Spatial and functional interrelationship of a heterotetramer Survivin-DNA-PKcs complex in the repair of DNA double-strand breaks

Güllülü, Ömer

(2020)

TECHNISCHE UNIVERSITÄT DARMSTADT

Spatial and functional interrelationship of a heterotetramer Survivin-DNA-PKcs complex in the repair of DNA double-strand breaks

Dem Fachbereich Biologie der Technischen Universität Darmstadt

zur Erlangung des akademischen Grades

eines *Doctor rerum naturalium*

genehmigte Dissertation von

M.Sc. Ömer Güllülü

aus Gebze - Türkei

Erstgutachter: Prof. Dr. Franz Rödel

Zweitgutachter: Prof. Dr. Markus Löbrich

Tag der Einreichung: 20.08.2020

Tag der mündlichen Prüfung: 02.12.2020

Darmstadt 2020

Güllülü, Ömer: Spatial and functional interrelationship of a heterotetramer Survivin-DNA-PKcs complex in the repair of DNA double-strand breaks

Darmstadt, Technische Universität Darmstadt

Jahr der Veröffentlichung der Dissertation auf TUprints: 2020

URN: urn:nbn:de:tuda-tuprints-154062

Tag der mündlichen Prüfung: 02.12.2020

Word of Honour

I hereby declare that I have written this dissertation independently and without undue assistance from third parties in accordance with the rules of good scientific practice. All thoughts taken directly or indirectly from external sources as well as all data, techniques and materials taken directly or indirectly from others are marked as such. The work has not yet been submitted to any other university for examination purposes. The submitted electronic version agrees with the written version.

_____

Ömer Güllülü

Darmstadt, den 20.08.2020

Contents

List of Figures

List of Tables

1. Summary

Survivin was discovered as a member of the Inhibitor of Apoptosis Protein (IAP) family showing high expression in almost all human cancers. Although primarily considered as a protein implicated apoptosis and cell cycle/mitotic spindle checkpoint regulation, Survivin is now recognized as a nodal factor involved in a multitude of cellular circuits. By this, Survivin covers a radiation resistance factor in a variety of cancer entities and enhances tumor cell survival upon radiation exposure by impacting DNA double-strand break (DNA DSB) repair. Following irradiation, nuclear accumulation of Survivin was mechanistically been linked to the activity of the DNA-dependent protein kinase, catalytic subunit (DNA-PKcs), a key component of DNA DSB repair pathway non-homologous end joining (NHEJ).

In this study, we aimed to unravel the determinants of the Survivin-DNA-PKcs interrelationship on a molecular level by computational investigations of the regions of interaction and biochemical approaches. 3D crystallographic structures of Survivin and catalytic PI3K domain of DNA-PKcs were virtually docked using advanced global docking algorithms, simulated by molecular dynamics, and were evaluated according to binding free energies (ΔG) and the spatial accessibility/physical proximity. Next, multiple residues derived from these analyses were mutated, and the functional consequences of the mutagenesis were assayed by flow cytometry-based Förster resonance energy transfer (FACS-FRET) and co-immunoprecipitation (co-IP) experiments. Radiation survival and DNA damage repair capacity were assayed by 3D colony formation assays and DNA foci analysis (γH2AX/53BP1), respectively. The effects of the Survivin-DNA-PKcs interrelationship were further analyzed by *in vitro* DNA-PKcs kinase activity assays and Liquid Chromatography-Mass Spectrometry (LC-MS2/3)-based multi-proteomic techniques. Finally, a virtual drug screening approach was employed in search for novel small-molecule radiosensitizers targeting the Survivin-DNA-PKcs interaction.

Molecular docking and advanced *in silico* analyses uncovered residues serine(S)20 and tryptophan(W)67 located in the baculovirus inhibitor of apoptosis protein repeat (BIR) domain of dimerized Survivin to interact with the PI3K domain of DNA-PKcs. Mutagenesis of these residues significantly decreased the interaction compared to wild-type (wt) Survivin, was correlated with an increased radiosensitivity of colorectal cancer cells and a hampered DNA repair capacity, measured by γH2AX/53BP1 foci analysis, after knockdown of endogenous Survivin. By contrast, overexpression of wt Survivin rescued radiation survival and DNA repair. In addition, advanced molecular docking and dynamics simulation analyses revealed a heterotetramer model, where Survivin binds to the surface of pre-existing DNA-PKcs dimer. Moreover, by investigating the effects of Survivin on DNA-PKcs' downstream regulatory functions, differentially abundant phosphopeptides and proteins were identified for multiple pathways, predominantly for DNA damage/repair. Binding of Survivin to a pre-existing DNA-PKcs dimer was lead to a conformational change on the PI3K domain and resulted in a differential change in substrate specificity. Particularly, the previously little-known DNA-PKcs' S/T-Hydr (hydrophobic residues: G, A, V, L, I, P, F, M, W) motif substrates including the FOXO3 S253 phosphosite displayed high conservation within the detected phosphosites. Further, proteomics analyses indicated that the Survivin-DNA-PKcs interrelationship not only displays post-translational but also protein expression-level regulatory properties. Ultimately, the virtual drug screening approach uncovered small-molecule compounds having strong binding affinity to S20, and W67 residues and

consequently might show promise for the development of future radiation sensitizing therapeutic approaches.

In summary, in this study, we identified specific residues of Survivin involved in the interaction with the PI3K domain of DNA-PKcs by implementing *in vivo* live cell protein interaction quantification and *in silico* structure-based molecular docking technologies. Besides that, findings on radiosensitivity, DNA foci formation, kinase activity, and phosphoproteomics and proteomics analyses further strengthen the notion that Survivin is a fine-tuning regulator of DNA DSB repair and impacts on substrate specificity by fostering the S/T-Hydr motif phosphorylation. Large-scale proteomics and phosphoproteomics studies further discovered novel candidate proteins and phosphosites, enlightening the underlying mechanistic relation between Survivin and DNA-PKcs in response to irradiation and may pave the way to novel Survivin-related cancer and DNA damage response marker discoveries.

Zusammenfassung

Survivin, das kleinste Mitglied der Inhibitor of Apoptosis Protein (IAP)-Familie ist durch eine hohe Expression in fast allen untersuchten humanen Tumoren gekennzeichnet. Obwohl Survivin primär als ein Protein mit Funktionalität in der Regulation von Apoptose und Zellzyklus/mitotischen Spindelkontroll- punkt beschrieben ist, wird das Protein aktuell als ein wesentlicher Knotenfaktor in einer Vielzahl zellulärer Reaktionskaskaden angesehen. In diesem Zusammenhang stellt Survivin in einer Vielzahl von Tumorentitäten einen Resistenzfaktor dar, der das Überleben der malignen Zellen nach Strahlenexposition verbessert indem er die Reparatur von DNA-Doppelstrangbrüchen (DNA-DSB) zu modulieren vermag. Dabei konnte eine nukleäre Akkumulation von Survivin nach Bestrahlung mechanistisch mit der Aktivität der DNA-abhängigen Proteinkinase (DNA-PKcs), einer Schlüsselkomponente des DNA-DSB Reparatur- Mechanismus der Nicht-Homologen Endverknüpfung (NHEJ), assoziiert werden.

Ziel der Studie war die Aufklärung der molekularen Determinanten der Survivin-DNA-PKcs Wechsel- Beziehung durch computergestützte Analysen der Interaktionsregionen und biochemische Ansätze. Dazu wurden die Bindung kristallographischer 3D-Strukturen von Survivin und die katalytische PI3Kinase-Domäne der DNA-PKcs virtuell mit Hilfe fortgeschrittener Algorithmen und molekular-dynamischer Berechnungen simuliert und in Abhängigkeit von freien Bindungsenergien (ΔG) und der räumlichen Zugänglichkeit/physischen Nähe bewertet. Anschließend wurden als Ergebnis dieser Analysen unter- schiedliche Aminosäuren von Survivin mutiert und die funktionellen Konsequenzen dieser Mutagenese mittels durchflusszytometrischer Förster-Resonanzenergietransfer (FACS-FRET) und Ko-Immunpräzipitations (co-IP) Experimenten untersucht. Das Überleben nach Bestrahlung und die Fähigkeit zur Reparatur von DNA-Schäden wurden mit 3-dimensionalen-Koloniebildungstests bzw. der Quantifizierung von DNA-Schadensmarker γH2AX/53BP1 analysiert, während die Effekte der Interaktion auf die Kinaseaktivität der DNA-PKcs durch *in-vitro* Kinase-Aktivitätsmessungen und Massenspektrometrie (LC-MS2/3) basierten multi-Proteomik-Ansätzen evaluiert wurden. Schließlich erfolgte mit Hilfe eines virtuellen Wirkstoff-Screening-Ansatzes auf Grundlage der Survivin-DNA-PKcs-Interaktion eine Suche nach neuartigen niedermolekularen Hemmstoffen der Interaktion mit möglicher strahlensensibilisierender Wirkung.

Durch molekulare Bindungs- und *in-silico* Analysen konnte eine Bindung von Survivin an die PI3Kinase-Domäne der DNA-PKcs nachgewiesen werden, die überwiegend durch eine Interaktion der Aminosäuren Serin (S)20 und Tryptophan (W)67 der Baculovirus-IAP repeat (BIR) Domäne von dimerisierten Survivin vermittelt wird. Im Vergleich zum Wildtyp (wt) Survivin verringerte eine spezifische Mutagenese dieser Aminosäuren signifikant die Interaktion mit der DNA-PKcs, korrelierte mit einer erhöhten Strahlen- sensibilität von kolorektalen Tumorzellen und einer verminderten DNA-Reparaturkapazität nach Hemmung von endogenem Survivin. Im Vergleich dazu konnte durch eine Überexpression von wt Survivin das klonogene Zellüberleben und die DNA-Reparaturkapazität wiederhergestellt werden. Darüber hinaus führten weiterführende molekulare Bindungsanalysen und dynamische Simulationen zur Entwicklung eines Heterotetramer-Modells, bei dem Survivin an die Oberfläche eines bereits existierenden DNA-PKcs-Dimers zu binden vermag. In Untersuchungen des Effekts dieser Bindung auf nachgeschaltete regulatorische Funktionen der DNA-PKcs konnte eine große Anzahl differentiell regulierter Phospho- peptide identifiziert werden, die vorwiegend Reaktionswegen der DNA-Schadensantwort/Reparatur betreffen. Dabei führt die Bindung von Survivin an ein präformiertes DNA-PKcs-Dimer zu einer Konformationsänderung der PI3K-Domäne, resultierte in einer signifikanten Steigerung der Kinaseaktivität und einer differentiellen Änderung der Substratspezifität. Insbesondere bisher wenig beschriebene DNA-PKcs S/T-Hydr (hydrophobe Aminosäuren: G, A, V, L, I, P, F, M, W) Motive einschließlich der FOXO3 Aminosäure S253 zeigten eine hohe Konservierung innerhalb der detektierten Phosphorylierungsstellen. Darüber hinaus zeigten Proteomanalysen, dass die Survivin-DNA-PKcs-Interaktion nicht nur post- translationale, sondern auch regulatorische Funktionen auf Proteinexpressionsebene ausüben kann. Schließlich konnten in ersten virtuellen Wirkstoff-Screening-Ansatz niedermolekulare Verbindungen identifiziert werden, die eine hohe Bindungsaffinität zu den Amiosäuren S20 und W67 aufweisen und für zukünftige strahlensensibilisierende Therapieansätze vielversprechend sein könnten.

Zusammenfassend konnte erstmals unter Verwendung einer Methodik zur Quantifizierung einer Proteineninteraktion in lebenden Zellen und durch *in-silico* strukturbasierte Bindungsanalysen spezifische Aminosäuren von Survivin identifiziert werden, die an der Wechselwirkung mit der PI3K-Domäne der DNA-PKcs beteiligt sind. Darüber hinaus bestätigen die Ergebnisse der Strahlensensibilitätsuntersuchungen, der Nachweis von DNA Reparatur-Foci, DNA-PKcs Aktivitätsmessungen und (Phospho)proteomik-Analysen die Vorstellung, dass Survivin einen (Fein)regulator der DNA-DSB Reparatur und insbesondere der Substratspezifität der DNA-PKcs hin zu S/T-Hydr-Motiven darstellt. Umfangreiche (Phospho)proteomik-Analysen führten zudem zur Aufdeckung neuer Kandidatenproteine und Phosphorylierungsstellen. Dies könnte dazu beitragen die zugrundeliegenden mechanistischen Beziehungen zwischen Survivin und DNA-PKcs weiter aufzuklären und den Weg zur Entdeckung neuer, Survivin-assoziierter Tumor und DNA-Schadenreaktionsmarkern und Therapieansätze zu ebnen.

2. Introduction

2.1. DNA damage response

2.1.1. Irradiation, DNA DSB repair and DNA-PKcs

125 years ago, physicist Wilhelm Conrad Röntgen has discovered a novel art of ionizing radiation (IR) known as X-Rays or Röntgen-Rays today (Röntgen, 1895). IR is a type of high-energy radiation that generates ions via releasing electrons from molecules that causes the breaking of covalent bonds. IR is measured in Gray (Gy) units and is defined as the amount of radiation energy absorbed by one kilogram (kg) of tissue. IR directly damages the deoxyribonucleic acid (DNA) structure by inducing DNA damage such as base damage, single-strand breaks (SSBs), DNA crosslinks, and most importantly double-strand breaks (DSBs) (Borrego-Soto et al., 2015; Jeggo and Lobrich, 2006).

IR-induced DNA DSBs initiate a cellular DNA damage stress response (DDR) by activating DNA repair pathways aiming to maintain genomic stability and fix the damage. Functional, disruption of DNA repair pathways ends up with anti-proliferative responses by regulation of cell cycle checkpoints, cellular senescence, and a variety of cell death pathways (Kantidze et al., 2018). Dependent on the cell cycle phase status, one of the two main DNA DSB repair pathways, homologous recombination (HR) or non-homologous end joining (NHEJ) is used for repair. HR is in service for S-phase diploid cells, while because of the absence of a homology donor nearby, haploid and G1/G2/M-phase diploid cells are repaired by NHEJ (Lieber, 2010). NHEJ functions throughout the cell cycle process, while during the late S/G2 phase, HR is more dominant (Brandsma and Gent, 2012).

Around 35 years ago, a study reported the discovery of a global increase of phosphorylation upon addition of double-stranded DNA (dsDNA) into cell extract phosphorylation assay. Of particular importance, this study revealed for the first time that some kinases have dependencies on the presence of dsDNA to function properly (Walker et al., 1985). Within a couple of years, specific identification, partial purification and characterization, and activity of DNA-dependent protein kinase catalytic subunit (DNA-PKcs) were reported (Carter et al., 1990; Lees-Miller and Anderson, 1989). DNA-PKcs is a serine/threonine protein kinase belonging to the phosphatidylinositol-3-kinase (PI3K)-like kinase (PIKK) family and is a major regulator of DDR. Lupus Ku autoantigen protein p70/80 (KU70/80) heterodimer binds to DNA and recruits the DNA-PKcs to the damage site to form an active DNA-PK holoenzyme (Hartley et al., 1995). The PI3K domain of DNA-PKcs is located at the C-terminus and flanked upstream by a FRAP-ATM-TRRAP (FAT) (Hammel et al., 2010) domain and downstream by a FAT C-terminal domain (FATC). All the members of PIKK family further include variable lengths of large helical supersecondary structured hydrophobic Huntingtin, Elongation Factor 3, PP2 A, and TOR1- (HEAT)-repeat domains (Sibanda et al., 2017) (**Figure 1**).

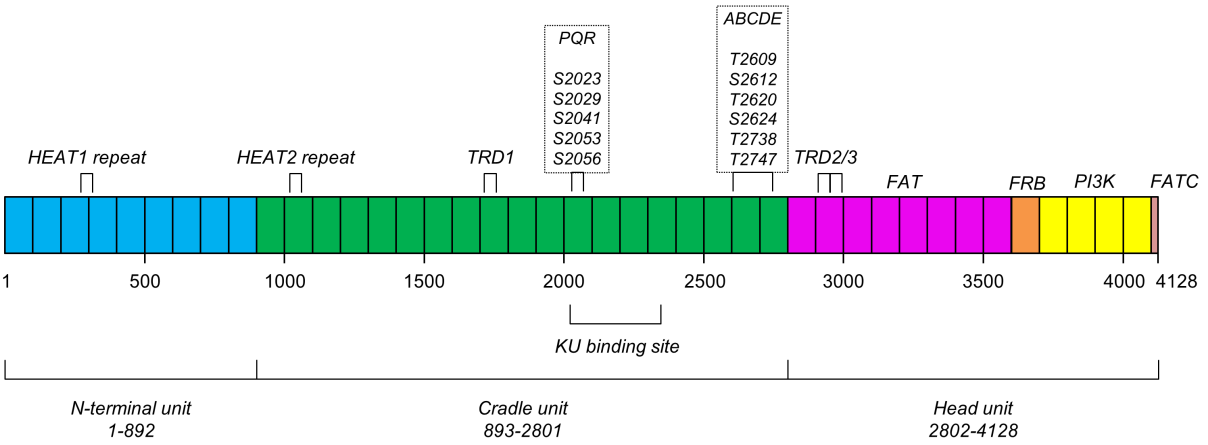

Figure 1. Schematic representation of the DNA-PKcs' subunits. 4128 amino acids long DNA-PKcs contains N-terminal, Cradle and Head units and a variety of different subspecialized domains/regions within these units. (Abbreviations: HEAT1/2, Huntingtin, Elongation Factor 3, PP2 A, and TOR1 repeat; TRD1/2/3, tetratricopeptide repeat domain 1/2/3; PQR, autophosphorylation sites; ABCDE, auto/transphosphorylation sites; FAT, FRAP-ATM-TRRAP domain; FRB, FKBP12-rapamycin binding domain; PI3K, phosphatidylinositol-3-kinase; FATC, FAT C-terminal domain). Figure modified from (Sibanda et al., 2017).

When a DNA DSB occurred, KU70/80 heterodimer was first thought to bind DNA DSB ends because of the high abundance (400,000 molecules/cell) and strong binding affinity (dissociation constant (K_d): $\sim 10^{-9}$ M) for dsDNA ends (Blier et al., 1993; Falzon et al., 1993; Lieber, 2010; Mimori and Hardin, 1986). Moreover, recently it has been reported that the C-terminal region of KU80 is responsible for recognizing the DNA DSB ends and to generate an extended flexible arm that connects DNA-PKcs to the KU70/80-DNA complex (Hammel et al., 2010; Hammel et al., 2016; Radhakrishnan and Lees-Miller, 2017). The recruitment of DNA-PKcs to the KU70/80-DNA complex is dependent on the presence of DNA DSB ends because in the absence of these ends a stable KU70/80-DNA-PKcs complex can not be established (Lieber, 2010; Yaneva et al., 1997). For the DNA DSB end processing stage of NHEJ repair, it is still unclear whether Artemis-based nuclease activity or polymerase (λ or μ)-based filling of overhangs are used. Artemis is a nuclease characterized by a variety of abilities such as 5´ and 3´ endonuclease activity, 5´ exonuclease activity, and hairpin opening activity (Lieber, 2010; Ma et al., 2002). On the other hand, polymerases λ and μ both are able to bind to KU70/80-DNA complex, and particularly polymerase μ has template-independent synthesis ability, which perfectly fits the needs of NHEJ (Lieber, 2010; Ma et al., 2004; Zhao et al., 2020). After the processing step, ultimately an X-ray repair cross complementing 4 (XRCC4)-DNA ligase IV-XRCC4-like factor (XLF) complex has to be recruited to ligate the processed ends. XLF stimulates the initial heterodimerization of XRCC4-DNA ligase IV, and interacts with XRCC4 by generating a bridge on DNA ends (Ahnesorg et al., 2006; Roy et al., 2015). The flexibility of DNA ligase IV permits ligation of a wide range of DNA end structures, even single strands of both ends. However, one consequence of this flexibility is that it may cause ligation of one or both strands of the left and right duplexes, which stimulates transient or permanent termination of the NHEJ ligation process. It seems likely that the dynamic NHEJ processor complexes need multiple rounds of actions to fix the damage (Lieber, 2010). NHEJ factors are in close functional relation to accurately carry out the repair function. XRCC4/XLF interaction is vital for DNA-PKcs since *xlf*-deficient cells or XRCC4 interaction-deficient XLF cause a

malfunction in terms of DNA-PKcs autophosphorylation (Roy et al., 2015). Furthermore, for the activation of the end-processing endonuclease process, Artemis requires either autophosphorylation of DNA-PKcs (Goodarzi et al., 2006) or DNA-PKcs- or Ataxia telangiectasia mutated- (ATM)-dependent phosphorylation (Jiang et al., 2015). DNA ligase IV which is a vital component of the NHEJ end-ligation step was found to be phosphorylated by DNA-PKcs whose deletion in V3 cells diminished the DNA ligase IV phosphorylation. The phosphorylation of DNA ligase IV by DNA-PKcs, particularly on T650 residue, was found to be essential for its stability (Wang et al., 2004). Additionally, the accumulation of XRCC4 at the DNA DSB site was found to be dependent on KU70/80 via direct interaction (Mari et al., 2006). Moreover, according to recent small angle X-ray scattering (SAXS) analyses, mainly KU80 was found to interact with the C-terminus region of XLF (Nemoz et al., 2018) (**Figure 2**).

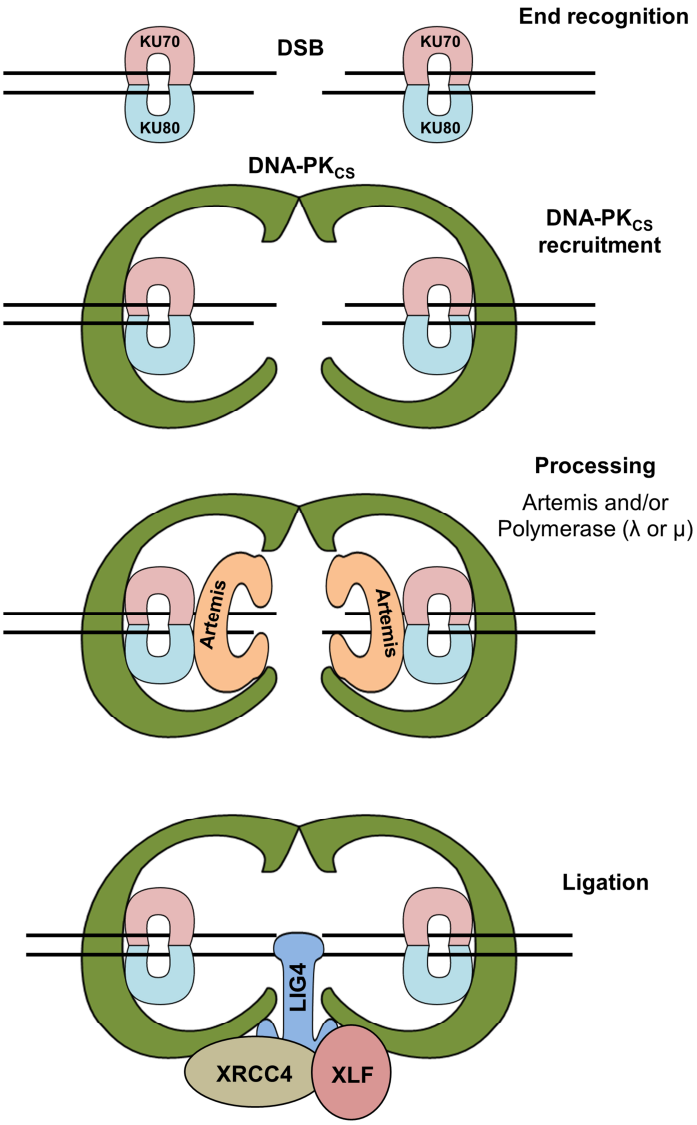

Figure 2. Non-homologous end joining (NHEJ) repair pathway. After DNA double-strand break (DSB) generation, NHEJ starts with the recognition of both DNA ends by the KU70/80 heterodimers, which then recruit the DNA-PKcs. If the ends are incompatible, Artemis and/or Pol λ or μ can be recruited as well to either trim or fill up the ends, respectively. Eventually, the XRCC4-DNA ligase IV-XLF complex ligates the break. Figure adapted from (Brandsma and Gent, 2012).

Notably, the PI3K domain of DNA-PKcs is vital both, on a cellular and organism level. Expression of catalytically inactive kinase-dead (KD) DNA-PKcs (DNA-PKcs $^{KD/KD}$) leads to embryonic lethality in mice via causing severe neuronal apoptosis and several defects in the G0/G1 phase of the cell cycle when NHEJ is more prominent. Furthermore, it causes increased genomic instability by showing a massive fraction of chromosomal abnormalities, severe NHEJ defects, including hypersensitivity to IR, and abrogation of end-ligation (Jiang et al., 2015). Biochemical studies revealed the DNA-PKcs' preference for phosphorylating a serine or threonine followed by a glutamine residue (S/T-Q) both *in vitro* and *in vivo*, with the exception of phosphorylation of some non-S/T-Q motifs only *in vitro* (Lees-Miller and Anderson, 1989).

Autophosphorylation sites of DNA-PKcs mostly cluster in the cradle unit, such as S2056 and T2609, which are particularly essential for activation. S2056 and T2609 activation phosphorylation sites of DNA-PKcs are phosphorylated by itself and ATM/Ataxia telangiectasia and RAD3-related (ATR) kinases, respectively in response to IR and ultraviolet (UV) (Chen et al., 2005; Chen et al., 2007a; Yajima et al., 2006). Another autophosphorylation site, T3950, is located in the kinase domain and regulates the kinase activity. Despite that the kinase domain is located in the C-terminal region, deletion of the N-terminal and cradle units also hamper the kinase activity, which indicate the importance of N-terminal unit and autophosphorylation sites. The kinase activity of DNA-PKcs is essential for the phosphorylation of a variety of substrates including H2A histone family member X (H2AX), tumor protein P53 binding protein 1 (53BP1), ATM, polynucleotide kinase 3'-phosphatase (PNKP), KU70/80, DNA ligase IV, and XRCC4 which mainly regulate the DNA damage response (Davis et al., 2014). Moreover, it has many additional functions, e.g. it confers a negative regulatory effect on ATM on both, translational and post-translational level. DNA-PKcs/*prkdc*-deficient cells clearly show decreased ATM protein expression. Moreover, S85, T86, T372, T373, T1985, S1987, and S1988 phosphorylation of ATM by DNA-PKcs represses ATM activation both *in vitro* and *in vivo*. Overexpression of ATM with the related phospho-mimetic mutations in *atm*-deficient cells fails to restore cell survival, DNA DSB end resection, or intra-S-phase checkpoint activation in response to DNA damage (Zhou et al., 2017a). Corroborating findings revealed as well that siRNA-mediated inhibition of DNA-PKcs hyperactivates ATM by increased phosphorylation of S1981 autophosphorylation site (Finzel et al., 2016).

The expected final step of NHEJ is the ligation of broken DNA ends, but the missing link was how DNA ends are brought together? The process called synapsis was studied by a variety of groups for many years yielding novel aspects. The first hypothesis to enlighten the process arised from electron microscopy (EM) studies by DeFazio and colleagues that suggested a DNA-PKcs dimerization (DeFazio et al., 2002). This hypothesis was further supported by other EM/cryogenic EM (cryo-EM) studies postulating that the DNA-PKcs either alone or as a holoenzyme with KU70/80 dimerized by the N-terminal HEAT repeats and/or mid part of cradle (Baretic et al., 2019; Sibanda et al., 2017; Spagnolo et al., 2006). By a different experimental approach, using SAXS, Hammel and colleagues further reported that DNA-PKcs was dimerized by the head domain, which incorporates the PI3K domain (Hammel et al., 2010). That was also supported by a recent cryo-EM study that indicated the FAT/kinase domain regions of DNA-PKcs to generate a self-heterodimer to autophosphorylate the PQR cluster (Baretic et al., 2019). Indeed, DNA-PKcs is not the only member of the PIKK family which dimerizes. According to crystallographic data, ATM and ATR seem to dimerize as well.

ATM was found to dimerize via long helical hairpin regions in the tetratricopeptide repeat domain 3 (TRD3) sub-domain located within the FAT and kinase (FATKIN) domain (Baretic et al., 2017; Wang et al., 2016; Waterman et al., 2020). However, ATR was found to generate a heterodimer with ATRIP (Wang et al., 2017; Waterman et al., 2020). In contrast to the DNA-PKcs dimerization hypotheses and findings, a recent study suggested a synapsis model predicting of a complex containing KU70/80, XRCC4, DNA ligase IV, XLF, and Paralog of XRCC4 and XLF (PAXX) but not DNA-PKcs by employing a single-molecule FRET (sm-FRET) method (Zhao et al., 2019). It is well known that synapsis processes are highly dynamic and this hypothesis definitely needs further investigations to elucidate its dynamic mechanism and mediators.

2.1.2. IAP family, Survivin and relations with DNA damage response

The inhibitor of apoptosis protein (IAP) family was first discovered by the characterization of a novel domain of baculoviral IAP repeat (BIR), which takes the name from the gene of a baculovirus that inhibit virally infected *Spodoptera frugiperda* insect cells (Crook et al., 1993). The IAP family is structurally characterized by a varying numbers of BIR domains. After the recent discovery of Baculoviral IAP repeat-containing protein 1 (gene name *birc8)*, the IAP family currently consists of eight members such as neuronal apoptosis inhibitory protein (NAIP)*/birc1*, cellular IAP 1 (cIAP1)*/birc2*, cellular IAP 2 (cIAP2)*/birc3*, X-chromosome-linked IAP (XIAP)*/birc4*, Survivin*/birc5*, BIR repeat-containing ubiquitin-conjugating enzyme (BRUCE)/Apollon*/birc6*, LIVIN*/birc7* and human IAP-like 2 (hILP2)/TS-IAP*/birc8* (Oberoi-Khanuja et al., 2013; Srinivasula and Ashwell, 2008) (**Figure 3**).

Besides the well-known function of IAP family members to inhibit apoptosis mainly mediated by BIR domains, they also consist of a variety of different domains which equip them with different functional abilities. Anti-apoptotic nucleoside triphosphatase (NTPase) NAIP*/birc1* includes a NAIP-C2TA-HETE-TEP1 nucleotide-binding and oligomerization domain (NACHT) which functions in a guanosine triphosphate (GTP)-dependent manner in apoptosis inhibition and major histocompatibility complex (MHC) class II transcription activation (Koonin and Aravind, 2000). Leucine-rich repeat (LRR) containing domains are conserved regions mainly playing roles on signalling pathways of innate immunity and host-pathogen recognition (Ng and Xavier, 2011). cIAP1/2 and hILP2 proteins consist ubiquitin-associated (UBA) domains that stimulate either the proteasomal degradation or protein stabilization via binding to ubiquitinated proteins (Su and Lau, 2009). Caspase recruitment domains (CARD) predominantly serve as protein-protein interaction region playing roles in the regulation of immune response signalling pathways, inflammation and apoptosis (Palacios-Rodriguez et al., 2011). BRUCE has an ubiquitin conjugating (UBC) domain which works sequentially with the ubiquitin facilitates the conjugation step of activation/conjugation/ligation cascade process of ubiquitination via catalysing the covalent attachment of ubiquitin to the target protein (Passmore and Barford, 2004). Really interesting new gene (RING) domain containing cIAP1/2, XIAP, LIVIN and hILP2 have E3 ubiquitin ligase activity which mediates ubiquitination and intrinsic protein degradation/stabilization dynamics. Further, RING domains mediate signal transduction, protein-protein interactions, transcription and recombination (Stone et al., 2005) (**Figure 3**).

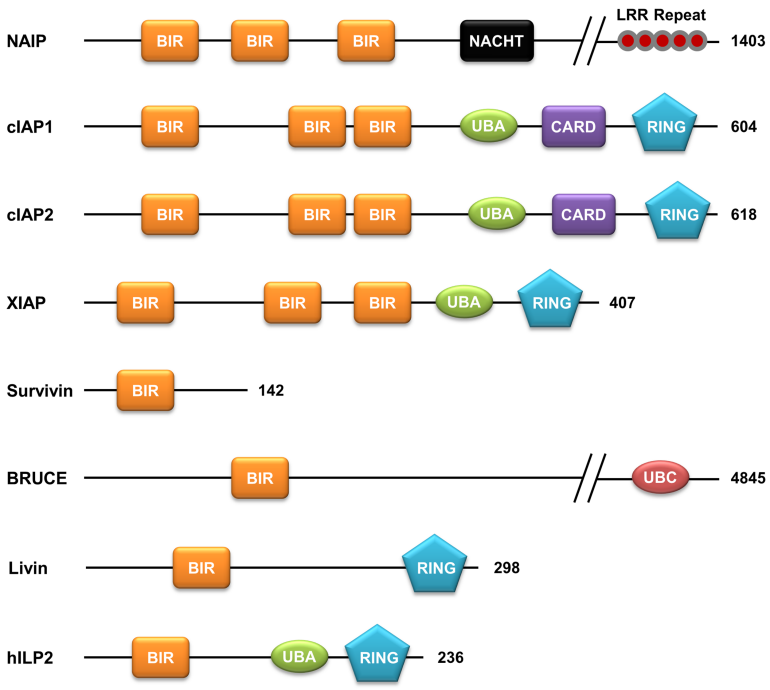

Figure 3. Domain architecture of the inhibitor of apoptosis (IAP) family members. IAPs are represented with their functional domains. Baculoviral IAP repeat (BIR), NAIP-C2TA-HETE-TEP1 nucleotide-binding and oligomerization domain (NACHT), leucine-rich repeats (LRR), ubiquitin-associated domain (UBA), caspase recruitment domain (CARD), really interesting new gene domain (RING), ubiquitin conjugating domain (UBC). Figure adapted from (Oberoi-Khanuja et al., 2013).

Survivin, encoded by the *birc5* gene, is a 16.5 kDa protein of 142 amino acid residues primarily described in the late nineties as a member of the mammalian IAP family (Ambrosini et al., 1997). In contrast to other members of the family, Survivin harbors only a single BIR domain that is reported to confer protein-protein interactions with caspases or kinases and an extended amphipathic α-helical coiled-coil domain at the C-terminus, common in microtubule-associated proteins (LaCasse et al., 1998; Verdecia et al., 2000). The conserved BIR domain (18-88 amino acids region) works as an interaction hub for many protein-protein interactions of Survivin to function correctly and maintain self-consistency. SMAC/DIABLO, which is essential for the anti-apoptotic function of Survivin, binds directly to the BIR domain, and D71R point mutation inhibits this interaction (Song et al., 2003). Further, as a chromosomal passenger complex (CPC) member, Survivin´s BIR domain residues D70 and D71 function as an anchorage to centromeres, which results in the proper karyokinesis during mitosis (Wang et al., 2010). Besides, binding of the ATPase domain of HSP90 to the BIR domain provides both, consistency for Survivin and regulation of cell cycle and apoptosis. Inhibition of this interaction leads to proteasomal degradation of Survivin, mitochondrial-dependent apoptosis, and cell cycle arrest with mitotic defects (Fortugno et al., 2003). These findings suggest a potential protein-protein interaction role mainly for the BIR domain of Survivin.

Although Survivin was primarily reported to constitute a bifunctional protein involved in the regulation of cell division/proliferation and apoptosis, it is now evident that it is a prime example of a multifunctional nodal protein implicated in multiple tumor signaling pathways. These cover transcriptional networks, autophagy, and stemness (Altieri, 2008, 2010; Wheatley and Altieri, 2019). In that context, one of the signature features of Survivin is its direct or indirect relationship with a multitude of protein partners, including tubulins, nuclear

and heat shock proteins, multiple kinases, caspases and other members of the IAP family such as the XIAP and cIAP-1 (Altieri, 2008, 2010; Jung et al., 2015; Rodel et al., 2012). Although the BIR domain of Survivin does not bind directly to caspases, in both homodimer and monomer forms, increased Survivin expression and prior mitochondrial residence reduce the caspase activity. For example, via prevention of the release of Apoptotic protease-activating factor 1 (APAF1) from mitochondria or direct association with XIAP and Hepatitis B X-interacting protein (HBXIP) in a complex with XIAP-associated factor 1 (XAF1), Survivin is reported to inhibit Caspase 3/7, 8 and 9 activities whereas association with second mitochondria-derived activator of caspases (SMAC)/direct IAP binding protein with low pI (DIABLO) counteracts this inhibitory activity (Dohi et al., 2004; Du et al., 2000; Hehlgans et al., 2015; Song et al., 2003; Wheatley and Altieri, 2019). Moreover, Survivin was found to orchestrate nuclear factor kappa B (NF-κB) dependent expression of fibronectin, integrin signalling, activation of focal adhesion kinase (FAK) and SRC or up-regulation of AKR thymoma serine/threonine-specific protein kinase (AKT) pathway to mediate tumor cell migration and metastatic dissemination (Chu et al., 2012; Hehlgans et al., 2013; Mehrotra et al., 2010; Wheatley and Altieri, 2019) (**Figure 4**).

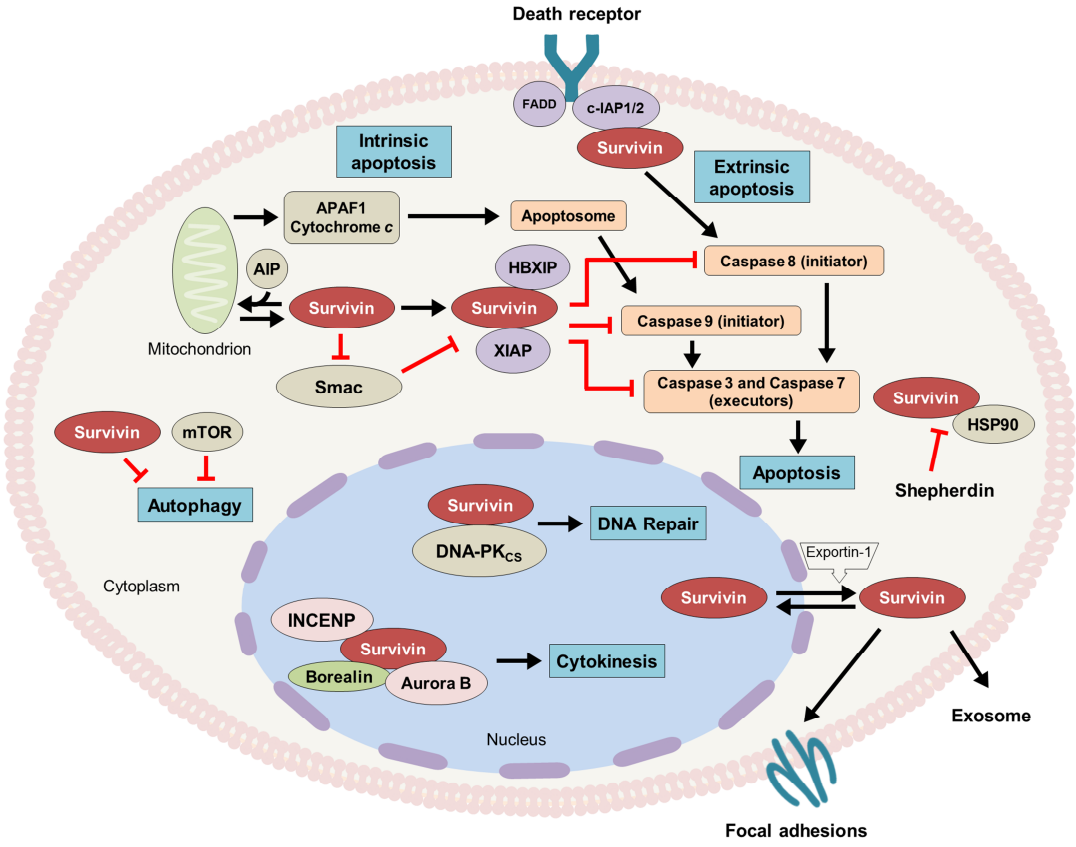

Figure 4. Schematic representation of the cellular functions of Survivin. Survivin acts in a variety of cellular pathways such as regulation of apoptosis (intrinsic and extrinsic), autophagy, DNA repair and cytokinesis via dynamic protein interactions in mitochondria, the cytoplasm and nucleus. (Abbreviations: FADD, FAS-associated death domain protein; cIAP1/2, cellular inhibitor of apoptosis protein 1/2; APAF1, apoptotic protease-activating factor 1; AIP, APAF1 inhibitory protein; SMAC, second mitochondria-derived activator of caspases; HBXIP, hepatitis B X-interacting protein; XIAP, X-chromosome-linked inhibitor of apoptosis protein; mTOR, mammalian target of rapamycin; HSP90, heat shock protein 90; Shepherdin, peptidomimetic antagonist of the HSP90-Survivin complex; DNA-PKcs, DNA-dependent protein kinase catalytic subunit; INCENP, inner centromere protein; Aurora B, aurora kinase B). Figure adapted from (Wheatley and Altieri, 2019).

Survivin works as a protector against either apoptotic or autophagic cell death. Cytoplasmic localization is essential for this activity, while nuclear relocation abrogates it. The basal level of autophagy is vital to remove defective organelles and unfolded/misfolded proteins. In the catabolic recycling system, an excessive amount of autophagy kills the cells, which might be a tumor suppression approach in a cancer-dependent manner (Chun and Kim, 2018). Survivin expression increases via hyperactivated AKT-PKB-PI3K signalling in response to cytokine treatment and results in the inhibition of autophagic death. In accordance, the association of Survivin with coiled-coil myosin-like BCL2-interacting protein (BECLIN-1) inhibits the excessive amount of autophagy, while inhibition of Survivin with small molecule YM155 inhibitor increases the interrelationship, which makes it a target as an autophagy-dependent cancer treatment (Wheatley and Altieri, 2019). Recently, the role of Survivin on autophagy was further investigated. It could be shown that Survivin works as a bridging molecule to provide interaction between autophagy related 12 (ATG-12) and ATG-5, and this interaction prevents the ATG-12/ATG-5/ATG16L1 heterotrimeric interaction that results in the suppression of autophagy-induced DNA damage (Lin et al., 2019).

Moreover, Survivin contains various phosphorylation sites such as Serine (S) 20 (Protein kinase A, Polo like kinase 1 and Aurora Kinase C), Threonine (T) 34 ($p34^{cdc2}$/cyclin-dependent kinase 1 and cyclin-dependent kinase 15) and T117 (Aurora kinase B) to facilitate both, protein stability and trafficking among various subcellular compartments (Colnaghi and Wheatley, 2010; Dohi et al., 2007; O'Connor et al., 2002; Park et al., 2014; Raab et al., 2015; Sasai et al., 2016; Wheatley et al., 2007).

In the clinical setting, it has consistently been demonstrated that Survivin is overexpressed in the majority of solid and liquid human tumors and significantly correlates with tumor onset, more aggressive and advanced pathologic features, metastasis and worse prognosis as well as impaired patients' survival (Kanwar et al., 2013; Miura et al., 2011; Rodel et al., 2012). In addition, due to its prognostic and predictive relevance along with a prominent role at disparate cellular networks, Survivin is considered to be a target for a molecular cancer drug development with the first inhibitors (antisense oligonucleotides, small molecules and immunotherapy) currently under clinical phase I/II/III investigation (http://clinicaltrials.gov) (Kanwar et al., 2011). Additionally, Survivin has been found on the surface of circulating exosomes in malignant glioma patients. A decrease in Survivin-positive exosomes following Survivin immunotherapy was reported to be associated with longer progression-free survival suggesting Survivin as potential prognostic marker in serum biopsies (Galbo et al., 2017). Beyond that, it has been shown in a multitude of both, *in vitro* and *in vivo* models that Survivin constitutes a radiation resistance factor and that attenuation of the protein radiosensitizes malignant cells (Rodel et al., 2012). The underlying mechanism(s) and molecular requirements, however, far exceed a simple inhibition of irradiation-induced caspase-dependent apoptotic cell death, including caspase-independent pathways like modulation of DNA damage repair (Chakravarti et al., 2004; Rodel et al., 2011). Thus, recent studies further demonstrate that a nuclear accumulation of Survivin following irradiation and an interaction with components of the DNA DSB repair apparatus like DNA-PKcs regulates DNA DSB repair, at least in part, by modulating DNA-PKcs kinase activity (Capalbo et al., 2010; Reichert et al., 2011).

Not only Survivin but also other IAP family members are directly involved in the DNA damage response and repair. In line with the characteristics of the IAP family members, BRUCE the largest member of the IAP family with a 528 kDa molecular weight, is a multifunctional

protein which regulates development (Hao et al., 2004; Lotz et al., 2004), cytokinesis (Pohl and Jentsch, 2008) and as recently reported DNA damage response (Ge et al., 2015) besides its apoptosis inhibitory role. BRUCE was found to act as a scaffold for DNA DSB-induced deubiquitination of BRCT-repeat inhibitor of TERT expression 1 (BRIT1) by ubiquitin specific peptidase 8 (USP8). Further, the complex BRUCE-BRIT1-USP8 facilitates chromatin relaxation for timely DNA repair in response to DNA DSB (Ge et al., 2015). The other member of IAP family that contributes to the DNA damage response is cIap1 which alongside three BIR domains, harbors a RING domain to modulate ubiquitin ligase activity and a CARD domain (Lopez et al., 2011). CIAP1 functions in the regulation of cell cycle (Samuel et al., 2005), nuclear factor kappa B (NF-κB) activation (Tang et al., 2003), and differentiation (Plenchette et al., 2004). Recently it has been reported that silencing of cIAP1/*birc2* impedes IR-induced transforming growth factor (TGF)-beta-activated kinase 1 (TAK1) activation and I-kappa B kinase (IKK) T-loop phosphorylation by ATM in DNA damage induced NF-κB pathway activation (Hinz et al., 2010). According to the previous findings on Survivin (Capalbo et al., 2010; Reichert et al., 2011; Wang et al., 2018c), the current study and studies on other IAPs such as Bruce and cIap1 mentioned above suggest potential regulatory roles for IAP proteins in DNA damage response and repair processes.

2.2. Aim of the thesis

Survivin is a multifunctional protein which plays essential roles in several cellular processes such as programmed cell death, cell cycle regulation, chromosome segregation, mitosis, cellular stress response and in particular DNA damage response (Wheatley and Altieri, 2019). Recently it was revealed that upon irradiation Survivin accumulated in the nucleus and participated in the regulation of DNA damage response by interacting with DNA-PKcs (Capalbo et al., 2010; Chakravarti et al., 2004; Iwasa et al., 2008; Reichert et al., 2011; Rodel et al., 2005; Wang et al., 2018c). However on the molecular level characterization, mechanistic functions and the downstream regulatory effects of this interrelationship still remain unknown. To fill in the gaps of knowledge on the irradiation-dependent DNA damage response roles of Survivin at the molecular level, we aimed to investigate in more detail the interaction of Survivin with DNA-PKcs, its role in radiation responsiveness/survival of tumor cells and the large-scale regulatory effects on DNA damage response.

Crystallographic structures of Survivin and DNA-PKcs were subjected to *in silico* molecular docking/dynamics simulations. Experimentally, a variety of amino acid and domain/region deletion mutants of Survivin and DNA-PKcs were generated and stably/transiently expressed in the colorectal cancer cell lines SW480, DLD-1 and HCT-15. Cells were subjected to functional analyses, including *in vivo* FACS-FRET, more physiological three-dimensional (3D) colony-forming assays, 3D immunofluorescence staining of γH2AX/53BP1 DNA repair foci, co-immunoprecipitation, *in vitro* kinase, multi-omics (phosphoproteomics and proteomics) and virtual drug screening analyses. Here we show that the BIR domain of Survivin and more specifically S20 and W67 amino acids located in the BIR domain of Survivin are essential for the regulation of 3D radiation survival and DNA damage repair via generating a heterotetramer complex interacting with catalytic PI3K domains of two DNA-PKcs' molecules and possibly modulating the kinase activity of DNA-PKcs. Eventually, this interaction leads to the regulation of critical cellular pathways such as DNA damage repair, apoptosis, cell cycle and transcriptional/post-transcriptional regulation.

3. Materials and Methods

3.1. Materials

3.1.1. Devices/Instruments

Device/Instrument	Model/Description	Manufacturer
Agarose gel electrophoresis chamber	-	PEQLAB Biotechnologie, Erlangen
Centrifuges	3-1810 Mini Spin UNIVERSAL 320R MEGA STAR 1.6R Ultracentrifuge, L8-M, SW32 Ti rotor	Neo Lab, Korea Eppendorf AG, Hamburg Hettich, Tuttlingen VWR, Darmstadt Beckman Coulter, Krefeld
Column oven	-	Sonation
Electrophoresis chamber for SDS gels + accessories	Mini-PROTEAN® Tetra Vertical Electrophoresis Cell	Bio-Rad, Munich
ELISA reader	TECAN infinite M200 pro	TECAN, Männedorf, Switzerland
Flow cytometer	CytoFLEX S	Beckman Coulter, Krefeld
Freezing container	Mr. Frosty™	Thermo Fisher Scientific, Dreieich
Gel electrophoresis power supply	Power Pack P25 T	Biometra, Göttingen
Heat sealer	Futura Junior	Audion, Weesp, the Netherlands
Hotplate/stirrer	C-MAG HS 7 -	IKA Labortechnik, Staufen VWR, Darmstadt
Imaging System	Odyssey® Fc Imaging System	LI-COR, Lincoln, NE, USA
Incubator	HERA cell 240 + 240i	Thermo Fisher Scientific, Dreieich
Laminar flow hood	HERA safe	Thermo Fisher Scientific, Dreieich
Linear accelerator	Synergy	Elekta, Crawley, UK
Magnet for Dynabeads	DynaMag™-2 Magnet	Thermo Fisher Scientific, Dreieich
Mass Spectrometer	Orbitrap Fusion™ Lumos™ Tribrid™ Mass Spectrometer (connected to EASY-nLC 1200 nano HPLC system)	Thermo Fisher Scientific, Dreieich
Microscopes	AxioVert A1 Axio Imager Z1 with AxioCam MRc	Zeiss, Jena Zeiss, Jena

	Axio Observer Z1 Inverted Phase Contrast Fluorescence	Zeiss, Jena
pH meter	pH Meter 765 Calimatic	Knick, Berlin
Phosphorimager	Fujifilm BAS-1500	GE Life Sciences, Japan
Scales	CP324S PRACTUM612-1S	Sartorius, Göttingen Sartorius, Göttingen
Semi-dry transfer system	Trans-Blot® Turbo™ Transfer System TE-77	Bio-Rad, Munich GE Healthcare, USA
Shakers	IKA® shaker MTS 4 IKA® KS 260 basic IKA® LOOPSTER digital Mixer HC ES-20 Biometra TS1 Vibramax 100	IKA Labortechnik, Staufen IKA Labortechnik, Staufen IKA Labortechnik, Staufen STARLAB, Hamburg BioSan, Riga, Latvia Analytik Jena, Jena Heidolph Instruments, Schwabach
Shaker for bacteria	MaxQ 4450	Thermo Fisher Scientific, Dreieich
Sonication device	Bioruptor Plus Bandelin Sonorex RK 31	Diagenode S.A., Belgium BANDELIN electronic, Berlin
Thermocycler	Primus 96 advanced Pro Flex	PeQLab Biotechnologie, Erlangen Applied Biosystems, Darmstadt
Vortex-Genie 2	-	Scientific Industries, Bohemia NY, USA
Water bath	Typ W/B 5	Gesellschaft für Labortechnik, Burgwedel

3.1.2. Consumables

Consumable	**Manufacturer**
100 mm cell culture dishes	Sarstedt, Nümbrecht
15/50 ml tubes	Greiner Bio-One, Frickenhausen
Cell scraper M	TPP, Trasadingen, Switzerland
CELLSTAR® 6/12/24/96-well cell culture plates	Greiner Bio-One, Frickenhausen
CELLSTAR® 96-well cell culture plates, white polystyrene wells flat bottom	Greiner Bio-One, Frickenhausen
CELLSTAR® Filter Top T25/T75 cell culture	Greiner Bio-One, Frickenhausen

flasks	
C-Chip Disposable Hemocytometer, Digital Bio	NanoEnTek, Seoul, South Korea
Cloning cylinders	Scienceware®, Pequannock, NJ, USA
Cover foil, Easy seal (80x140 mm)	Greiner Bio-One, Frickenhausen
CryoPure Tube 1.8 ml	Sarstedt, Nümbrecht
Culture slides 8 chambers	BD Falcon, Erembodegem, Belgium
FACS tubes, flow cytometry	Sarstedt, Nümbrecht
Filter paper	Whatman, Kent, UK
Glass beakers	Schott, Mainz
Microscope cover glasses (24x60 mm)	Marienfeld, Lauda-Königshofen
Microscopic slides	Thermo Fisher Scientific, Dreieich
Mini-PROTEAN® TGX™ Precast Gels	Bio-Rad, Munich
PCR tubes (0.2 ml)	Thermo Fisher Scientific, Dreieich
Petri dish (sterile, 92x16 mm)	Sarstedt, Nümbrecht
Pipette-tips, TipOne®, graduated, blue 1000μl/ yellow 200μl / white 20μl	Starlab, Hamburg
Polystyrene Round-Bottom tubes (14 ml)	Becton Dickinson, Heidelberg
Reaction tubes (0.5/1.5/2.0 ml)	Eppendorf, Hamburg Sarstedt, Nümbrecht
LoBind reaction tubes (1.5 ml)	Eppendorf, Hamburg
Trans-Blot® Turbo™ Mini Nitrocellulose Transfer Packs (mini format 0.2 μm nitrocellulose)	Bio-Rad, Munich
Amersham™ Protran™ Premium 0.45 μm Nitrocellulose membrane	Sigma-Aldrich, Munich

3.1.3. Reagents

Reagent	Manufacturer
3-(N-morpholino)propanesulfonic acid (MOPS)	Carl Roth, Karlsruhe
4 .6-Diamidin-2-phenylindol (DAPI)	Molecular Probes, Eugen, OR, USA
Agarose NEEO Ultra-Quality	Carl Roth, Karlsruhe
Glacial Acetic acid	J. T. Baker (Fisher Scientific), Schwerte

Acetonitrile	Sigma-Aldrich, Munich
Albumin Fraction V (pH 7)	AppliChem, Darmstadt
Ammonium peroxodisulfate (APS)	Carl Roth, Karlsruhe
Ampicillin	Carl Roth, Karlsruhe
^{32}P ATP (250 μCi)	PerkinElmer, Waltham, MA, USA
Benzonase® Nuclease	Merck Millipore, Darmstadt
Bromophenol blue	AppliChem, Darmstadt
Bovine Serum Albumin (BSA)	AppliChem, Darmstadt
Calcium chloride	AppliChem, Darmstadt
Chloroacetamide	Thermo Fisher Scientific, Dreieich
Chloroform	Fisher Scientific, Hampton, New Hampshire, USA
cOMPLETE mini EDTA-free protease inhibitor	Sigma-Aldrich, Munich
Cultrex 3D Culture Matrix BME Reduced Growth Factor Basement Membrane Extract Pathclear	R&D Systems, Wiesbaden
CytoFLEX Sheath Fluid	Beckman Coulter, Brea, CA, USA
Deoxynucleotides (dNTP) (10 mM)	Thermo Fisher Scientific, Dreieich
Dichloroacetic acid (DCA)	AppliChem, Darmstadt
Dimethyl sulfoxide (DMSO)	AppliChem, Darmstadt
Dithiothreitol (DTT)	Sigma-Aldrich, Munich
DNA-PK inhibitor (KU 0060648)	Tocris Bioscience, Bristol, UK
DNase I	Thermo Fisher Scientific, Dreieich
Dulbecco's Modified Eagle Medium (DMEM)	Thermo Fisher Scientific, Dreieich
Dulbecco's Phosphate Buffered Saline (PBS)	Thermo Fisher Scientific, Dreieich
Dynabeads™ Protein G	Thermo Fisher Scientific, Dreieich
Empore™ C18 (Octadecyl) resin material	3M, St. Paul, Minnesota, USA
EPPS	Sigma-Aldrich, Munich
Ethylenediaminetetraacetic acid (EDTA)	AppliChem, Darmstadt
EDTA Disodium Salt 2-hydrate (Na_2EDTA)	
Ethidium bromide (EtBr)	Carl Roth, Karlsruhe
Fetal bovine serum (FBS)	Thermo Fisher Scientific, Dreieich
Formaldehyde – Solution 37%	AppliChem, Darmstadt

Formic acid	Fisher Scientific, Hampton, New Hampshire, USA
Geneticin (G418)	AppliChem, Darmstadt
Glycerine	Carl Roth, Karlsruhe
Glycine	AppliChem, Darmstadt
Halt™ Protease Inhibitor Single-Use Cocktail	Thermo Fisher Scientific, Dreieich
Hydrogen chloride (HCl)	AppliChem, Darmstadt
Hydroxylamine	Sigma-Aldrich, Munich
Isopropanol	Sigma-Aldrich, Munich
jetPRIME Transfection Reagent	Polyplus-transfection SA, Illkirch-Graffenstaden, France
Kanamycin	Carl Roth, Karlsruhe
LB medium	Carl Roth, Karlsruhe
LB agar	Carl Roth, Karlsruhe
LysC	Fujifilm Wako Chemicals, Osaka, Japan
Methylene blue C.I. 52015	AppliChem, Darmstadt
$MgCl_2$	Sigma-Aldrich, Munich
Milk powder	Carl Roth, Karlsruhe
Nonidet P-40	AppliChem, Darmstadt
Non-reducing Lane Marker, Sample Buffer	Thermo Fisher Scientific, Dreieich
Opti-MEM I	Thermo Fisher Scientific, Dreieich
Penicillin 10.000 Units, Streptomycin 10 mg/ml (P/S)	Sigma-Aldrich, Munich
peqGREEN DNA/RNA Dye	PEQLab Biotechnologie, Erlangen
PhosSTOP phosphatase inhibitor	Roche Diagnostics, Mannheim
Pierce® ECL, Western Blotting Substrate	Thermo Fisher Scientific, Dreieich
Polyethylenimine, Linear, Transfection Grade (PEI 25K)	Polysciences, Inc., Warrington, USA
Ponceau S	AppliChem, Darmstadt
Propidium iodide	Thermo Fisher Scientific, Dreieich
ReproSil-Pur Basic 1.9 μm C18 particles	Dr. Maisch HPLC GmbH, Ammerbuch
RNAse/DNase-free water	Thermo Fisher Scientific, Dreieich

Roti-Fect PLUS	Carl Roth, Karlsruhe
Rotiphoresis gel 30	Carl Roth, Karlsruhe
Roswell Park Memorial Institute (RPMI)-1640 medium	Thermo Fisher Scientific, Dreieich
Rubidium chloride	Sigma-Aldrich, Munich
SepPak C18 column	Waters, Milford, Massachusetts, USA
Silicon for cloning cylinders	Momentive performance materials, Albany, NY, USA
Sodium hydroxide (NaOH)	Sigma-Aldrich, Munich
Sodium chloride (NaCl)	Sigma-Aldrich, Munich
Sodium dodecylsulfate (SDS) pellets	Carl Roth, Karlsruhe
Sodium dodecylsulfate (SDS) 20% solution	AppliChem, Darmstadt
Sodium fluoride	Sigma-Aldrich, Munich
Sodium orthovanadate	Sigma-Aldrich, Munich
TCEP	Thermo Fisher Scientific, Dreieich
Tetramethylethylenediamin (TEMED)	Carl Roth, Karlsruhe
Tandem Mass Tag (TMT) reagent	Thermo Fisher Scientific, Dreieich
Trichloroacetic acid (TCA)	AppliChem, Darmstadt
Trifluoroacetic acid (TFA)	Sigma-Aldrich, Munich
Trypan Blue Stain 0.4%	Thermo Fisher Scientific, Dreieich
Trypsin/Ethylene diamine tetraacetic acid (EDTA, 0.25%)	Thermo Fisher Scientific, Dreieich
Trypsin	Promega, Madison, WI, USA
Tween® 20	AppliChem, Darmstadt
Tris hydroxymethyl aminomethane (Tris)	Carl Roth, Karlsruhe
Triton X-100	AppliChem, Darmstadt
Urea	Carl Roth, Karlsruhe
Vectashield® Mounting Medium	Vector, Burlingame, CA, USA
WesternSure® PREMIUM Chemiluminescent Substrate	LI-COR, Lincoln, NE, USA

3.1.4. Solutions and buffers

Agarose gel electrophoresis

DNA loading dye Blue Run (5x)

1.25 ml	1 M Tris/HCl, pH 7.0
15 ml	0.5 M EDTA
25 mg	Bromophenol blue
12.5 ml	Glycerine

adjust volume to 50 ml with distilled water

Tris acetate EDTA (TAE) buffer (50x)

242 g	Tris (in 500 ml distilled water)
100 ml	0.5 M Na_2EDTA, pH 8.0
57.1 ml	glacial acetic acid

adjust volume to 1 l with distilled water

Growth media for bacteria

LB agar plates

35 g	LB agar

adjust volume to 1 l with distilled water

LB medium

20 g	LB medium

adjust volume to 1 l with distilled water

Immunostaining

Blocking/antibody dilution solution	5% BSA in PBS
DAPI staining solution	1000 ng/ml in PBS
Fixing/permeabilisation solution	3.7% Formaldehyde/0.25% Triton X-100 in PBS

Preparation of competent *Escherichia coli (E. coli)*

MOPS I solution

10 ml	0.5 M MOPS
5 ml	0.1 M RbCl

adjust volume to 50 ml with distilled water and pH to 7.0 with 1 M NaOH.

MOPS II solution

10 ml	0.5 M MOPS
5 ml	0.1 M RbCl
5 ml	0.7 M $CaCl_2$

adjust volume to 50 ml with distilled water and pH to 6.5 with 1 M NaOH

SDS-PAGE and immunoblotting

1 M Tris HCl, pH 6.8

60.6 g	Tris

dissolve in 450 ml distilled water

adjust volume to 500 ml with distilled water and pH to 6.8 with HCl

1 M Tris HCl, pH 8.8

121.2 g	Tris

dissolve in 900 ml distilled water

adjust volume to 1000 ml with distilled water and pH to 8.8 with HCl

Antibody diluent (5% BSA)

0.5 g	BSA

adjust volume to 10 ml with TBS-T

IP lysis buffer (1x)

2 ml	1 M Tris, pH 8.2
15 ml	1 M NaCl
1 ml	Triton X-100

adjust volume to 100 ml distilled water

Milk powder solution (5% Milk Powder)

0.5 g	milk powder

adjust volume to 10 ml with TBS-T

Ponceau solution

0.5 g	Ponceau S
37.5 ml	TCA

adjust volume to 250 ml with distilled water

Radio-immunoprecipitation assay (Pandey et al., 2015) buffer (10x)

1.752 g	NaCl
2 ml	Nonidet P-40
1 g	DCA
1 ml	SDS (20% solution)
6.67 ml	1.5 M Tris, pH 8.0

adjust volume to 20 ml distilled water

Reducing electrophoresis buffer (6x)

25 ml	Glycerine
4.63 g	DTT
5.14 g	SDS pellet
17.5 ml	1 M Tris/HCl, pH 6.8
0.25 mg	Bromophenol blue

adjust volume to 50 ml with distilled water

SDS electrophoresis buffer (10x)

30.3 g	Tris
144 g	Glycine
10 g	SDS pellets

adjust volume to 1 l with distilled water

Tris-buffered saline (TBS, 10x), pH 7.5

87.7 g	NaCl
12.1 g	Tris

dissolve in 900 ml distilled water

adjust volume to 1000 ml with distilled water and pH to 7.5 with HCl

TBS-Tween 20 (TBS-T)

100 ml	TBS (10x)
1 ml	Tween 20

adjust volume to 1 l with distilled water

3.1.5. Plasmids, Oligonucleotides, siRNAs and Antibodies

Table 1. Characteristics of plasmids used for site-directed mutagenesis and cellular transfection assays.

Plasmid	Description	Reference
pEYFP-N1	MCS at N-terminus of EYFP tag	Clontech
pEYFP-C1	MCS at C-terminus of EYFP tag	Clontech
pECFP-N1	MCS at N-terminus of ECFP tag	Clontech
pECFP-C1	MCS at C-terminus of ECFP tag	Clontech
pECFP-EYFP	ECFP and EYFP fusion construct	Kind gift from Prof. Dr. Michael Schindler – University Hospital Tubingen (Banning et al., 2010)
pEYFP-Survivin-N1	Survivin at N-terminus of EYFP tag	Provided by Melanie Hoffmann – Master study - University Hospital Frankfurt (Hoffmann, 2017)
pEYFP-Survivin-C1	Survivin at C-terminus of EYFP tag	Provided by Melanie Hoffmann – Master study - University Hospital Frankfurt (Hoffmann, 2017)
pECFP-Survivin-N1	Survivin at N-terminus of ECFP tag	Provided by Melanie Hoffmann – Master study - University Hospital Frankfurt (Hoffmann, 2017)
pECFP-Survivin-C1	Survivin at C-terminus of ECFP tag	Provided by Melanie Hoffmann – Master study - University Hospital Frankfurt (Hoffmann, 2017)
pEYFP-Survivin S20A-N1	S20A mutated Survivin at N-terminus of EYFP tag	Generated in this study
pEYFP-Survivin S20D-N1	S20D mutated Survivin at N-terminus of EYFP tag	Generated in this study
pEYFP-Survivin W25A-N1	W25A mutated Survivin at N-terminus of EYFP tag	Generated in this study
pEYFP-Survivin F27A-N1	F27A mutated Survivin at N-terminus of EYFP tag	Generated in this study
pEYFP-Survivin L28A-N1	L28A mutated Survivin at N-terminus of EYFP tag	Generated in this study
pEYFP-Survivin E29A-N1	E29A mutated Survivin at N-terminus of EYFP tag	Generated in this study
pEYFP-Survivin C31A-N1	C31A mutated Survivin at N-terminus of EYFP tag	Generated in this study
pEYFP-Survivin T34A-N1	T34A mutated Survivin at N-terminus of EYFP tag	Generated in this study
pEYFP-Survivin T34D-N1	T34D mutated Survivin at N-terminus of EYFP tag	Generated in this study
pEYFP-Survivin D53A-N1	D53A mutated Survivin at N-terminus of EYFP tag	Generated in this study
pEYFP-Survivin W67A-N1	W67A mutated Survivin at N-terminus of EYFP tag	Generated in this study

pEYFP-Survivin E76A-N1	E76A mutated Survivin at N-terminus of EYFP tag	Generated in this study
pEYFP-Survivin K79A-N1	K79A mutated Survivin at N-terminus of EYFP tag	Generated in this study
pEYFP-Survivin T117A-N1	T117A mutated Survivin at N-terminus of EYFP tag	Generated in this study
pEYFP-Survivin T117D-N1	T117D mutated Survivin at N-terminus of EYFP tag	Generated in this study
pEYFP-Survivin S20D-W67A-N1	S20D and W67A mutated Survivin at N-terminus of EYFP tag	Generated in this study
pEYFP-Survivin S20D-C31A-D53A-N1	S20D, C31A, and D53A mutated Survivin at N-terminus of EYFP tag	Generated in this study
pEYFP-Survivin C31A-D53A-N1	C31A and D53A mutated Survivin at N-terminus of EYFP tag	Generated in this study
pEYFP-Survivin C31A-D53A-W67A-N1	C31A, D53A, and W67A mutated Survivin at N-terminus of EYFP tag	Generated in this study
pEYFP-Survivin ΔBIR-N1	BIR domain deleted Survivin at N-terminus of EYFP tag	Generated in this study
pEYFP-PI3K-N1	PI3K domain of DNA-PKcs at N-terminus of EYFP tag	Provided by Melanie Hoffmann – Master study - University Hospital Frankfurt (Hoffmann, 2017)
pEYFP-PI3K-C1	PI3K domain of DNA-PKcs at C-terminus of EYFP tag	Provided by Melanie Hoffmann – Master study - University Hospital Frankfurt (Hoffmann, 2017)
pECFP-PI3K-N1	PI3K domain of DNA-PKcs at N-terminus of ECFP tag	Provided by Melanie Hoffmann – Master study - University Hospital Frankfurt (Hoffmann, 2017)
pECFP-PI3K-C1	PI3K domain of DNA-PKcs at C-terminus of ECFP tag	Provided by Melanie Hoffmann – Master study - University Hospital Frankfurt (Hoffmann, 2017)
pEYFP-HEAT1-N1	HEAT1 repeat of DNA-PKcs at N-terminus of EYFP tag	Provided by Melanie Hoffmann – Master study - University Hospital Frankfurt (Hoffmann, 2017)
pEYFP-FATC-N1	FATC domain of DNA-PKcs at N-terminus of EYFP tag	Provided by Melanie Hoffmann – Master study - University Hospital Frankfurt (Hoffmann, 2017)
pEYFP-PI3K-ATM-N1	PI3K domain of ATM at N-terminus of EYFP tag	Provided by Melanie Hoffmann – Master study - University Hospital Frankfurt (Hoffmann, 2017)
p3xFlag-CMV10-Survivin	Survivin at C-terminus of 3xFlag tag	Sigma Aldrich - Generated in this study by inserting the Survivin to EcoRI/KpnI restriction sites
p3xFlag-CMV14-PI3K	PI3K domain of DNA-PKcs at N-terminus of 3xFlag tag	Sigma Aldrich - Generated in this study by inserting the PI3K to EcoRI/KpnI restriction sites

pEGFP-N1	MCS at N-terminus of EGFP tag (contains neomycin/kanamycin resistance gene)	Clontech
pEGFP-Survivin-N1	Survivin at N-terminus of EGFP tag (contains neomycin/kanamycin resistance gene)	Provided by Chrysi Petraki – Doctorate study (Petraki, 2014) / Dr. Stephanie Hehlgans - University Hospital Frankfurt
pEGFP-Survivin S20D-N1	S20D mutated Survivin at N-terminus of EGFP tag (contains neomycin/kanamycin resistance gene)	Provided by Chrysi Petraki – Doctorate study (Petraki, 2014) / Dr. Stephanie Hehlgans - University Hospital Frankfurt
pEGFP-Survivin W67A-N1	W67A mutated Survivin at N-terminus of EGFP tag (contains neomycin/kanamycin resistance gene)	Generated in this study
pEGFP-Survivin S20D-W67A-N1	S20D and W67A mutated Survivin at N-terminus of EGFP tag (contains neomycin/kanamycin resistance gene)	Generated in this study
pEGFP-Survivin ΔBIR-N1	BIR domain deleted Survivin at N-terminus of EGFP tag (contains neomycin/kanamycin resistance gene)	Provided by Chrysi Petraki – Doctorate study (Petraki, 2014) / Dr. Stephanie Hehlgans - University Hospital Frankfurt

Table 2. Characteristics of oligonucleotides used for cloning and site-directed mutagenesis.

Oligo	Sequence (5' → 3')	Tm (°C)	Manufacturer
S20A-Fw	tcaaggaccaccgcatcgctacattcaagaactgg	79.27	Eurofins Genomics, Ebersberg
S20A-Rev	ccagttcttgaatgtagcgatgcggtggtccttga	79.27	Eurofins Genomics, Ebersberg
S20D-Fw	ctcaaggaccaccgcatcgatacattcaagaactggcc	78.97	Eurofins Genomics, Ebersberg
S20D-Rev	ggccagttcttgaatgtatcgatgcggtggtccttgag	78.97	Eurofins Genomics, Ebersberg
W25A-Fw	atctctacattcaagaacgccccttcttggagggctgc	74.7	Eurofins Genomics, Ebersberg
W25A-Rev	gcagccctccaagaaggggcgttcttgaatgtagagat	74.7	Eurofins Genomics, Ebersberg
F27A-Fw	attcaagaactggcccgccttggagggctgcg	74.6	Eurofins Genomics, Ebersberg
F27A-Rev	cgcagccctccaaggcgggccagttcttgaat	74.6	Eurofins Genomics, Ebersberg
L28A-Fw	attcaagaactggcccttcgccgagggctgcgcctgca	78.1	Eurofins Genomics, Ebersberg
L28A-Rev	tgcaggcgcagccctcggcgaagggccagttcttgaat	78.1	Eurofins Genomics, Ebersberg
E29A-Fw	aagaactggcccttcttggccggctgcgcctgca	76.7	Eurofins Genomics, Ebersberg
E29A-Rev	tgcaggcgcagccggccaagaagggccagttctt	76.7	Eurofins Genomics, Ebersberg
C31A-Fw	ttcttggagggcgccgcctgcaccccgga	76.6	Eurofins Genomics, Ebersberg
C31A-Rev	tccggggtgcaggcggcgccctccaagaa	76.6	Eurofins Genomics, Ebersberg
T34A-Fw	gctgcgcctgcgccccggagcgg	81.67	Eurofins Genomics, Ebersberg
T34A-Rev	ccgctccggggcgcaggcgcagc	81.67	Eurofins Genomics, Ebersberg
T34D-Fw	gggctgcgcctgcgacccggagcggatg	81	Eurofins Genomics, Ebersberg

T34D-Rev	catccgctccgggtcgcaggcgcagccc	81	Eurofins Genomics, Ebersberg
D53A-Fw	actgagaacgagccagccttggcccagtgtttctt	73	Eurofins Genomics, Ebersberg
D53A-Rev	aagaaacactgggccaaggctggctcgttctcagt	73	Eurofins Genomics, Ebersberg
W67A-Fw	ttcaaggagctggaaggcgccgagccagatgacga	75.3	Eurofins Genomics, Ebersberg
W67A-Rev	tcgtcatctggctcggcgccttccagctccttgaa	75.3	Eurofins Genomics, Ebersberg
E76A-Fw	atgacgaccccatagaggcccataaaaagcattcgtcc	72.7	Eurofins Genomics, Ebersberg
E76A-Rev	ggacgaatgctttttatgggcctctatggggtcgtcat	72.7	Eurofins Genomics, Ebersberg
K79A-Fw	cccatagaggaacataaagcccattcgtccggttgcgcttt	74.4	Eurofins Genomics, Ebersberg
K79A-Rev	aaagcgcaaccggacgaatgggctttatgttcctctatggg	74.4	Eurofins Genomics, Ebersberg
T117A-Fw	gccaagaacaaaattgcaaaggaagccaacaataagaagaaagaat	78.02	Eurofins Genomics, Ebersberg
T117A-Rev	attctttcttcttattgttggcttcctttgcaattttgttcttggc	78.02	Eurofins Genomics, Ebersberg
T117D-Fw	gagccaagaacaaaattgcaaaggaagacaacaataagaagaaagaatttgagg	78.96	Eurofins Genomics, Ebersberg
T117D-Rev	cctcaaattctttcttcttattgttgtcttcctttgcaattttgttcttggctc	78.96	Eurofins Genomics, Ebersberg
HEAT1-Fw	cggaattcggcggcatggcgggctccggagccggt	74.3	Eurofins Genomics, Ebersberg
HEAT1-Rev	ggggtaccgtgtttataaccttgcacggtcc	70.8	Eurofins Genomics, Ebersberg
FATC-Fw	cggaattcggcggcatgctgaaaaaaggagggtcatgg	74.9	Eurofins Genomics, Ebersberg
FATC-Rev	ggggtaccgtcatccagggctcccatcct	73.7	Eurofins Genomics, Ebersberg
PI3K-Fw	cggaattcggcggcatggaacacccttttcctggtgaag	75.9	Eurofins Genomics, Ebersberg
PI3K-Rev	ggggtaccgtatttttccaatcaaaggagggc	69.5	Eurofins Genomics, Ebersberg
PI3K-ATM-Fw	cggaattcggcggcatggtggaccacacaggagaat	75.2	Eurofins Genomics, Ebersberg
PI3K-ATM-Rev	ggggtaccgtcctctgctgtaaatacaaagct	69.5	Eurofins Genomics, Ebersberg
Surv-Fw	ggggtaccggcggcatgggtgccccgacgttgc	80.7	Eurofins Genomics, Ebersberg
Surv-Rev	cgggatcccgatccatggcagccagctgctc	76.1	Eurofins Genomics, Ebersberg
ΔBIR-Fw1	catgggtgccccgacgttgccccctgcctggcagccctttctct	82.5	Eurofins Genomics, Ebersberg
ΔBIR-Rev1	ctagagagaaagggctgccaggcaggggggcaacgtcgggcacccatggtac	83.6	Eurofins Genomics, Ebersberg
ΔBIR-Fw2	gctctagatctgtcaagaagcagtttgaaga	65.5	Eurofins Genomics, Ebersberg
ΔBIR-Rev2	cgggatcccgatccatggcagccagctgctc	76.1	Eurofins Genomics, Ebersberg

Table 3. Characteristics of sequencing primers for confirmation of mutations/deletions.

Oligo	Sequence (5' → 3')	Tm (^{o}C)	Manufacturer
pEGFPC1for	gatcactctcggcatggac	58.8	Eurofins Genomics, Ebersberg
pEGFPC1rev	cattttatgtttcaggttcaggg	57.1	Eurofins Genomics, Ebersberg
CMVfor	cgcaaatgggcggtaggcgtg	65.7	Eurofins Genomics, Ebersberg
pEGFPN1rev	gtccagctcgaccaggatg	61	Eurofins Genomics, Ebersberg

Table 4. Characteristics of siRNAs used for control or knockdown of endogenous Survivin expression.

siRNA	Sequence (5' → 3')	Manufacturer	Catalog number
AllStars Neg. Control siRNA (20 nmol)	-	QIAGEN, Hilden	1027281
BIRC5 Survivin 3 siRNA	Sense: GCAGGUUCCUUAUCUGUCAtt Antisense: UGACAGAUAAGGAACCUGCag	Ambion, Austin, TX, USA	s1458

Table 5. Characteristics of primary antibodies used for immunoblotting, immunoprecipitation and immunofluorescence staining.

Target	Host	Type	Stock solution [μg/ml]	Dilution	Molecular weight [kDa]	Manufacturer	Catalog number
Anti-β-Actin	mouse	IgG	1000	1:10 000	42	Sigma-Aldrich	A5441
Anti-Survivin	rabbit	IgG	200	1:1000	16.5	R&D Systems	AF886
Anti-phospho-H2AX (Ser139)	mouse	IgG1	1000	1:1000	17	Millipore	05-636
Anti-53BP1	rabbit	IgG	1	1:1000	250	Novus Biologicals	NB100-304
Anti-FOXO3	rabbit	IgG	15	1:1000	82-97	Cell Signaling	2497S
Anti-phospho-FOXO3 (Ser253)	rabbit	IgG	908	1:500	97	Cell Signaling	9466S
Anti-GFP	rabbit	IgG	2000	1:2000	27	Abcam	ab290
Anti-FLAG	rabbit	IgG	84	1:1000	1	Cell Signaling	2368S
Anti-FLAG (HRP)	mouse	IgG1	1100	1:1000	1	Abcam	ab49763
Anti-DNA-PKcs	mouse	IgG	200	1:500	470	Thermo	MS-370-P1
Isotype control	rabbit	IgG	400	1:100	-	Santa Cruz Biotechnology	SC-2027
Isotype control	mouse	IgG	400	1:100	-	Santa Cruz Biotechnology	SC-2025

Table 6. Characteristics of secondary antibodies used for immunofluorescence staining.

Target	Host	Type	Dilution	Label	Manufacturer	Catalog number
Anti-rabbit	goat	IgG	1:500	Alexa Fluor^{R} 488	Life technologies	A11034
Anti-mouse	goat	IgG	1:500	Alexa Fluor^{R} 594	Life technologies	A11032

Table 7. Characteristics of secondary antibodies used for immunoblotting.

Coupled enzyme	Specificity	Host	Type	Dilution	Manufacturer	Catalog number
Horse radish peroxidase	rabbit	goat	IgG	1:1000	Southern Biotech	4050-05
Horse radish peroxidase	mouse	goat	IgG	1:1000	Southern Biotech	1030-05

3.1.6. Commercial kits

Description	Manufacturer
High-Select™ Fe-NTA Phosphopeptide Enrichment Kit	Thermo Fisher Scientific, Dreieich
Micro BCA™ Protein Assay Kit	Thermo Fisher Scientific, Dreieich
NucleoBond® Xtra Midi Plus EF	Macherey-Nagel, Dueren
NucleoSpin® Plasmid Kit	Macherey-Nagel, Dueren
NucleoSpin® Gel and PCR Clean-Up Kit	Macherey-Nagel, Dueren
NucleoSpin® RNA	Macherey-Nagel, Dueren
Pierce™ BCA™ Protein-Assay, (RAC)	Thermo Fisher Scientific, Dreieich
Pierce™ High pH Reversed-Phase Peptide Fractionation Kit	Thermo Fisher Scientific, Dreieich
PCR Mycoplasma Test Kit	AppliChem, Darmstadt
SignaTECT® DNA-Dependent Protein Kinase Assay	Promega, Madison, WI, USA

3.1.7. Enzymes and respective buffers

Description	Manufacturer
PfuUltra High-Fidelity DNA Polymerase	Strategene, La Jolla, CA, USA
PfuUltra HF Reaction Buffer (10x)	Strategene, La Jolla, CA, USA
DNA-dependent protein kinase (DNA-PK) 199 U/μl	Promega, Madison, WI, USA
T4 DNA Ligase	New England Biolabs, Frankfurt
T4 DNA Ligase Buffer (10x)	New England Biolabs, Frankfurt
ApaLI, 10 U/μl	New England Biolabs, Frankfurt
NEB Buffer 10x	New England Biolabs, Frankfurt
EcoRI 10 U/μl	New England Biolabs, Frankfurt
HindIII 10 U/μl	New England Biolabs, Frankfurt
KpnI 10 U/μl	New England Biolabs, Frankfurt
BamHI 10 U/μl	New England Biolabs, Frankfurt

3.1.8. Electrophoresis markers

Description	Manufacturer
ProSieve QuadColor Protein Marker	Lonza, Cologne
GelPilot 1kb Plus Ladder	QIAGEN, Hilden

3.1.9. Cells

Bacteria

Escherichia coli (*E. coli*) DH5α (Promega, Madison, WI, USA) were used for all site-directed mutagenesis and cloning procedures.

Human cell lines

SW480: The SW480 cell line was established from a primary adenocarcinoma of the colon by A. Leibovitz in the 1970s (Leibovitz et al., 1976). It has two p53 mutations, a G/A mutation at codon 273 and a C/T mutation at codon 309. The cells were cultured in DMEM supplemented with 10% FBS, 50 U/ml penicillin, 50 μg/ml streptomycin and 1000 μg/ml G418 (for stably transfected cells) at 37 °C in a humidified atmosphere containing 5% CO_2. The cells were obtained from the American Type Culture Collection (ATCC, Promochem, Germany).

DLD-1: DLD-1 cell line was established from colorectal adenocarcinoma by D.L. Dexter and colleagues during a period from 1977-1979 (Dexter et al., 1979). It is positive for p53 antigen expression by having a C -> T mutation resulting in Ser -> Phe at position 241. The cells were cultured in DMEM supplemented with 10% FBS, 50 U/ml penicillin, 50 μg/ml streptomycin and 1000 μg/ml G418 (for stably transfected cells) at 37 °C in a humidified atmosphere containing 5% CO_2. The cells were obtained from the American Type Culture Collection (ATCC, Promochem, Germany).

HCT-15: HCT-15 cell line like DLD-1 was established from colorectal adenocarcinoma by D.L. Dexter and colleagues during a period from 1977-1979 (Dexter et al., 1979). DNA fingerprinting evidence indicates that this line and DLD-1 are derived from the same individual; however, isoenzymology and cytogenetic data are not same. The cells were cultured in RPMI supplemented with 10% FBS, 50 U/ml penicillin, and 50 μg/ml streptomycin at 37 °C in a humidified atmosphere containing 5% CO_2. The cells were obtained from the American Type Culture Collection (ATCC, Promochem, Germany).

3.2. Methods

3.2.1. Cell Culture

SW480 and DLD-1 cells were cultured in Dulbecco's Modified Eagle Medium (DMEM; Invitrogen, Karlsruhe, Germany) containing glutamax-I (L-alanyl-L-glutamine) while HCT-15 cells were maintained in Roswell Park Memorial Institute (RPMI) 1640 Medium, both supplemented with 10% fetal bovine serum (FBS), 50 U/ml penicillin and 50 μg/ml streptomycin at 37 °C in a humidified atmosphere containing 5% CO_2.

For freezing, cells resuspended in precooled cryomedium (DMEM/RPMI + 20% FBS + 5% DMSO) and transferred into a cryotube, followed by storage in a freezing container at -80 °C for gradient cool-down. Three days later, the cryotube was transferred into storage boxes and kept at -80 °C. For thawing, cells were resuspended in prewarmed medium, followed by centrifugation (100 x g, 3 min, RT); then resuspended in 12 ml fresh medium and plated on a T-75 flask.

3.2.2. Transfection

Many cell lines exhibit different transfection efficiencies in response to the usage of different transfection reagents. For that reason, Polyethylenimidine (PEI) and Roti-Fect PLUS transfection reagents were used for SW480 colorectal cancer cells, JetPRIME transfection reagent for DLD-1 and HCT-15 colorectal cancer cells and Roti-Fect PLUS transfection reagent for all knockdown experiments.

PEI procedure (for 6-well plate): 2 μg plasmid DNA (1 μg/μl) were mixed with 3 volume (6 μl) of PEI (1 μg/μl) in 500 μl medium without FBS (DMEM + 1% P/S) and incubated in the dark at room temperature for 20 min. After incubation, the transfection mix was added to 40-50% confluent SW480 colorectal cancer cells dropwise. After 24h incubation at 37 °C and 5% CO_2, medium was renewed with normal medium (DMEM + 10% FBS + 1% P/S) and incubated for another 24h at 37 °C and 5% CO_2. After incubation, cells were harvested.

Roti-Fect PLUS procedure (for 6-well plate): 2 μg plasmid DNA (1 μg/μl) was mixed with 123 μl of Opti-MEM. In a second tube 5 μl Roti-Fect PLUS was mixed with 120 μl Opti-MEM and incubated at room temperature for 5 min. After incubation, the content of the tubes was combined, mixed and incubated at room temperature for 20 min. Next, transfection mix was added to 40-50% confluent SW480 colorectal cancer cells dropwise and supplemented with 1ml Opti-MEM. After an 8h incubation at 37 °C and 5% CO_2, 1.25 ml of 20% FBS medium (Opti-MEM + 20% FBS) was added (to adjust to a final concentration of 10% FBS), and incubated for another 40h at 37 °C and 5% CO_2. For knockdown experiments, the procedure was highly similar with a minor exception: 2.5 μl of 20 nM siRNA was mixed with 122.5 μl of Opti-MEM instead of 2 μg plasmid DNA.

JetPRIME procedure (for 6-well plate): 2 μg plasmid DNA (1 μg/μl) was mixed with 200 μl of JetPRIME buffer, spinned down for 10s and incubated in the dark at room temperature for 5 min. Afterwards, 4 μl of JetPRIME transfection reagent was added, mixed, spinned down for 10s, and incubated in the dark at room temperature for 10 min. Then, transfection mix was

added to 40-50% confluent DLD-1 and HCT-15 colorectal cancer cells dropwise and supplemented with 1.8 ml medium (Opti-MEM + 10% FBS). After 48h incubation at 37 °C and 5% CO_2 cells were harvested.

3.2.3. Stable cell line generation

For stable transfection of SW480 and DLD-1 colorectal cancer cells, the constructs (pEGFP-N1, Survivin-EGFP, SurvivinΔBIR-EGFP, Survivin-S20D-EGFP, Survivin-W67A-EGFP and Survivin-S20D-W67A-EGFP) were linearized using 30 μg of plasmid DNA, 10 μl 10x NEBuffer, 4 μl ApaLI enzyme (10 U/μl), 1 μl BSA (100x) and volumes were adjusted to 100 μl with RNase/DNase-free water in 1.5 ml tubes. After incubation at 37 °C overnight, samples were subjected to agarose gel electrophoresis, the linearized plasmid was resected and subjected to Gel clean-up using the NucleoSpin® Gel and PCR Clean-Up Kit (Macherey-Nagel) following the manufacturer's instructions. SW480 and DLD-1 colorectal cancer cells with 50-60% confluency were then stably transfected with corresponding linearized vectors using JetPRIME transfection reagent followed by incubation for 24 h at 37 °C and 5% CO_2. The next day, cells were transferred to 100 mm petri dishes where colonies were allowed to grow. For the selection of transfected cells, the DMEM medium supplemented with 10% FBS and 1% P/S was supplemented with 1000 μg/ml G418 (Geneticin: Commonly used for neomycin resistance gene selection).

The fluorescence intensities of clones were visually checked with a fluorescence microscope, then silicon-embedded cloning cylinders were carefully placed on the selected colonies. Cells within the cloning cylinders were detached with 60 μl trypsin/EDTA, incubated for 5 min at 37 °C and 5% CO_2, resuspended with 60 μl medium (DMEM + 10% FBS + 1% P/S + 1000 μg/ml G418) and transferred into 12-well plates (one clone per well) along with 1 ml medium (DMEM + 10% FBS + 1% P/S + 1000 μg/ml G418). When cells were grown to a confluency of approximately 60-80% they were transferred to T-25 flasks and later (when 80-100% confluent) harvested for cryostocks. The corresponding protein expressions of clones were verified via flow cytometry, and ≥60% $EGFP^+$ clones further verified by immunoblotting (**Figure 18**).

3.2.4. Competent *E.coli* DH5α preparation and transformation

Preparation of competent *Escherichia coli (E. coli)* DH5α cells

For the preparation of competent *E. coli* DH5α, 5 ml LB medium were inoculated with a cryo stock of *E. coli* DH5α, followed by overnight incubation at 37 °C while shaking at 250 rpm. The following day, 400 μl of the overnight culture was transferred into 200 ml LB medium. Incubation at 37 °C while shaking at 250 rpm was continued until an optical density $(OD)_{600}$ of 0.2 was reached. The cells were then pelleted at 4100 x g and 4 °C for 10 min and resuspended in 20 ml MOPS I buffer. After 10 min incubation on ice, the cells were centrifuged again at 4100 x g and 4 °C for 10 min, followed by resuspension of the pellet in 20 ml MOPS II buffer. Due to the $CaCl_2$ in the MOPS buffer, membrane permeability is changed which leads to the possibility of DNA uptake through the membrane (Mandel and

Higa, 1970). After another incubation at 4 °C for 30 min and centrifugation at 4100 x g and 4 °C for 10 min, the pellet was resuspended in 2 ml MOPS II buffer and aliquoted into 200 µl portions in precooled 1.5 ml tubes containing 50 µl glycerine. After mixing carefully, the competent cells were snap-frozen in liquid nitrogen and stored at -80 °C.

Transformation

For the transformation of chemically competent *E. coli* DH5α cells with plasmids, 30 µl cells per transformation were thawed on ice and mixed with 10 ng plasmid DNA. In case of site-directed mutagenesis plasmids, 5 µl of the DpnI digested and ligated plasmid was used. DNA and cells were gently mixed and incubated on ice for 30-60 min, followed by a heat-shock for 45 sec at 42 °C in a water bath. Then, the transformation mix was immediately cooled on ice for 5 min. Afterwards, 500 µl sterile LB medium was added and cells were incubated in a shaker by 300 rpm for 1 h at 37 °C, followed by plating on LB-agar plates containing the appropriate antibiotics and incubated overnight at 37 °C.

3.2.5. Site-Directed Mutagenesis

Survivin single/multiple amino acid mutants were generated using the appropriate primers (**Table 2**) and the QuikChange II Site-Directed Mutagenesis Kit (Agilent Technologies, La Jolla, USA) following the manufacturer's instructions. Briefly, PCR was performed according to the components and procedure in **Table 8** and **Table 9**, followed by verification of amplification by agarose gel electrophoresis. Then, samples were subjected to DpnI restriction enzyme digestion for 1 h at 37 °C followed by overnight ligation at 16 °C. The next day, samples were transformed into E.coli DH5α competent cells, incubated overnight at 37 °C and plasmid isolation was performed by using NucleoSpin® Plasmid Kit (for large scale stocks NucleoBond® Xtra Midi Plus EF kit), following the manufacturer's instructions from individual clones. Plasmids were digested by appropriate restriction endonucleases and subjected to agarose gel electrophoresis which then were further confirmed by sequencing (Eurofins Genomics, Ebersberg) (**Figure 5**).

Table 8. Site-directed mutagenesis components of PCR reaction.

Component	Volume (µl)
ddH_2O	36.5
10X Reaction Buffer	5
Forward Primer (10 pmol)	2
Reverse Primer (10 pmol)	2
dNTPs mix (10 mM each)	2.5
Template (20 ng)	1
PfuUltra II HF Polymerase	1
Total	50

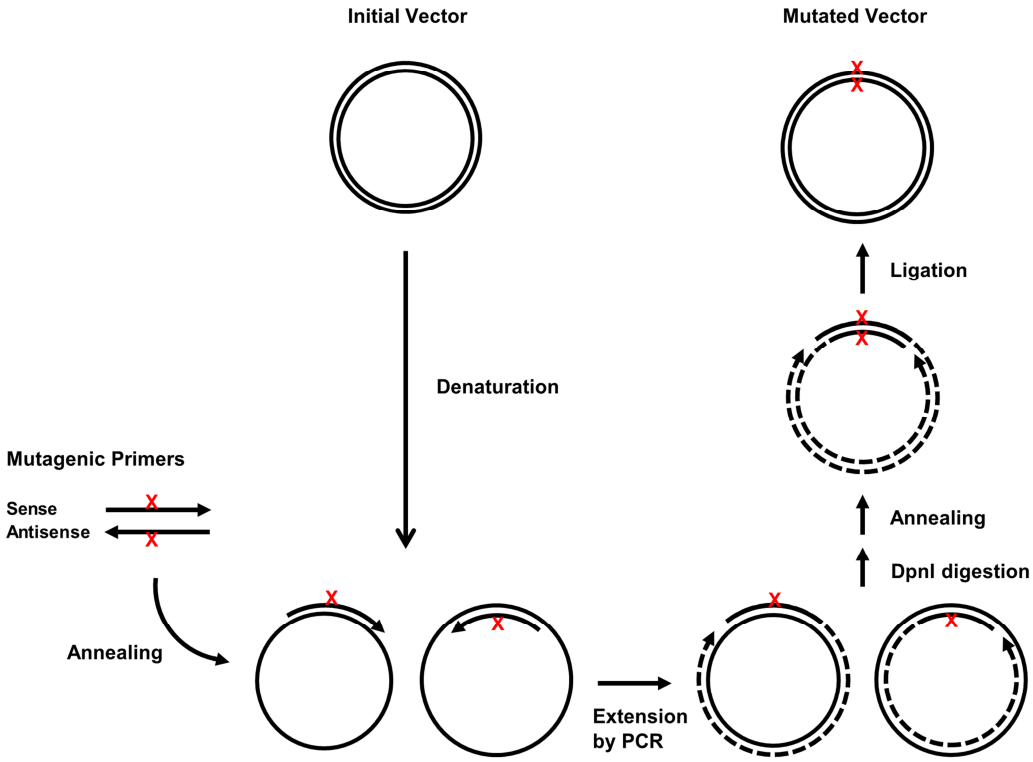

Figure 5.Brief workflow of the site-directed mutagenesis method. Sense and antisense mutagenic primers were designed and used for the PCR amplification of wild type vectors. After DpnI restriction endonuclease treatment, methylated input wild type templates were digested while amplified non-methylated mutant vectors not. Samples were further ligated with T4 Ligase on amplification end-nicks.

Table 9. Site-directed mutagenesis PCR protocol for plasmid DNA amplification with PfuUltra II HF. Annealing temperature and elongation time were adjusted according to primer melting temperature and length of the template, respectively.

Step	Temperature [°C]	Time [min:sec]	
Initial denaturation	95	0:30	1x
Denaturation	95	0:30	18x
Annealing	55	1:00	
Elongation	68	1:00/kb	
Final elongation	68	15:00	1x
-	4	∞	

Agarose gel electrophoresis

Agarose gels were prepared using 50-80 ml of a 0.8-2% agarose gel/TAE buffer solution, supplemented with 5-8 μl peqGREEN in order to visualize DNA. Before loading on the gel, DNA was mixed with an appropriate volume of DNA loading dye (5x). Gel electrophoresis was performed at 100-120 V for approximately 1 h. Thereafter, DNA was visualized using the Odyssey Fc Imaging System and Image Studio Version 5.2 Software. The size of the DNA was determined with the GelPilot 1kb Plus DNA ladder.

3.2.6. Preliminary Molecular Docking Analysis

The X-ray crystal structure of Survivin -PDB: 1E31- (Chantalat et al., 2000) and DNA-PKcs -PDB: 5LUQ- (Sibanda et al., 2017) were used as input for the molecular docking conducted in a preliminary approach. First, structures were pre-processed using the Protein Preparation Wizard (Sastry et al., 2013) in the Schrödinger Release 2018-1 (Schrödinger, LLC, New York, NY): In brief, missing/truncated hydrogen atoms, side chains, loops, cap-termini, disulfide bonds were re-created, all non-complexed ions and solvents were deleted and selenomethionines converted to methionines. The hydrogen bonding network was optimized and protonation states assigned at pH 7.0. Finally, a restrained minimization was performed using the OPLS3 force field (Harder et al., 2016). Prepared structures were docked by using PIPER (Kozakov et al., 2006) and PatchDOCK (Schneidman-Duhovny et al., 2005) programs. Top-ranked poses were post-processed and refined by FireDOCK (Mashiach et al., 2008). Then, interactions between residues were determined according to their binding energies by using PRIME MM-GBSA (Jacobson et al., 2004) in the Schrödinger Release 2018-1 and distances by Find Clashes/Contacts tool of Chimera 1.13.1 (Pettersen et al., 2004). Interaction pairs that have lower binding energy values and distances between backbones/side chains atoms lower than 5Å were qualified as potential interactors. *In silico* mutagenesis was performed by Rotamer tool of Chimera 1.13.1 (Pettersen et al., 2004) by using the Dunbrack Rotamer Library (Shapovalov and Dunbrack, 2011).

3.2.7. Large-scale Molecular Docking Analysis

Preparation and Refinement of DNA-PKcs head domain: The DNA-PKcs head domain (residues 2802 - 4128) model was extracted from the latest crystal structure of DNA-PKcs (PDB code: 5LUQ) (Sibanda et al., 2017). As parts of the structure are not resolved, the missing residues were modelled using the MODELLER software (Fiser et al., 2000; Marti-Renom et al., 2000; Sali and Blundell, 1993; Webb and Sali, 2016). In order to ensure that the structure is adequately folded, i.e., it is in a low-energy conformation, an MD simulation using Gromacs 2018 (Abraham et al., 2015) was performed. The AMBER14 force field (Maier et al., 2015) was used for the simulation. The head domain was simulated in a dodecahedron box with 150 mM NaCl. The minimum distance between the box edge and the system was set to 0.6 nm. TIP3P was used as a water model (Jorgensen et al., 1983). The energy minimization was performed using the steepest descent algorithm in 10,000 steps with a step size of 1 fs. The equilibration was conducted over 2.5 ns (2 fs step size). In order to achieve fast equilibration V-rescale for temperature coupling and a Berendsen thermostat for pressure coupling were chosen. The system was equilibrated to 300 K temperature and 1 bar pressure. The leapfrog algorithm was used for integration. The MD production run was simulated over 50 ns (2 fs step size) using a Nose-Hoover thermostat and a Parrinello-Rahman barostat. Again, the leapfrog integrator was used. The RMSD (orange) and radius of gyration (gray) are plotted for the whole trajectory. The RMSD initially exhibited upward rising movement but converged against a saturated trend after approximately 30 ns, and the radius of gyration was constant on average. So the structure seems stable, and no structural changes are observed that can be used for the following analyses (**Figure 6**).

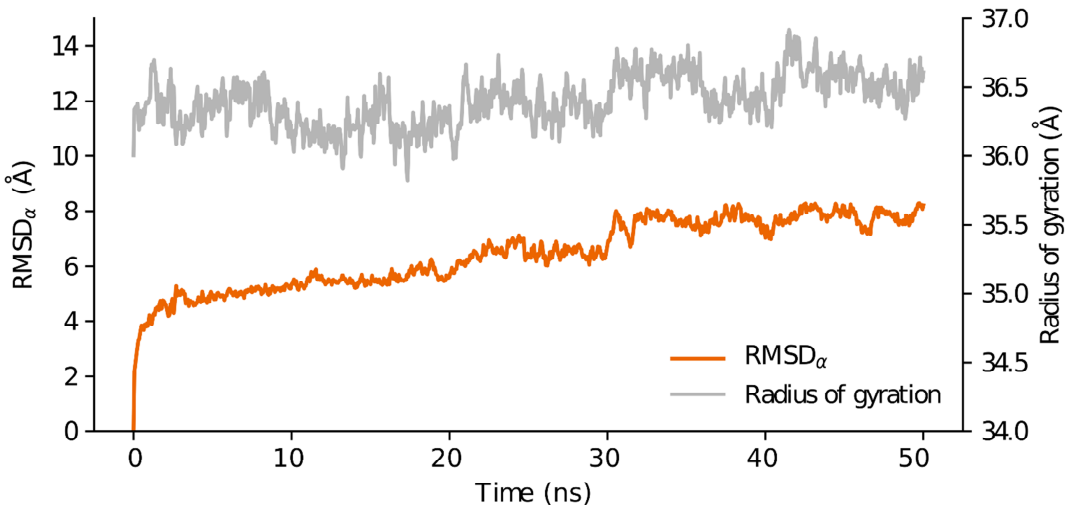

Figure 6.Initial molecular dynamics simulation of the head domain of DNA-PKcs. The simulation lasts over the course of 50 ns to verify the stability for the RMSD and the radius of gyration.

Large-scale Molecular Docking Analysis: For the *in silico* large-scale protein docking analysis, we used the latest crystal structures from the Protein Data Bank (PDB), PDB codes: 5LUQ for DNA-PKcs, and 1E31 for Survivin (Chantalat et al., 2000; Sibanda et al., 2017). The crystal structure for 5LUQ has some smaller regions where electron density could not be sufficiently resolved and has a larger missing region in what is known as the cradle domain (Sibanda et al., 2017). Refinement was performed using the Rosetta (Gray et al., 2003) and MODELLER (Fiser et al., 2000; Marti-Renom et al., 2000; Sali and Blundell, 1993; Webb and Sali, 2016). A 50 ns molecular dynamics simulation was performed to verify the refined subdomain of 5LUQ is stable within simulations. A detailed summary of the steps taken to refine the structure can be found in **Section 3.2.8**. Global molecular docking was performed using the head domain, where Survivin was docked in different poses covering the head domains' surface. For this approach, a global docking protocol from Rosetta was applied, where a coarse backbone based force field is used (Leaver-Fay et al., 2011). The generated 98884 poses were then used as input for the local docking protocol, which in contrast uses Rosetta all-atom energy function (Alford et al., 2017). The subsequent analysis regarding the proximity of BIR domain residues and the PI3K domains was done using custom python scripts and relies on the bioinformatics library Biotite (Kunzmann and Hamacher, 2018).

3.2.8. Molecular Dynamics Simulation

To analyze the stability and dynamics of the heterotetramer structure, molecular dynamics simulations were performed by employing Gromacs 2019.4 (Abraham et al., 2015) with the Charm36 force field (Vanommeslaeghe et al., 2010) and the Tip3P water model (Jorgensen et al., 1983). All simulations were performed inside a dodecahedron water box with periodic boundary conditions. The first step was energy minimization to remove potential clashes, followed by short equilibration in canonical (NVT) and isothermal-isobaric (NPT) ensembles for 100 ps, respectively. Finally, a 200 ns productive run was performed, which produces the trajectories used for analysis. Structural changes were measured by root mean square

deviation (RMSD) and radius of gyration (Rg) analyses: The trajectories were analyzed using the RMSD, which measures the positional deviation between simulation frame and reference structure to examine the stability of simulation. Furthermore, the Rg was used to measure the global protein changes.

$$RMSD = \sqrt{\frac{1}{N}\sum_{i=1}^{N}\left(r_i - r_{i,0}\right)^2}$$

$$R_g = \sqrt{\frac{\sum_i m_i |\vec{r_i}|^2}{\sum_i m_i}}$$

Finally, a unique and simple quantitative measurement strategy was generated and implemented for the opening and closing dynamics of the active site. Briefly, the base of a cylindrical reference volume was fitted to the outer surface of the PI3K active site. The measurement of opening and closing of the active site cavity was performed by counting the atoms which were inside the cylindrical reference volume during the molecular dynamics simulations. Scripts and raw data are available at https://github.com/entropybit/survivinpkcs and http://www.cbs.tu-darmstadt.de/SurvivinDnaPkcs.

Measuring active site opening/closing dynamics using a cylindrical probe: To measure the opening of the kinase active site, a cylindrical volume is fitted to the atoms defining the active site (**Figure 7**). Where the base is defined by the center of mass of the active site G3919 – V3930 residues´ atoms and the atoms of lysine (K)3586, aspartic acid (D)3661, leucine (L)3668, proline(P)3832, K3840 and glycine (G)4024 residues located around the entry to the active site. The center of mass of these atoms is used as the coordinate systems origin. Measuring whether an atom lies within the probe cylinder can easily be achieved by considering the cylindrical coordinate system defined by the probe cylinder. In this coordinate system, we have the following equation:

$$\begin{pmatrix} x \\ y \\ z \end{pmatrix} = \begin{pmatrix} \rho cos(\phi) \\ \rho sin(\phi) \\ z \end{pmatrix},$$

ρ is the radius measured from the cylinder's main axis and ϕ the angle around it. Using this equation, the following inequalities have to be checked:

$$\rho \leq R_p,$$

$$z \leq L_p,$$

R_p and L_p are the radius and length of the cylindrical probe. Counting the number of atoms fulfilling these conditions and normalizing by the probe´s volume gives the particle number density:

$$n(t) = \frac{\sum_{i=1}^{N_a}\left(\rho_i(t) \leq R_p\right) \cdot \left(z_i(t) \leq L_p\right)}{\rho_p \cdot L_p}$$

The unit is measured in $N/Å^3$, so the number of particles per volume. This is the density of particles *blocking* the active site accessibility.

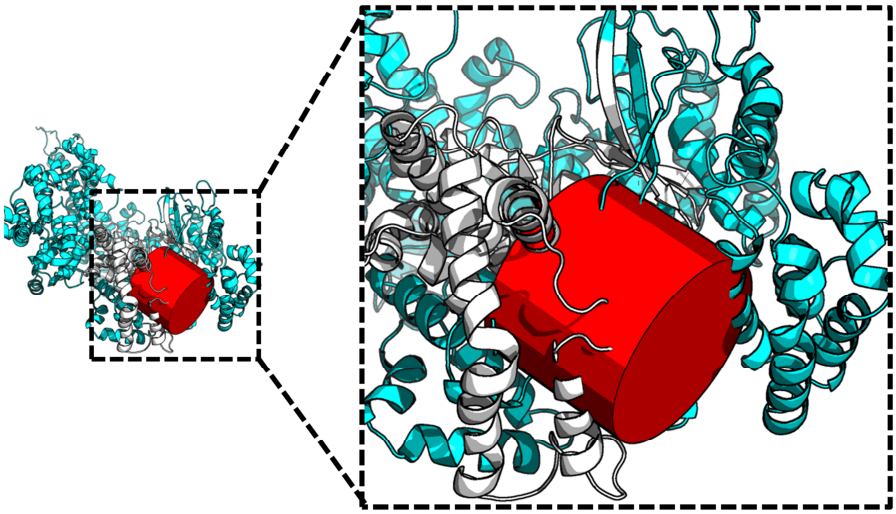

Figure 7.Illustration the fitting of cylindrical reference volume to the active site cavity. Exemplary depiction of the cylindrical reference volume (red) at the active site cavity of PI3K domain within the head domain (cyan) of DNA-PKcs.

3.2.9. Calculation of the molecular *in silico* attraction between catalytic PI3K domain of DNA-PKcs and BIR domain of Survivin

To analyze the interaction between the BIR domain and PI3K domain in the large-scale docking (98884 poses), the minimum distance between the docked Survivin and the whole PI3K region (d_{BIR}) was calculated by the following formula:

$$d_{BIR} = min\{|\vec{x} - \vec{y}|: x \in R_{PI3K}, y \in R_{BIR}\}$$

R_{PI3K} and R_{BIR} indicate the collection of atom coordinates from the PI3K domain and BIR domain of Survivin, respectively. The minimum distance between the related atoms provides a sensible distance measurement that examines whether and how effective these two domains interact with each other. The docking quality is described by increasingly negative Rosetta interface scores. This score is defined as the difference in Rosettas score for the structure with two docking poses together and separated by 100 Å, eventually mimicking no interaction (Gray et al., 2003).

3.2.10. Virtual drug screening analysis

The X-ray crystal structure of monomer Survivin -PDB: 2QFA- (Jeyaprakash et al., 2007) was used as input for the virtual drug screening analysis. Primarily, the structure was subjected to the Protein Preparation Wizard (Sastry et al., 2013) in the Schrödinger Release 2018-1 (Schrödinger, LLC, New York, NY) as mentioned in **Section 3.2.6**. To prepare the Survivin structure as a receptor, Receptor Grid Generation – Glide module of Schrödinger Release 2018-1 (Friesner et al., 2004; Friesner et al., 2006; Halgren et al., 2004) was employed by

setting the receptor enclosing box as the centroid of S20 and W67 residues. As input ligands, in total 7,919,071 drug/drug-like ligands from the repositories of Asinex (Gold&Platinium Collections – 263,557 ligands) (http://www.asinex.com/libraries-html/), ChemBridge (Core Library Stock – 2,238,050 ligands, Core Extended Library Stock – 943,422 ligands) (https://www.chembridge.com/screening_libraries/), Specs (ExAcD library release May 2018 - 474,042 ligands) (www.specs.net) and MolPort (4,000,000 ligands) (https://www.molport.com/shop/screeening-compound-database) were used. Further, the ligands were prepared by LigPrep – Glide module of Schrödinger Release 2018-1 (Friesner et al., 2004; Friesner et al., 2006; Halgren et al., 2004). Briefly, OPLS3 force field was used, and possible ionization states and tautomers were generated at pH 7.0 ± 2.0 with a desaltation step. Specific chiralities were retained for stereoisomer computation and maximal 32 stereoisomers were generated per ligand. Additionally, three low energy ring conformations were generated per ligand. Prepared receptor and ligands were further subjected to a global virtual screening approach by using the Virtual Screening Workflow – Glide module of Schrödinger Release 2018-1 (Friesner et al., 2004; Friesner et al., 2006; Halgren et al., 2004). Briefly, rapid ADME (absorption, distribution, metabolism, and excretion) properties of ligands were predicted by QikProp, followed by prefiltering by Lipinski rules (Molecular mass <500 Da, high lipophilicity LogP <5, hydrogen bond donors <5, hydrogen bond acceptors <10, molar refractivity in between 40-130) (Lipinski et al., 2001). Afterwards, prefiltered ligands were docked with receptors: Planarity of conjugated pi groups was enhanced and Epik state penalties were used for docking. Docking was performed in three steps: High-throughput Virtual Screening (HTVS), Standard Precision (SP), and Extra Precision (XP) with enhanced sampling and flexible docking configurations followed by post-docking minimization. Post-docking processing was performed by Prime MM-GBSA in the Schrödinger Release 2018-1 (Jacobson et al., 2004).

3.2.11. Irradiation procedure

Irradiation of cells with single photon doses ranging from 2 to 6 Gy was performed using a linear accelerator (Agility, ELEKTA, Crawley, UK) with 6 MeV/100 cm focus-surface distance and a dose rate of 4 Gy/min. Mock-irradiated cultures were kept at room temperature in the X-ray control room while the other samples were being irradiated.

3.2.12. FACS-FRET

Since the ground-breaking investigation and description of the Förster resonance energy transfer (FRET) by Theodor Förster, this method has been established of as a potential biosensor for macromolecular interactions in the cell and implemented into the solutions for many questions in the field of cell biology. FRET is a highly sensitive method based on the energy transfer from an excited donor fluorophore to the acceptor fluorophore in less than 10 nm distance, which provides a reasonable distance for potential macromolecule-macromolecule interactions. In addition, the emission spectrum of the donor fluorophore and the absorption spectrum of the acceptor fluorophore have to be overlapping (Clegg, 1995; Jares-Erijman and Jovin, 2003; Sun et al., 2013) (**Figure 8a**). With the technological advancements currently achieved, there are many donor and acceptor pair alternatives for

practical usage such as CFP-YFP, GFP-RFP, far-red fluorescence proteins (FFP), Infrared FPs (IFP), large stokes shift (LSS) FPs, Dark FPs, phototransformable (PT) FPs and multicolor systems (Bajar et al., 2016; Forster, 1946). Still, there are some major limitations and difficulties such as spectral overlaps for some donor and acceptors, artefact proneness, and microscopy-based analysis limit the evaluation of a large number of cells. To overcome these challenges, a non-invasive, sensitive, and quantitative method FACS-FRET (Flow cytometry-based FRET) has been adapted from Banning and co-workers. This method is easy to apply for many FRET experiments, allows analyzing the protein interactions in living cells, and well-controlled, standardized, reliable and quantitative assessments which overcomes many limitations in FRET and proteomics (Banning et al., 2010). In the experimental approaches used within this thesis, the FACS-FRET methodology was applied to ECFP-EYFP based fusion constructs with Survivin and different domains of DNA-PKcs. By this, SW480 colorectal cancer cells were transfected with plasmids (**Section 3.2.2**) and harvested 1 h after irradiation with 4 Gy, followed by the quantitative measurement by FACS (**Figure 8b**). FACS-FRET measurements were performed using a CytoFLEX S cytometer (Beckman Coulter) equipped with 405 nm, 488 nm and 638 nm lasers. To measure ECFP and FRET, cells were excited with the 405 nm laser and fluorescence was collected in the ECFP channel with a standard 450/45 filter, while the FRET-signal was measured with a 525/40 filter. To measure EYFP, cells were excited with the 488 nm laser, while emission was taken with a 525/40 filter. For each sample, we evaluated a minimum of one thousand ECFP/EYFP positive cells that fell within the background adjusted gate, as described previously (Banning et al., 2010). Analysis was performed with CytExpert software version 1.2.11.0.

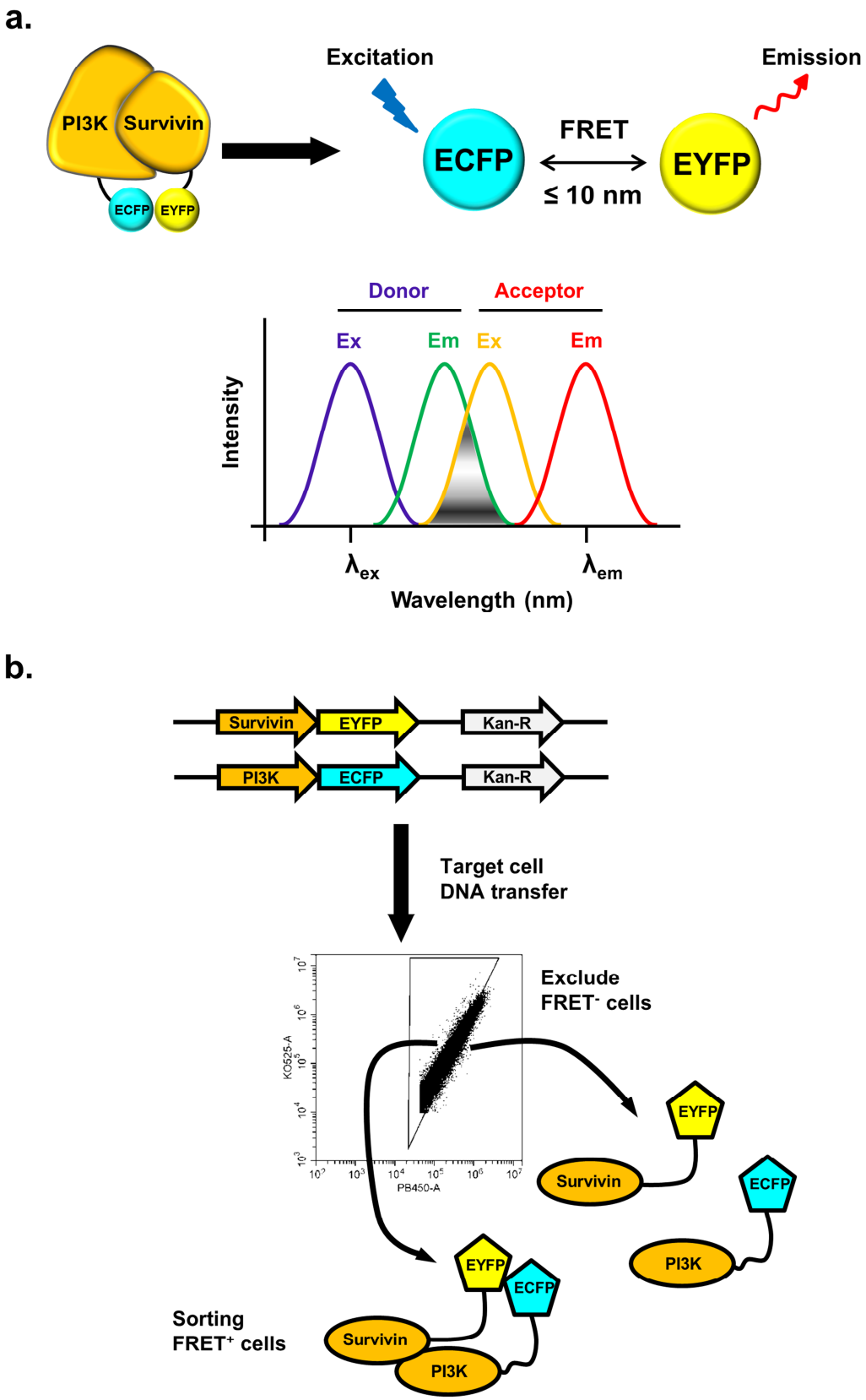

Figure 8. Overview of the FACS-FRET methodology. (**a**) Requirements for FRET: less than 10 nm proximity between the donor (ECFP) and acceptor (EYFP), and overlap of the spectra of donor emission and acceptor absorption. (**b**) Cells were co-transfected with Gene of interest (GOI)-Fusion protein constructs, 48 h later irradiated with 4 Gy, harvested and measured one hour after irradiation. Figures were modified from (Banning et al., 2010; Hoffmann, 2017).

3.2.13. 3D colony formation assay

Measurement of 3D cell survival was carried out as reported before (Eke et al., 2012; Hehlgans et al., 2018; Hehlgans et al., 2012). In brief, single cells were plated in 0.5 μg/μl laminin rich extracellular matrix; Cultrex 3D Culture Matrix BME Reduced Growth Factor Basement Membrane Extract PathClear; supplemented with medium (DMEM + 10% FBS + 1% penicillin/streptomycin) in 50 μl 1% agarose coated 96-well plates 24 h after siRNA transfection. Cells were irradiated (0, 2, 4, 6 Gy) 24 h thereafter and colonies (> 50 cells) were microscopically counted 7 days after plating. Experiments were performed in triplicates and at least three independent experiments were performed for each condition. Plating efficiencies were determined as numbers of colonies formed (0 Gy) / numbers of cells plated. Surviving fractions were calculated as numbers of colonies formed / (numbers of cells plated (irradiated) × plating efficiency (mock-irradiated)). Each point on survival curves represents the mean surviving fraction from at least three independent experiments. Survival variables α and β were fitted according to the linear quadratic equation ($SF = \exp\ [-\alpha \times D - \beta \times D^2]$ with D = dose using Microsoft Excel software ver. 2010 (Microsoft, Redmond, USA).

3.2.14. Co-Immunoprecipitation

Co-Immunoprecipitations were carried out using Dynabeads™ Protein G (#10004D ThermoFisher Scientific) and SW480 colorectal cancer cell lysates. The protocol was followed according to the manufacturer's instructions; beginning with the addition of 3 μg antibody: Anti-GFP (#ab290 Abcam), anti-Flag (#2368S Cell Signaling Technology), anti-DNA-PKcs (#MS-369-P1 ThermoFisher Scientific) or 3 μg of IgG (Mouse #SC-2025, Rabbit #SC-2027 Santa Cruz Biotechnology) and incubated in the rotating mixer at 5rpm overnight at 4°C to create the co-IP bead complex. SW480 colorectal cancer cells (40-50% confluency) were transfected with related vectors for 48 h and cell lysates prepared 1 h after single-dose 4 Gy irradiation. Densitometrically equal amount of lysates were added to the related antibody or IgG-Dynabead complexes and incubated in the rotating mixer at 5rpm overnight at 4°C. Beads were washed gently 5 times with 700 μl PBS followed the renewal of co-IP tubes to prevent non-specific binding and then the bound proteins were eluted by boiling; subsequently, the samples were electrophoresed (**Section 3.2.15**).

3.2.15. Protein extraction, SDS-PAGE and Immunoblotting

For cell lysis using radioimmunoprecipitation assay (RIPA) buffer (Pandey et al., 2015), cells were washed once with ice-cold PBS and scraped in RIPA buffer on ice 1 h after irradiation. The lysates were transferred to a precooled 1.5 ml tube and incubated on ice for 1 h, followed by centrifugation at 18000 x g for 15 min at 4 °C. The supernatant containing the proteins was then transferred into a new precooled 1.5 ml tube and stored at -80 °C.

For the cell lysis of immunoprecipitation experiments, IP lysis buffer (1x) was used. Cells were washed with ice-cold PBS, scraped in ice-cold PBS and transferred to a precooled 50 ml falcon tube. After centrifugation at 100 x g for 5 min at 4 °C, the pellet was resuspended in IP lysis buffer, followed by sonication three times for 1 min (in between 10s vortexing) and incubation on a rotator by 5rpm speed for 1 h at 4 °C. Then, the lysates were centrifuged at

18000 x g for 15 min at 4 °C and the supernatant containing the proteins was transferred into a precooled 1.5 ml tube. Concentrations of protein samples determined with Micro BCA™ Protein Assay Kit following the manufacturer's instructions then were subjected to densitometric immunobloting to determine the relative amounts of bait/prey proteins. Densitometrically equal amounts of proteins were subjected to co-IP assay (**Section 3.2.14**), and the rest of the lysate stored at -80 °C.

For immunoblotting, sodium dodecyl sulphate polyacrylamide gel electrophoresis (SDS-PAGE) gels (8-10% for high, 12% for medium, 15% for low molecular weight proteins) were prepared according to **Table 10**. Briefly, protein samples including 6x reducing electrophoresis buffer were heated at 99 °C for 10 min then immediately cooled down in ice box and spinned down for 10s. Samples were loaded on the gels and electrophoresis was performed with 25 mA current per gel. Following SDS-PAGE, Bio-Rad Transfer-Blot Turbo Transfer Pack pre-designed membranes were used. The electrophoresed SDS gel was placed on the membrane (bubbles between gel and membrane were removed) followed by top filter papers soaked in transfer buffer, followed by transfer at 2.5 A and 25 V per gel for 25 min. To confirm the correct protein transfer and equal loading of the SDS gel, the membranes were next incubated in Ponceau S solution for 5 min on a shaker, subsequently washed with distilled water and destained with TBS-T. For blocking, the membranes were incubated in 5% milk powder/TBS-T at room temperature (RT) for 1 h, followed by overnight incubation at 4 °C while shaking with the respective primary antibodies (**Table 5**), diluted in 5% BSA/TBS-T. After incubation with the primary antibodies, the membranes were washed three times with TBS-T for 10 min at RT. Thereafter, horseradish peroxidase (HRP)-conjugated secondary antibodies (**Table 7**), diluted in 5% milk powder/TBS-T were applied to the membranes for 1 h at RT. Finally, membranes were washed three times with TBS-T and once with TBS for 10 min at RT. Next, the membranes were placed on an imaging tray and incubated for 3 min with working solutions of LI-COR WesternSure® PREMIUM Chemiluminescent Substrate. Odyssey Fc Imaging System and Image Studio Version 5.2 software were used for the detection of the chemiluminescent signal.

Densitometric analysis

Image Studio Version 5.2 software was used for the densitometrical analyses. Briefly, the corresponding protein bands were selected by using 'Draw Rectangle, tool under the 'Analysis, module. For the automatic background subtraction, 'Average–Border width, parameter was set to '1, and segment parameter was set to 'Top/Bottom,.

Table 10. Ingredients and pipetting scheme for SDS electrophoresis gels (8.3 cm x 7.3 cm x 1 mm).

	Separation gel 8%	**Separation gel 10%**	**Separation gel 12%**	**Separation gel 15%**	**Collection gel 5%**
Distilled water	5.8 ml	4.7 ml	3.6 ml	2.0 ml	3.52 ml
Rotiphorese® Gel 30 (37.5:1)	4.3 ml	5.4 ml	6.5 ml	8.1 ml	0.836 ml
1M Tris HCl (pH 8.8)	6.0 ml	6.0 ml	6.0 ml	6.0 ml	-
1 M Tris HCl (pH 6.8)	-	-	-	-	0.626 ml
10% SDS	0.162 ml	0.162 ml	0.162 ml	0.162 ml	0.05 ml
20% APS	0.054 ml	0.054 ml	0.054 ml	0.054 ml	0.04 ml
TEMED	0.012 ml	0.012 ml	0.012 ml	0.012 ml	0.005 ml

3.2.16. Immunofluorescence staining and imaging

Residual DNA DSBs of 3D cell cultures were counted using the foci assay as previously described (Hehlgans et al., 2018; Storch et al., 2010). Briefly, 3D cell cultures were isolated 24 h after irradiation with 2 Gy. Subsequently, cells were fixed and stained with anti-phospho-histone γH2AX antibody (clone JBW301; Millipore), anti-53BP1 antibody (NB100-304, Novus Biologicals), then labelled with Alexa Fluor 488 goat anti-rabbit secondary antibody (Invitrogen), Alexa Fluor 594 goat anti-mouse secondary antibody, 4',6-diamidino-2-phenylindole (DAPI) and covered with Vectashield mounting medium. γH2AX/53BP1-positive foci were microscopically counted from at least 50 nuclei per single experiment. Fluorescence images of stably transfected cells were obtained using an Axio Imager Z1 microscope (Carl Zeiss, Göttingen, Germany) after staining the nuclei with DAPI.

3.2.17. *In vitro* kinase assay

The kinase activity of DNA-PK was measured using a SignaTECT DNA-Dependent Protein Kinase Assay System. The biotinylated peptide substrate was incubated with 30 units purified DNA-PK and (γ-^{32}P)ATP in the presence or absence of immunoprecipitated Survivin-EGFP, EGFP or DNA-PK inhibitor (KU 0060648, 1 μM) in a thermoshaker at 1100rpm, 30 °C for 45 min according to the manufacturer's instructions. The biotinylated substrate was captured on a streptavidin membrane, washed and quantified by the Fujifilm BAS-1500 Phosphorimager (GE Life Sciences, Tokyo, Japan). Results were evaluated by using TINA Image Analysis Environment (OSMIA Project, EU IST Program) (**Figure 9**).

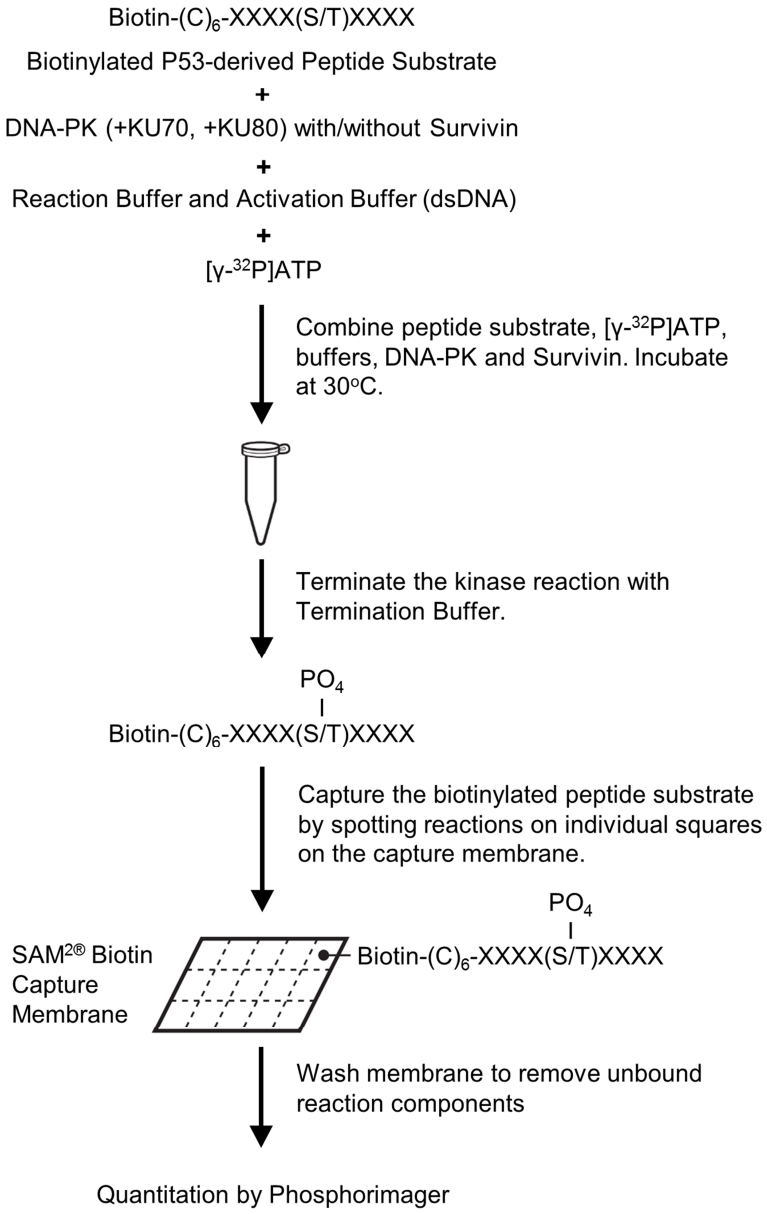

Figure 9. Schematic presentation of the SignaTECT® DNA-dependent Protein Kinase Assay Protocol. The biotinylated peptide, DNA-PK, reaction and activation buffers and γ-^{32}P ATP were mixed, incubated at 30 °C and the reaction was terminated by termination buffer. Further, the sample was probed on the SAM$^{2®}$ biotin capture membrane and unbound components were washed away. Subsequently, the membrane was quantified by Phosphorimager. Figure modified from Promega (https://www.promega.de).

3.2.18. Cell harvest and lysis for LC-MS

The SW480 human colorectal carcinoma cells (wild type, stably EGFP or Surv.wt transfected) were transfected with control siRNA or Survivin siRNA for 48 hours followed by DNA-PK inhibitor treatment (1 μM) 1 h before irradiation with 4 Gy. 1 h after irradiation, cells were harvested with ice-cold PBS, centrifuged at 100 x g for 5 min at 4 °C, and the supernatant was removed. Lysis was performed according to a previously described procedure (Potel et al., 2018). Briefly, one volume of cell pellet was resuspended with five volumes of lysis buffer composed of 100 mM Tris-HCl pH 8.5, 7 M Urea, 1% Triton X-100, 10U/ml DNase I, 1 mM

$MgCl_2$, 100U/ml Benzonase, 1 mM Sodium Orthovanadate, 1X PhosSTOP phosphatase inhibitor, and 1X cOMPLETE mini EDTA-free protease inhibitor then further lyzed by sonication for 45 min (30 s on, 30 s off) using a Bioruptor Plus. Residual cell debris removal was performed by ultracentrifugation (140,000 x g for 1 h at 4 °C). The lysates were further incubated at room temperature for 2 h then stored at -80 °C.

3.2.19. Sample preparation for LC-MS

Lysates were incubated with 10 mM TCEP and 40 mM chloroacetamide for 30 min at 37 °C. Proteins were precipitated using three volumes of ice-cold methanol, one volume of chloroform, and 2.5 volumes of ddH_2O. After centrifugation at 3,000 x g for 30 min at 4 °C, the upper aqueous phase was aspirated, and three volumes of ice-cold methanol added. Samples were mixed and proteins pelleted by centrifugation at 3,000 x g for 5 min at 4 °C. The supernatant was discarded and pellets were washed one additional time with ice-cold methanol. Protein pellets were resuspended in 8 M Urea, 10 mM EPPS pH 8.2 and protein concentration was determined using the BCA assay. Samples were diluted to 2 M Urea using digestion buffer (10 mM EPPS pH 8.2) and incubated with LysC at 1:50 (w/w) ratio for 3 h at 37 °C. Digestion reactions were further diluted to 1 M Urea using digestion buffer and incubated at 1:125 (w/w) ratio with trypsin overnight at 37 °C. Digests were acidified using trifluoroacetic acid (TFA) to pH 2.0, and peptides were purified using SepPak C18 columns according to the manufacturer's protocol. The elution was split into the proteome and phosphoproteome sample and dried separately. Proteome peptides were resuspended in TMT-labelling buffer (0.2 M EPPS pH 8.2, 20% acetonitrile) and peptide concentration was determined by using μBCA assay. Phosphopeptides were enriched by using High-Select™ Fe-NTA Phosphopeptide Enrichment Kit according to the manufacturer's protocol. Phospho peptides were purified using Empore™ C18 (Octadecyl) resin material. The material was activated by incubation with methanol for 10 min, followed by one wash with each buffers; 70% acetonitrile/0.1% TFA and 3% acetonitrile/0.1% TFA. Samples were resuspended in 3% acetonitrile/0.1% TFA, acidified to pH 2.0, and loaded on the resin material. Peptides were washed once with 3% acetonitrile/0.1% TFA and eluted with 70% acetonitrile. Samples were dried and resuspended in TMT labeling buffer. Equal amounts of proteome peptides and phosphopeptides were mixed with TMT reagents at a 2:1 (w/w) ratio. Reactions were incubated for one hour at RT and subsequently quenched by the addition of hydroxylamine to a final concentration of 0.5% at RT for 15 min. Samples were pooled in equimolar ratio and analyzed by test shot to verify equal mixing and labeling efficiency. Adjusted peptide amounts were used for Pierce™ High pH Reversed-Phase Peptide Fractionation Kit, according to the manufacturer's protocol. Samples were dried and resuspended in 0.1% formic acid (FA) for LC-MS2/3 analysis.

3.2.20. Liquid chromatography-mass spectrometry (LC-MS)

All mass spectrometry data were acquired in centroid mode on an Orbitrap Fusion Lumos mass spectrometer hyphenated to an easy-nLC 1200 nano HPLC system using a nanoFlex ion source applying a spray voltage of 2.6 kV with the transfer tube heated to 300 °C and a funnel RF of 30%. Internal mass calibration was enabled (lock mass 445.12003 m/z). Peptides were

separated on a self-made 32 cm long, 75 μm ID fused-silica column, packed in house with ReproSil-Pur Basic 1.9 μm C18 particles and heated to 50 °C using an integrated column oven. HPLC solvents consisted of 0.1% formic acid in water (Buffer A) and 0.1% formic acid/80% acetonitrile in water (Buffer B).

For total proteome analysis, a synchronous precursor selection (SPS) multi-notch MS3 method was used in order to minimize ratio compression, as previously described (McAlister et al., 2014). Individual peptide fractions were eluted by a non-linear gradient optimized for each fraction, spanning from 3 to 50% B over 210 min. The effective gradient was followed by a step-wise increase to 95% B in 6 min, which was held for another 9 min. Full scan MS spectra (350-1400 m/z) were acquired with a resolution of 120,000 at m/z 200, maximum injection time of 100 ms, and AGC target value of 4 x 10^5. The 20 most intense precursors with a charge state between 2 and 6 per full scan were selected for fragmentation ("Top 20") and isolated with a quadrupole isolation window of 0.7 Th. MS2 scans were performed in the Ion trap (Turbo) using a maximum injection time of 50 ms, AGC target value of 1.5 x 10^4, and fragmented using collision-induced dissociation with normalized collision energy (NCE) of 35%. SPS-MS3 scans for quantification were performed on the 10 most intense MS2 fragment ions with an isolation window of 0.7 Th (MS1) and 2 m/z (MS2). Ions were fragmented using higher-energy collisional dissociation (HCD) with an NCE of 65% and analyzed in the Orbitrap with a resolution of 50,000 at m/z 200, scan range of 110-500 m/z, AGC target value of 1.5 x10^5 and maximum injection time of 120 ms. Repeated sequencing of already acquired precursors was limited by setting a dynamic exclusion of 45 sec and 7 ppm and advanced peak determination was deactivated.

For phosphopeptide analysis, each peptide fraction was eluted by a linear gradient optimized for each fraction, spanning from 4 to 40% B over 120 min followed by a step-wise increase to 95% B in 8 min which was held for another 7 min. Full scan MS spectra (350-1400 m/z) were acquired with a resolution of 120,000 at m/z 200, maximum injection time of 100 ms, and AGC target value of 4 x 10^5. The 20 most intense precursors per full scan with a charge state between 2 and 5 were selected for fragmentation ("Top 20"), isolated with a quadrupole isolation window of 0.7 Th and fragmented via HCD applying an NCE of 38%. MS2 scans were performed in the Orbitrap using a resolution of 50,000 at m/z 200, maximum injection time of 86 ms, and AGC target value of 1 x 10^5. Repeated sequencing of already acquired precursors was limited by setting a dynamic exclusion of 60 sec and 7 ppm and advanced peak determination was deactivated.

3.2.21. Processing of raw LC-MS files and data analysis

Raw files were analyzed using Proteome Discoverer (PD) 2.4 software (Thermo Fisher Scientific). Files were recalibrated using the Homo sapiens SwissProt database (TaxID:9606, version 2017-09-11). Fixed modifications for proteome analyses were carbamidomethyl (C,+57.021) and TMT6 (N-terminal, +229.1629) and dynamic modification was methionine oxidation (M, +15.995). For phosphoproteomics fixed modifications were phosphorylation (S, T, Y, +79.966), carbamidomethyl (C,+57.021) and TMT6 (N-terminal, +229.1629).

Spectra were selected using default settings and database searches performed using SequestHT node in PD. Database searches were performed against trypsin digested Homo

sapiens SwissProt database and FASTA files of common contaminants ('contaminants.fasta' provided with MaxQuant) for quality control. Fixed modifications were set as TMT6 (N-terminal, +229.1629 and K, +229.1629) and carbamidomethyl (C,+57.021). Dynamic modifications for proteome analysis were oxidation (M, +15.995) and acetylation (N-terminal, +42.011) and for phosphoproteomics dynamic modifications were oxidation (M, +15.995), acetylation (N-terminal, +42.011) and phosphorylation (S, T, Y, +79.966).

After the search, posterior error probabilities were calculated, and PSMs filtered using Percolator with default settings. The consensus workflow for reporter ion quantification was performed with default settings. Results were then exported to Excel files for further processing.

The mass spectrometry proteomics data have been deposited to the ProteomeXchange Consortium (Vizcaino et al., 2014) via the PRIDE partner repository (Vizcaino et al., 2016) with the dataset identifier **PXD020489** (Reviewer account details: Username: reviewer58550@ebi.ac.uk; Password: oWwUa3dj).

Log_2 fold changes were calculated by Log_2 transformation of the ratio between the treated sample versus the control sample. Hierarchical clustering analysis was performed using the Perseus software package (version 1.6.10.45) with Euclidean distance and default settings after centering and scaling of data (Z scores).

3.2.22. Data analysis

Experimental data are presented as mean ± standard deviation (SD). At least three independent experiments were performed. A two-sided unpaired Student's t-test was performed using Microsoft Excel software to test statistical significance. Results were considered statistically significant when a p-value of less than 0.05 (*) was reached, more significant with $p < 0.01$ (**), and highly significant with $p < 0.001$ (***), respectively.

4. Results

4.1. Initial findings on the involvement of Survivin BIR domain in radiation survival and DNA damage repair

Initial experimental studies of our group have analyzed the effect of Survivin domain deletion mutants on DNA damage repair, and radiation response in 3D clonogenic assays that may reflect a physiological environment more closely than conventional 2D cultures (Eke et al., 2013; Storch et al., 2010). Under these conditions, cells stably expressing recombinant Survivin with a deletion of the BIR domain (ΔBIR) were significantly radiosensitized while the expression of Survivin mutants lacking the microtubule binding domain (ΔMicTub) fully rescued radiation survival following siRNA-mediated knockdown of endogenous Survivin (Petraki, 2014) (**Figure 10a**).

Our group and others have recently shown that nuclear accumulation of Survivin contributes to the repair of radiation-induced DNA DSBs (Chakravarti et al., 2004; Iwasa et al., 2008; Rodel et al., 2005) probably via interaction with members of the NHEJ apparatus such as DNA-PKcs (Capalbo et al., 2010; Reichert et al., 2011; Wang et al., 2018c). The molecular basis for this interrelationship, however, remains elusive. Thus, we analyzed the impact of Survivin deletion mutants on DNA DSB repair. Residual DNA damage in 3D cell cultures was significantly increased upon knockdown of endogenous Survivin in EGFP and ΔBIR expressing cells, as evaluated by the assessment of γH2AX foci at 24 h after irradiation with 2 Gy. On the contrary, overexpression of Survivin wild type (Surv. wt) and ΔMicTub constructs rescued DNA repair following the knockdown of endogenous Survivin (Petraki, 2014) (**Figure 10b**). This suggested a potential role of the BIR domain of Survivin in response to DNA damage. In the lights of these findings, investigations were further focused on *in silico* molecular interaction potential of Survivin-DNA-PKcs interaction in **Section 4.2** to elucidate the functional and molecular relevance of these preliminary findings.

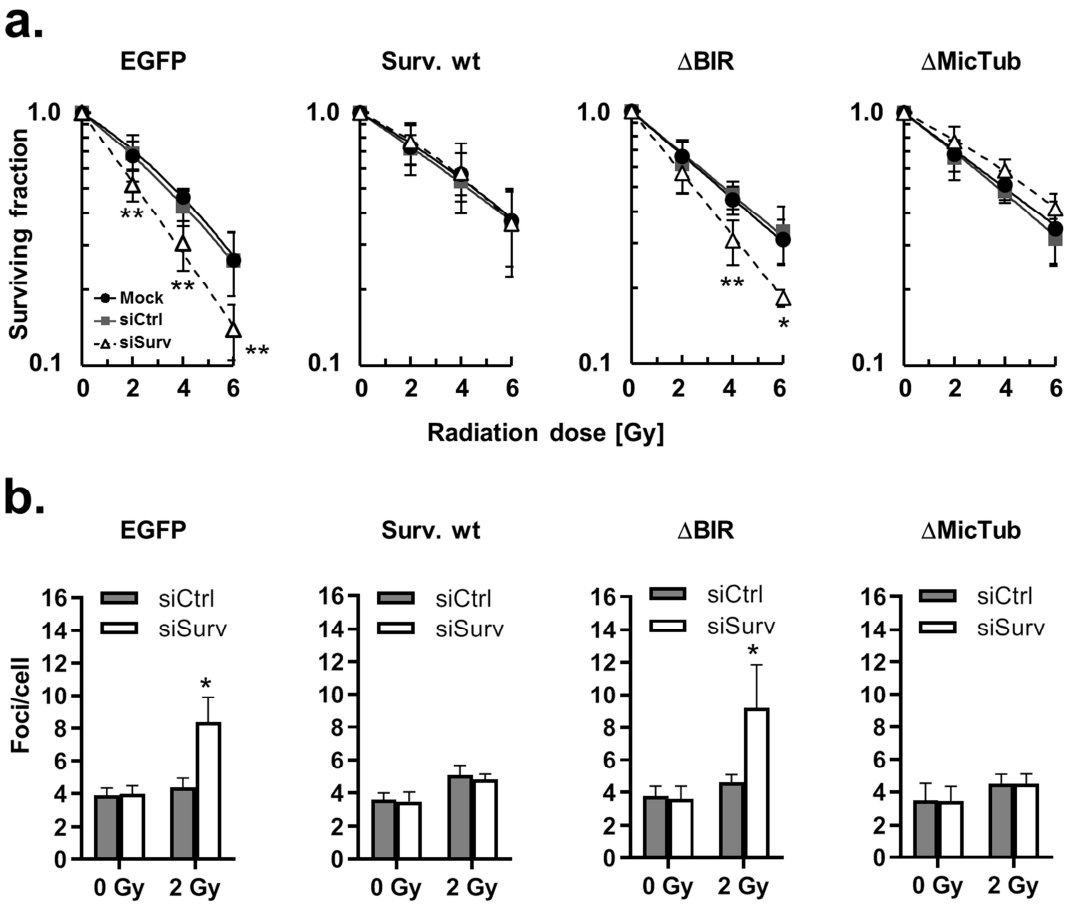

Figure 10. The Survivin BIR domain is essential for 3D clonogenic radiation survival and DNA damage repair. (**a**) Clonogenic radiation survival of the indicated 3D cell cultures was analyzed after irradiation with 0, 2, 4 or 6 Gy (single dose). Results represent means ± SD (n = 4; * $p < 0.05$; ** $p < 0.01$; t-test). (**b**) SW480 cells, stably expressing indicated Survivin mutants were subjected to siRNA transfection (siCtrl, non-specific control siRNA; siSurv, Survivin siRNA) and subsequently irradiated with 2 Gy. At 24 h after irradiation, cells were fixed and stained for γH2AX/53BP1 while nuclei were counterstained with DAPI. Nuclear γH2AX foci were microscopically counted (50 nuclei per experiment). Results represent mean foci per cell ± SD (n = 3; * $p < 0.05$; t-test). Figure provided by Dr. Chrysi Petraki (PhD thesis) (Petraki, 2014).

4.2. Molecular docking analysis of Survivin and DNA-PKcs interaction

Molecular crystallographic structures of proteins can be determined from protein crystals using a variety of methods, including nuclear magnetic resonance spectroscopy (NMR), X-ray crystallography, SAXS, cryogenic electron microscopy (Cryo-EM), neutron diffraction, electron crystallography and microcrystal electron diffraction (Wang and Wang, 2017). Even with these cutting-edge technological advances, still, many of the generated structures have a variety of structural defects, including missing atoms, missing/incomplete side chains, residues or loops, incorrect bond orders, and missing bonds, which can negatively affect the molecular docking analysis and further evaluations. To overcome those potential problems, pre-docking protein preparations were performed by the Protein Preparation Wizard module of Schrödinger Release 2018-1 (Sastry et al., 2013). The X-ray crystal structure of Survivin -PDB: 1E31- (Chantalat et al., 2000) and DNA-PKcs -PDB: 5LUQ- (Sibanda et al., 2017) were used as input and missing/truncated atoms, side chains, loops (Prime module of Schrödinger

Release 2018-1, (Jacobson et al., 2002; Jacobson et al., 2004)) were filled, cap-termini, disulfide bonds were re-created, all non-complexed ions and solvents were deleted and selenomethionines converted to methionines. The hydrogen-bonding network was optimized, and protonation states assigned at pH 7.0. Finally, protein preparations were completed by performing a restrained minimization using the OPLS3 force field (Harder et al., 2016) (**Figure 11**).

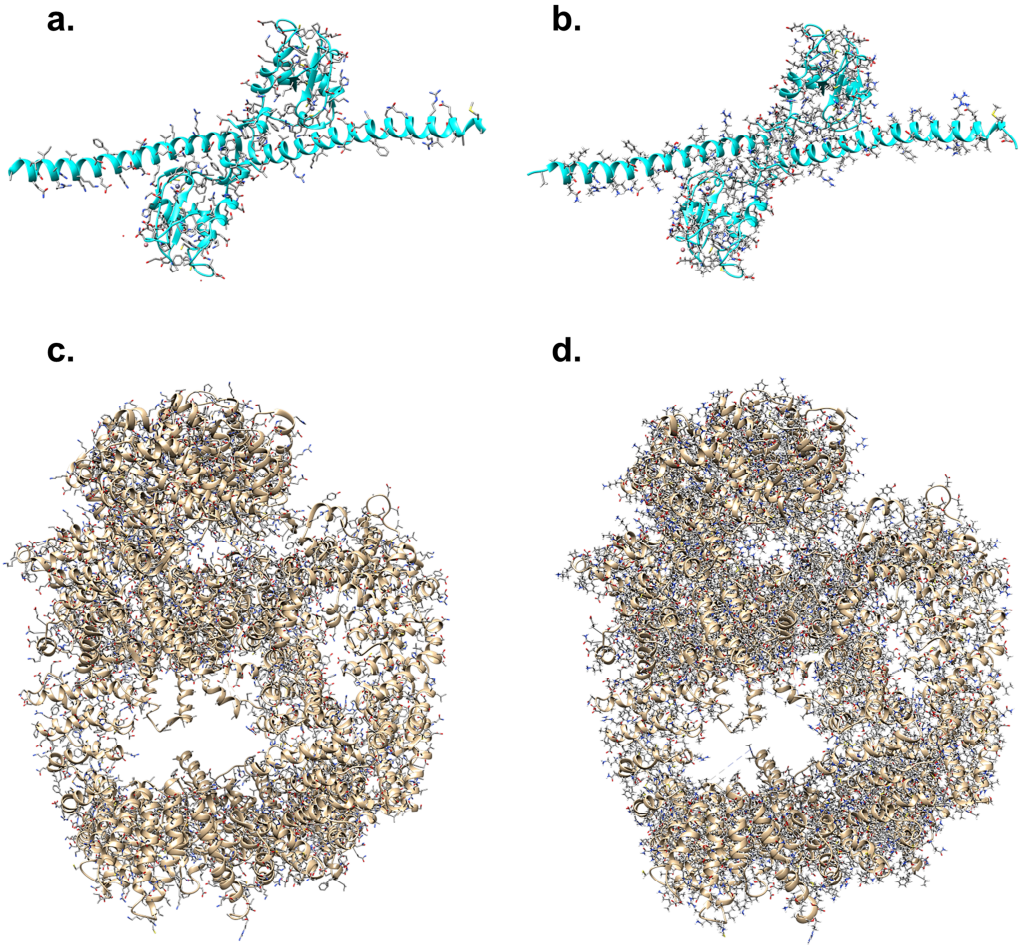

Figure 11. Protein preparation fixes crucial crystallographic errors. Survivin (PDB: 1E31), (**a**) before preparation, and (**b**) after preparation. DNA-PKcs (PDB: 5LUQ), (**c**) before preparation, and (**d**) after preparation.

Next, optimized proteins were molecularly docked by employing the PIPER module of Schrödinger Release 2018-1 (Chuang et al., 2008; Kozakov et al., 2006) and PatchDock webserver analyses (Schneidman-Duhovny et al., 2005) and top-ranked 150 poses were further refined with FireDock (Mashiach et al., 2008). Qualification of hot-spot potential interaction residues were based on the binding free energy and distances: Interaction pairs that have lower binding free energy values compared to pre-docking conditions and distances between backbone/side chains atoms lower than 5Å were qualified as potential interactors. Post-docking binding free energy and potential bond-forming proximity analyses revealed that some specific residues such as S20, F27, C31, D53 and W67 located in the BIR domain (18-88 amino acids (aa)) of Survivin showed low binding free energy compared to pre-docking conditions and showed high affinity to the catalytic PI3K domain (3747-4015 aa) of DNA-

PKcs (**Figure 12a**). By contrast, phospho-mimicking form of S20 (S20D) and alanine substitution form of W67 (W67A) residues *in silico* generated by Rotamer tool of Chimera 1.13.1 (Pettersen et al., 2004) using the Dunbrack Rotamer Library (Shapovalov and Dunbrack, 2011) showed greater side-chain distances and a potential decrease was observed in the attraction/bond formation compared to wild-type conditions by two representative molecular interaction poses (**Figure 12b**).

a.

Survivin	Survivin ΔG (kJ mol^{-1})	DNA-PKcs	DNA-PKcs ΔG (kJ mol^{-1})	Proximity (Å)
S20	-0.366	Y3828	-3.183	2.623
F27	-0.318	W3842	-1.452	0.890
C31	-0.206	M3846	-1.102	2.540
D53	-0.281	R3874	-2.085	2.588
W67	-0.487	E3838	-4.876	1.810

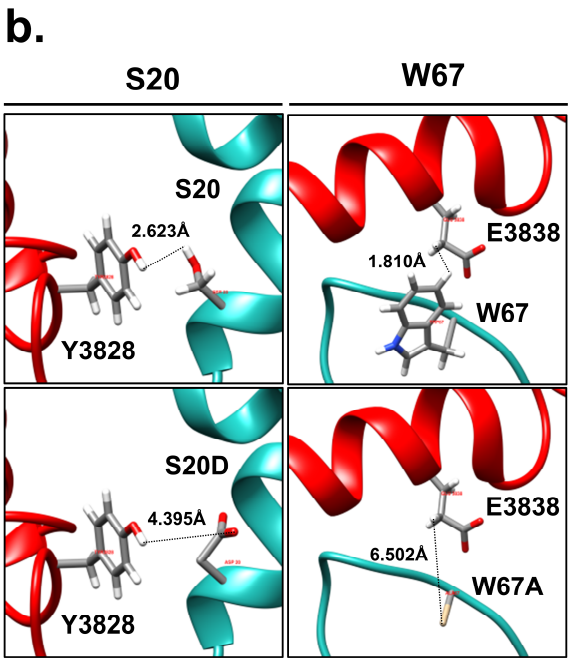

Figure 12. Molecular *in silico* docking and energy analyses of the interaction of Survivin and DNA-PKcs. (**a**) Pair-wise binding free energies and distances of Survivin and DNA-PKcs' amino acids. (**b**) Two representative docking poses indicating potential interactions between wild type or phospho-mimicking form of S20 (S20D) and wild type or alanine substitution form of W67 (W67A) residues of Survivin (cyan) with Y3828 and E3838 residues of DNA-PKcs (red) respectively.

4.3. BIR domain of Survivin is essential for the interaction with the PI3K domain of DNA-PKcs

In the light of all findings mentioned before, the interaction potential between Survivin and DNA-PKcs has been verified by testing different domains/regions of DNA-PKcs by FACS-FRET to unravel which domains/regions are responsible for this interaction. Survivin wt or BIR domain deletion mutants and domains/regions of DNA-PKcs (HEAT-1, FATC, PI3K) were sub-cloned into FRET vectors and co-transfected into SW480 colorectal cancer cells (**Figure 13a**). Analyses by cytofluorometry revealed a significant interaction of Survivin with the PI3K domain of DNA-PKcs, and deletion of the BIR domain of Survivin significantly diminished the interaction between Survivin and DNA-PKcs. Moreover, the interaction potentials between Survivin and the HEAT-1 and FATC domains of DNA-PKcs and as well as PI3K domain of ATM resulted in low interaction potentials compared to PI3K domain of DNA-PKcs. These results suggest that the BIR domain of Survivin is indispensably involved in the interaction with the PI3K domain of DNA-PKcs (**Figure 13b**).

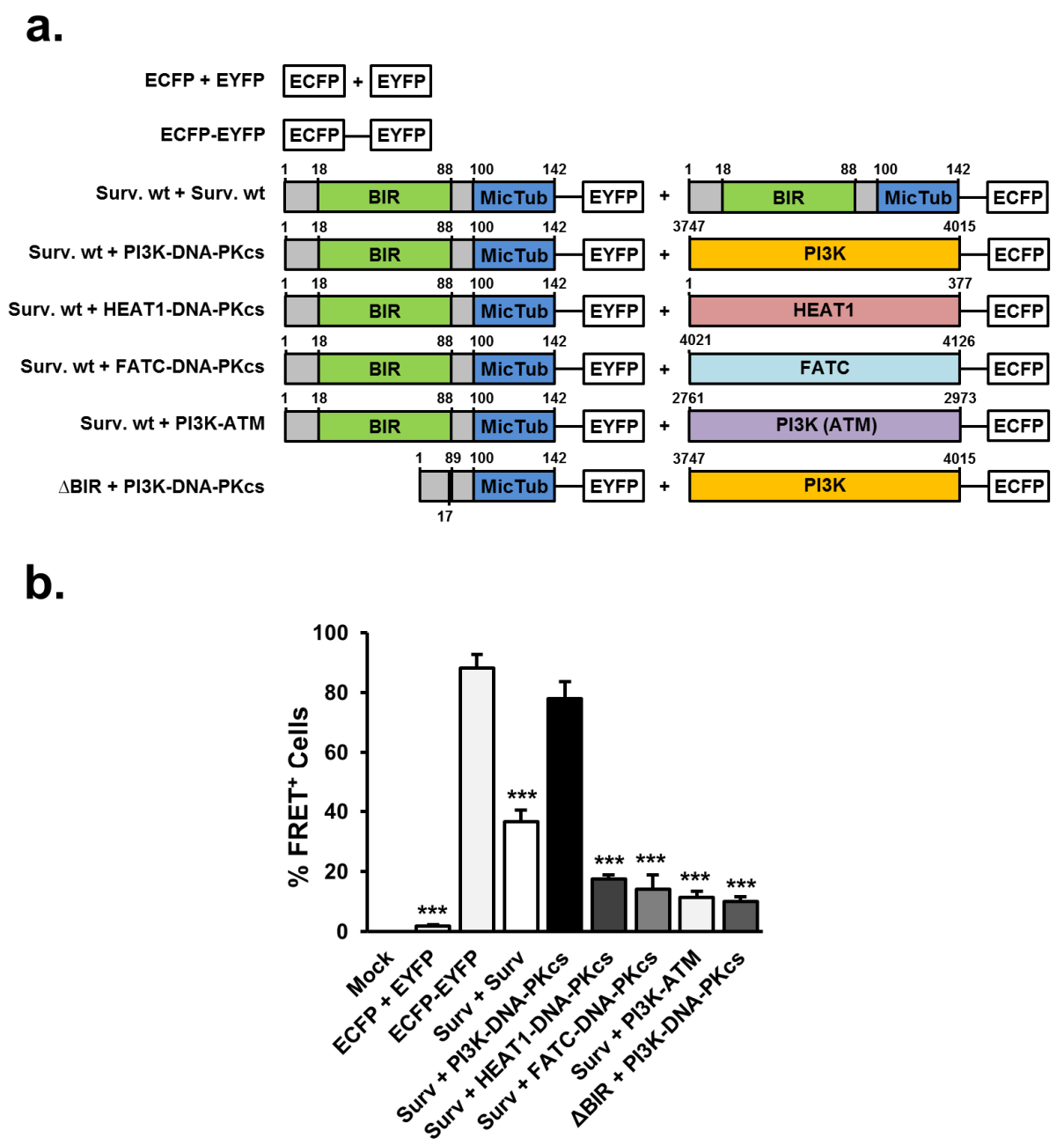

Figure 13. Domain-based FACS-FRET analysis for DNA-PKcs. (**a**) Schematic representation of the domains of Survivin, DNA-PKcs and ATM which subjected to FACS-FRET analyses. Vectors expressing enhanced yellow fluorescent protein (EYFP), Surv. wt, Survivin wild type-EYFP; ΔBIR, Survivin baculovirus inhibitor of apoptosis protein repeat (BIR) domain deletion mutant-EYFP. Vectors expressing enhanced cyan fluorescent protein (ECFP), Surv. wt, Survivin wild type-ECFP; PI3K, DNA-PKcs phosphatidylinositol-3-kinase (PI3K) domain-ECFP; HEAT1, DNA-PKcs Huntingtin-Elongation Factor 3-PP2A-TOR1 (HEAT1) domain-EYFP; FATC, FRAP-ATM-TRRAP C-terminal (FATC) domain-ECFP; PI3K-ATM, ATM phosphatidylinositol-3-kinase (PI3K) domain-ECFP. Numbering of residues correspond to the original positions in the complete protein sequence. (**b**) Analyses were performed to measure the interaction potentials between Survivin and the HEAT1-repeat, PI3K, and FATC domains of DNA-PKcs and as a negative control PI3K domain of ATM. Proteins were fused with ECFP and/or EYFP fluorescence tags and SW480 cells were co-transfected with the corresponding constructs. The interaction potentials depending on the proximity-based energy transfer from ECFP to EYFP fluorescence tag resulting in the EYFP emission fluorescence signal were measured by flow cytometry. Results represent means ± SD (n = 3; * $p < 0.05$; ** $p < 0.01$; *** $p < 0.001$; t-test).

To further confirm the importance of the BIR domain for the interaction with DNA-PKcs, co-IP assay were performed. Recombinant Survivin wild type/BIR domain deletion mutant expressing SW480 colorectal cancer cells were irradiated with 4 Gy, lysates were harvested 1 hour after irradiation. co-IP was performed for both DNA-PKcs and Survivin. As indicated in Figure 14, Surv. wt co-immunoprecipitated with DNA-PKcs while deletion of BIR domain (ΔBIR) or EGFP control did not display an interaction. Vice versa, DNA-PKcs co-immunoprecipitated with Surv. wt while deletion of the BIR domain (ΔBIR) or EGFP control lack an interaction. In summary, these findings revealed that the BIR domain is essential for this interaction (**Figure 14**).

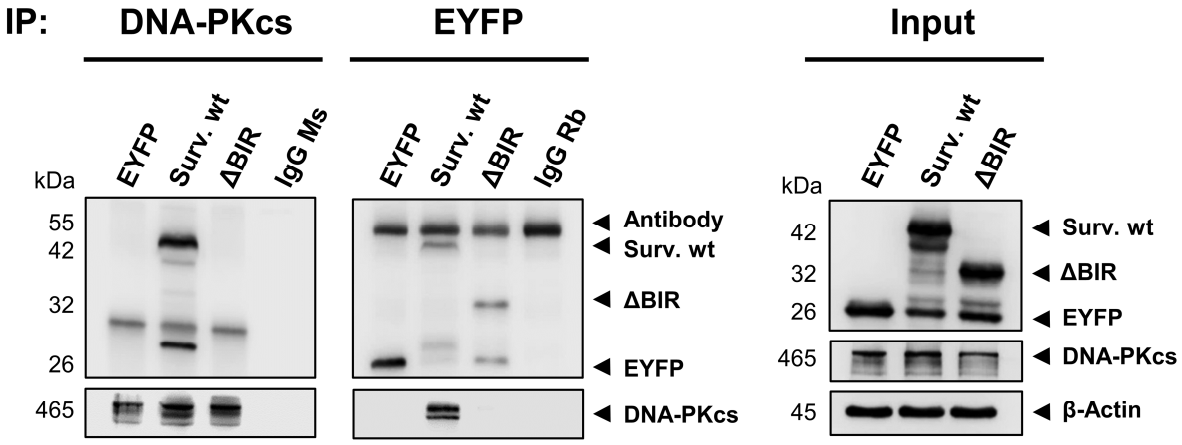

Figure 14. BIR domain is essential for the interaction between Survivin and DNA-PKcs. Whole cell lysates of SW480 cells, transiently transfected with EYFP, Surv. wt or ΔBIR expression constructs, were isolated one hour after irradiation with 4 Gy. EYFP fusion proteins were immunoprecipitated (IP) using an anti-GFP antibody, and DNA-PKcs was immunoprecipitated with an anti-DNA-PK antibody. Mouse and rabbit mAb isotype controls (IgG) served as controls. Subsequently, EYFP constructs and DNA-PKcs were detected by immunoblotting.

4.4. Specific amino acids located in the BIR domain of Survivin are important for the interaction with the PI3K domain of DNA-PKcs

Single mutation vectors of qualified potential interactor residues (S20, F27, C31, D53 and W67) (**Figure 12a**), negative control residues (W25, L28, E29, E76 and K79), and known post-translational phosphorylation sites (T34 and T117) of Survivin, also combined double/triple alanine and/or phosphomimetic mutation vectors were prepared by employing site-directed mutagenesis techniques. Correct mutation vectors were validated by sequencing and appropriate constructs were introduced into SW480 colorectal cancer cells and appropriate protein construct expression and stability were confirmed by immunoblotting (**Figure 15**).

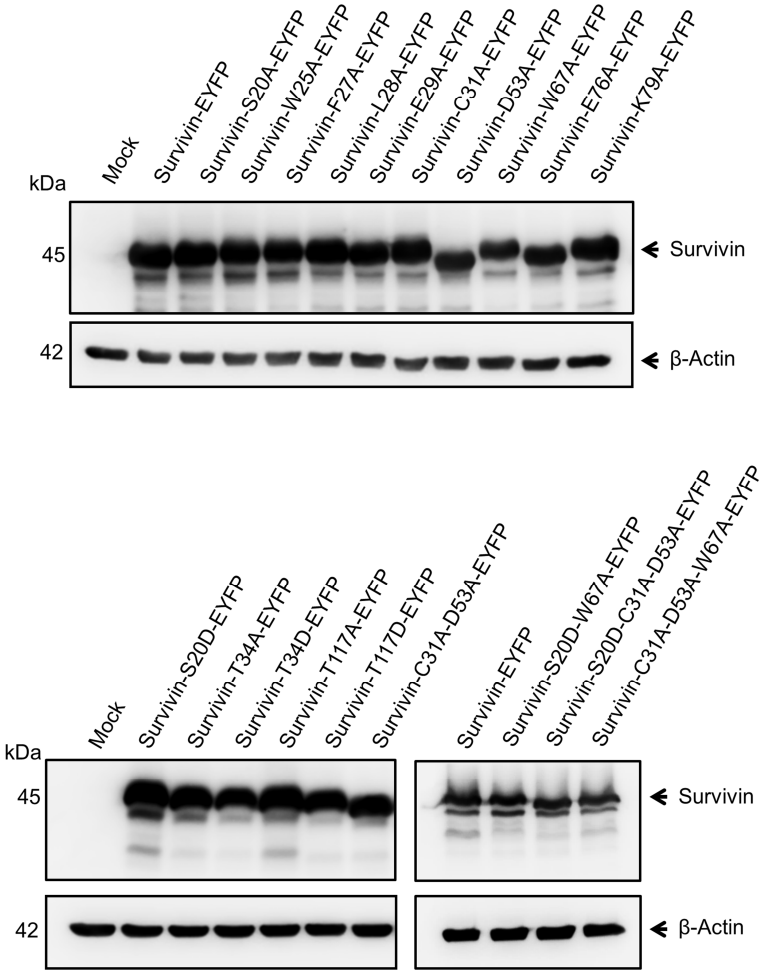

Figure 15. Protein expression levels of single/multiple amino acid mutations of Survivin. The scope of mutations comprises high/low potential molecular docking candidates, known post-translational phosphorylation sites and double/triple combinations of mutations. (β-actin served as a loading control).

Alanine substitution forms of hot-spot residues of Survivin predicted by molecular docking analysis and PI3K domain coding sequences were cloned into acceptor and donor EYFP/ECFP vectors, respectively, and co-transfected into SW480 cells to test the interaction potential by residue-level mutations. Predicted S20, F27, C31, D53, and W67 residues of Survivin were highly involved in this interaction, while alanine substitutions (exceptionally aspartic acid for S20) highly diminished the interaction of Survivin with PI3K domain of DNA-PKcs (**Figure 16a**). To further investigate the potentially involved residues, the known post-translational phosphorylation sites of Survivin (S20, T34, and T117) were tested in both alanine substitution and phospho-mimicking conditions while S20 was already predicted by molecular docking analysis. Phospho-mimicking aspartic acid mutations of S20, T34 and T117 and alanine substitution of T34 significantly decreased the interaction potential by more than 30% (**Figure 16b**). Further combined double/triple mutations cumulatively decreased the potential, and the S20D-W67A double mutant was found the most promising, displaying around 70% decrease in the interaction between Survivin and PI3K domain of DNA-PKcs (**Figure 16c**). The importance of the S20D-W67A double mutant was further verified by using additional colorectal cancer cell lines DLD-1 and HCT-15 (**Figure 16d,e**).

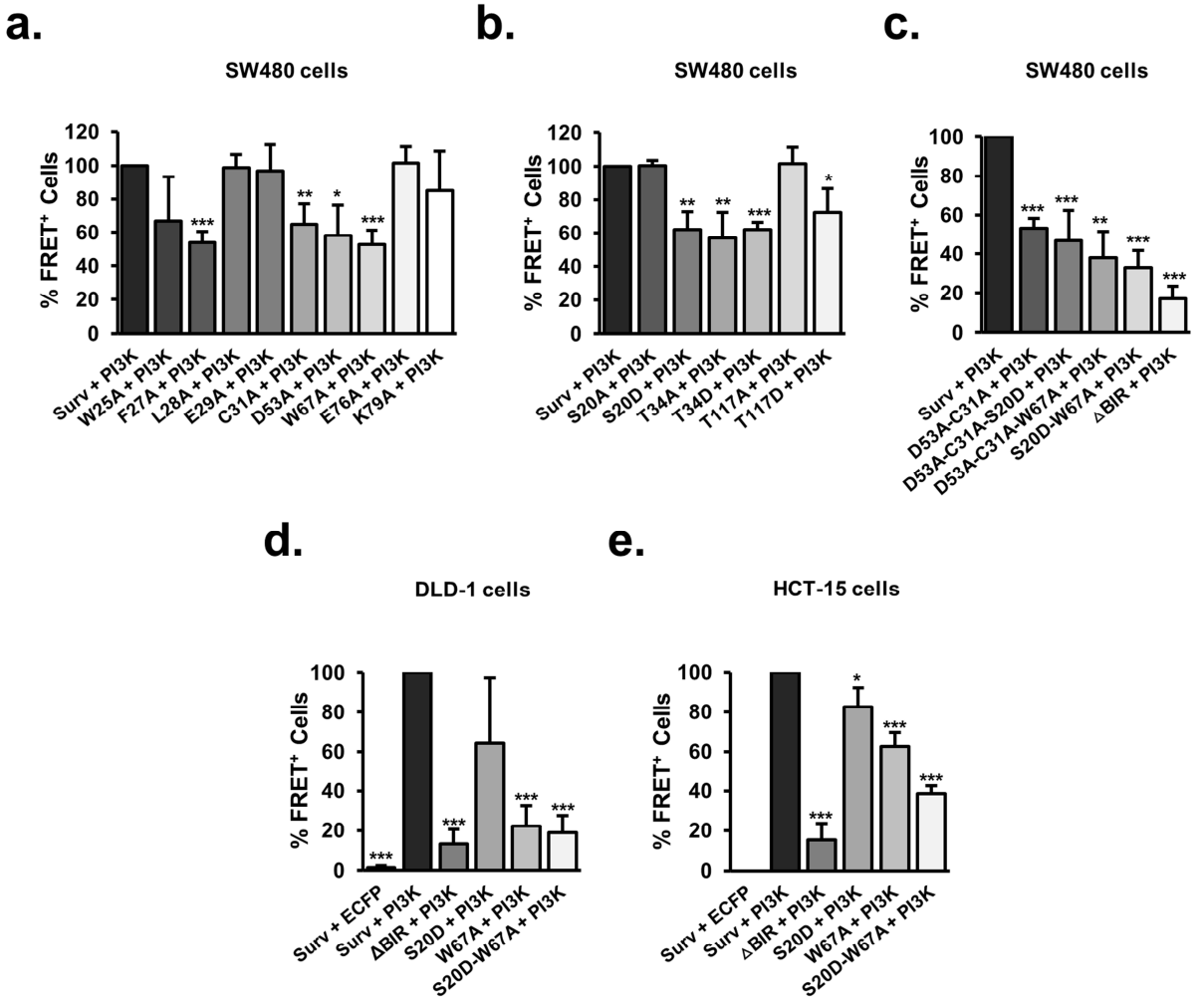

Figure 16. Specific amino acids located in the BIR domain of Survivin are essential for the interaction with the PI3K domain of DNA-PKcs. (**a**) Fluorescence-based FACS-FRET analysis of the interaction potentials of alanine substitution forms of various Survivin sites in the interaction with PI3K domain of DNA-PKcs in SW480 cells. Substitutions were generated by site-directed mutagenesis and SW480 cells were transfected with corresponding constructs (Surv, Survivin-EYFP; PI3K, PI3K domain of DNA-PKcs-ECFP; W25A, Tryptophan 25 Alanine-EYFP; F27A, Phenylalanine 27 Alanine-EYFP; L28A, Leucine 28 Alanine-EYFP; E29A, Glutamic acid 29 Alanine-EYFP; C31A, Cysteine 31 Alanine-EYFP; D53A, Aspartic acid 53 Alanine-EYFP; W67A, Tryptophan 67 Alanine-EYFP; E76A, Glutamic acid 76 Alanine-EYFP; K79A, Lysine 79 Alanine-EYFP;). Results represent means ± SD (n = 3; * $p < 0.05$; ** $p < 0.01$; *** $p < 0.001$; t-test). (**b**) FACS-FRET analysis of the interaction potentials of alanine and phospho-mimicking substitution forms of known Survivin post-translational phosphorylation sites with PI3K domain of DNA-PKcs in SW480 cells (S20A, Serine 20 Alanine-EYFP; S20D, Serine 20 Aspartic acid-EYFP; T34A, Threonine 34 Alanine-EYFP; T34D, Threonine 34 Aspartic acid-EYFP; T117A, Threonine 117 Alanine-EYFP; T117A, Threonine 117 Aspartic acid-EYFP). Results represent means ± SD (n = 3; * $p < 0.05$; ** $p < 0.01$; *** $p < 0.001$; t-test). (**c**) Fluorescence-based FACS-FRET analysis of the interaction potentials of BIR domain deletion (ΔBIR, Survivin-ΔBIR-EYFP) and double/triple mutations of the Survivin candidate sites which generated according to relative decrease on the interaction with PI3K domain of DNA-PKcs in SW480 cells. Results represent means ± SD (n = 3; * $p < 0.05$; ** $p < 0.01$; *** $p < 0.001$; t-test). (**d**) FACS-FRET analysis results of the interaction potentials of candidate mutants (ECFP/EYFP, Surv-wt, ΔBIR, S20D, W67A, S20D-W67A) in DLD-1, and (**e**) HCT-15 cells. Results represent means ± SD (n = 3; * $p < 0.05$; ** $p < 0.01$; *** $p < 0.001$; t-test).

Finally, the interaction between Survivin S20D, W67A single; S20D-W67A double mutant constructs, and PI3K domain was tested by performing immunoprecipitation experiments and it was found that single mutants showed significant decrease while double mutant diminished further the interaction with PI3K domain. PI3K domain co-immunoprecipitated with recombinant Surv. wt (and vice versa) but not with the ΔBIR Survivin mutant which verified the direct involvement of the BIR domain in the interaction between Survivin and DNA-PKcs via its catalytic PI3K domain (**Figure 17a,b**).

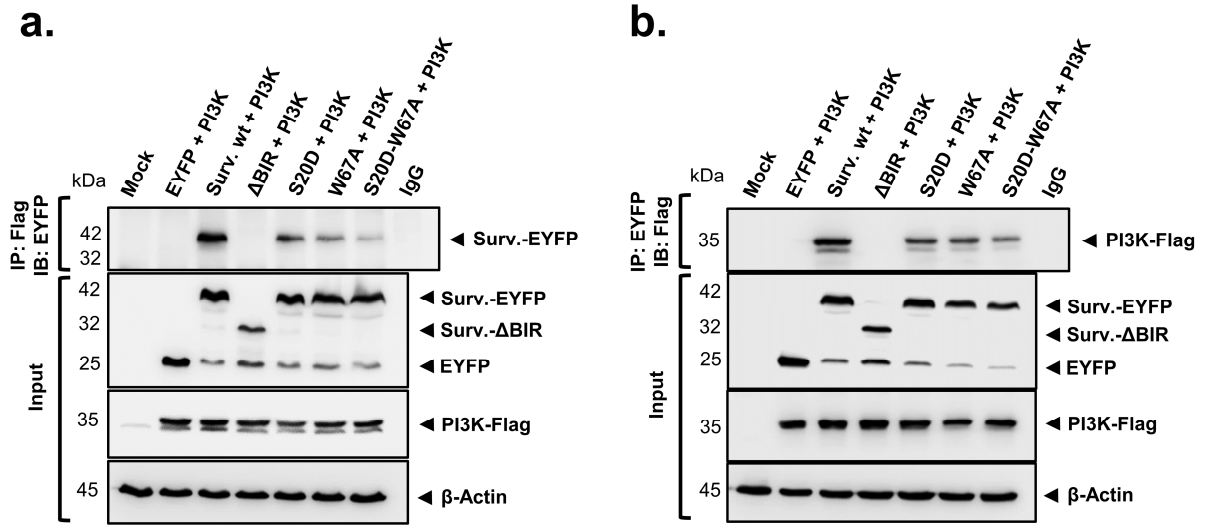

Figure 17. S20D-W67A double mutant hampers the interaction between Survivin and the PI3K domain of DNA-PKcs. Whole cell lysates of SW480 cells, transiently transfected with Mock (Transfection reagent-treated cells), PI3K-Flag, EYFP, Surv, ΔBIR, S20D, W67A and S20D-W67A expression constructs as depicted in the figure, were isolated one hour after irradiation with 4 Gy. (**a**) The PI3K domain of DNA-PKcs was immunoprecipitated with an anti-Flag antibody and (**b**) EYFP fusion proteins were immunoprecipitated (IP) using an anti-GFP antibody. Mouse and rabbit mAb Isotype controls (IgG) served as controls. Subsequently, EYFP constructs and PI3K domain of DNA-PKcs were detected by immunoblotting. β-actin served as a loading control.

4.5. S20 and W67 residues located in the Survivin BIR domain are essential for 3D clonogenic radiation survival and DNA repair of SW480 and DLD-1 colorectal cancer cells

In order to investigate a functional involvement of Survivin S20 and W67 residues in the DNA damage response, SW480 and DLD-1 colorectal cancer cells were stably transfected with the EGFP-fused Survivin mutants. Recombinant protein expression and efficient knockdown of endogenous Survivin were confirmed by immunoblotting (**Figure 18**). Then, 3D colony formation assays were performed by using SW480 and DLD-1 cells stably expressing Surv.wt or Survivin mutant constructs which were subjected to siRNA-mediated knockdown of endogenous Survivin. SW480 colorectal cancer cells expressing W67A, S20D-W67A, and ΔBIR mutant Survivin failed to rescue 3D clonogenic radiation survival while compared to the other mutants S20D displayed a weak but significant effect (**Figure 19a**). However, for the DLD-1 colorectal cancer cells all the mutations (S20D, W67A, S20D-W67A, and ΔBIR) resulted in significant radiosensitization (**Figure 20a**). These findings identify the S20 and W67 residues located in the BIR domain as important mediators of Survivin-dependent radiation survival.

Representative pictures of 3D colonies showing the radiosensitization effect are depicted in **Figure 19b and 20b**.

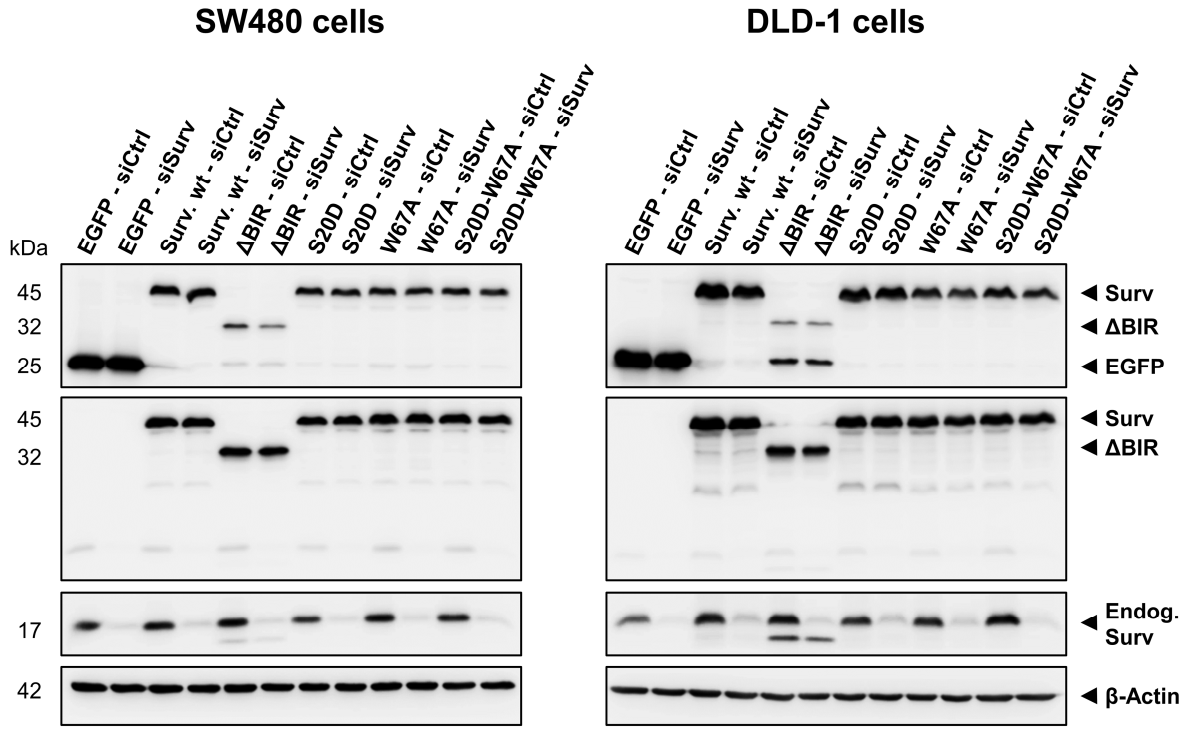

Figure 18. Recombinant protein expression of Survivin wt/mutant fusion proteins in SW480 and DLD-1 colorectal cancer cells. SW480 and DLD-1 cells, stably transfected with EGFP, Surv.wt, ΔBIR, S20D, W67A and S20D-W67A expression constructs in both control siRNA (siCtrl) and Survivin siRNA (siSurv) conditions were immunoblotted. Detection was performed by anti-GFP antibody (first blots for both cell lines) and anti-Survivin antibody (second blots for both cell lines). β-actin served as a loading control.

Next, the impact of Survivin ΔBIR, S20D, W67A and S20D-W67A mutants on DNA DSB repair capacity was analyzed. Residual DNA damage in SW480 and DLD-1 3D cell cultures was significantly increased upon knockdown of endogenous Survivin in EGFP, ΔBIR, W67A, and S20D-W67A expressing cells while S20D expressing cells exhibited a non-significant increase, as evaluated by the assessment of γH2AX/53BP1 foci at 24 h after irradiation with 2 Gy. In contrast, overexpression of Surv. wt rescued DNA repair following the knockdown of endogenous Survivin (**Figure 21a and 22a**). Representative pictures of SW480 3D colorectal cancer cells show the DNA repair effect of experimental conditions (**Figure 21b**).

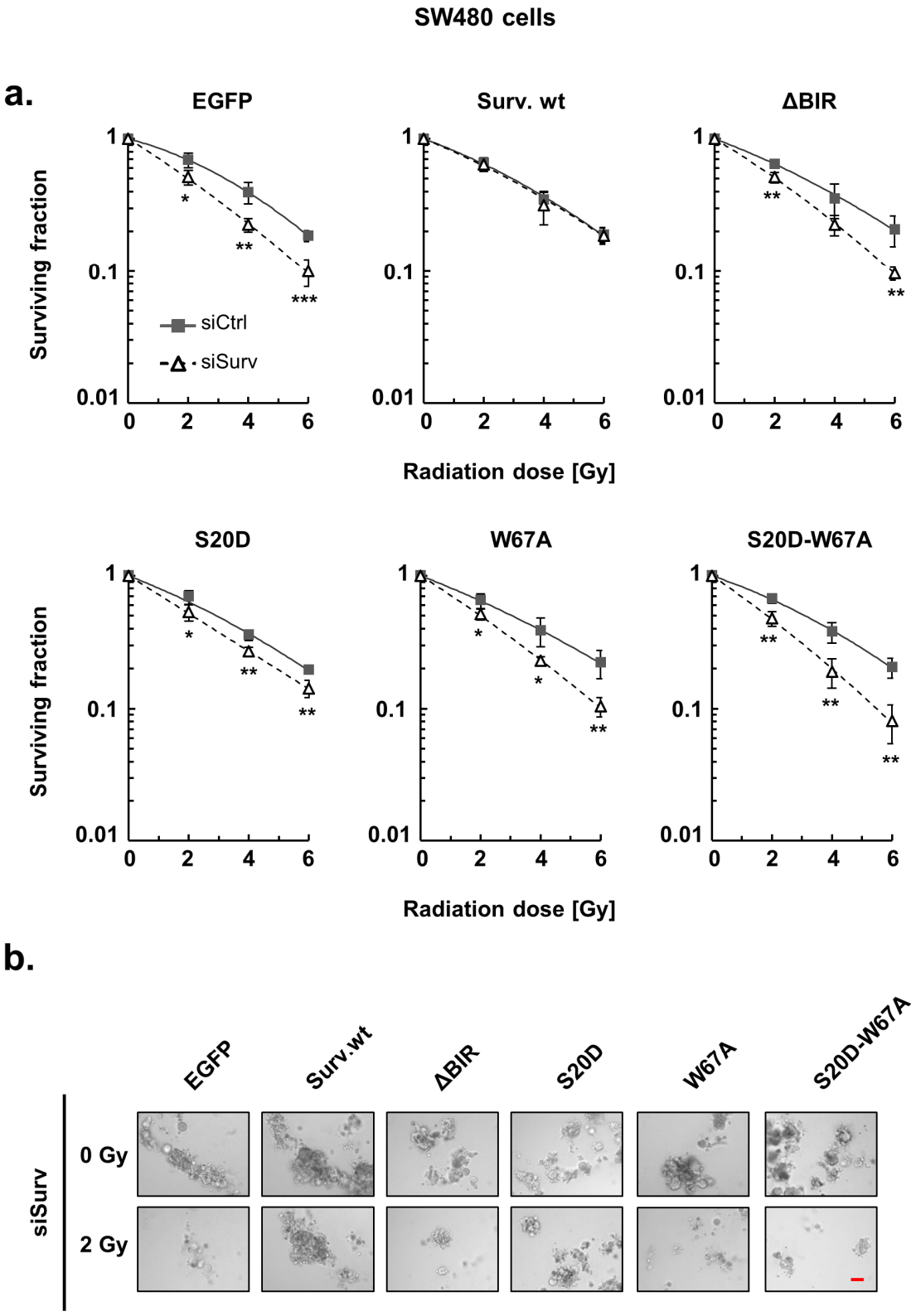

Figure 19. Mutation of W67A, S20D-W67A and ΔBIR deletion radiosensitize 3D-cultured SW480 colorectal cancer cells. (**a**) Clonogenic radiation survival of EGFP, Surv. wt, BIR, S20D, W67A, and S20D-W67A mutant-expressing SW480 3D cells after knockdown of endogenous Survivin (siSurv) or control siRNA (siCtrl) transfected cells were measured after irradiation with 0, 2, 4 or 6 Gy (single dose) using a 3D colony forming assay. Results represent means ± SD ($n \geq 3$; * $p < 0.05$; ** $p < 0.01$; *** $p < 0.001$; t-test). (**b**) Representative pictures of 3D SW480 cell colonies (Axio Observer Z1; 10x objective). Scale bar: 100 μm.

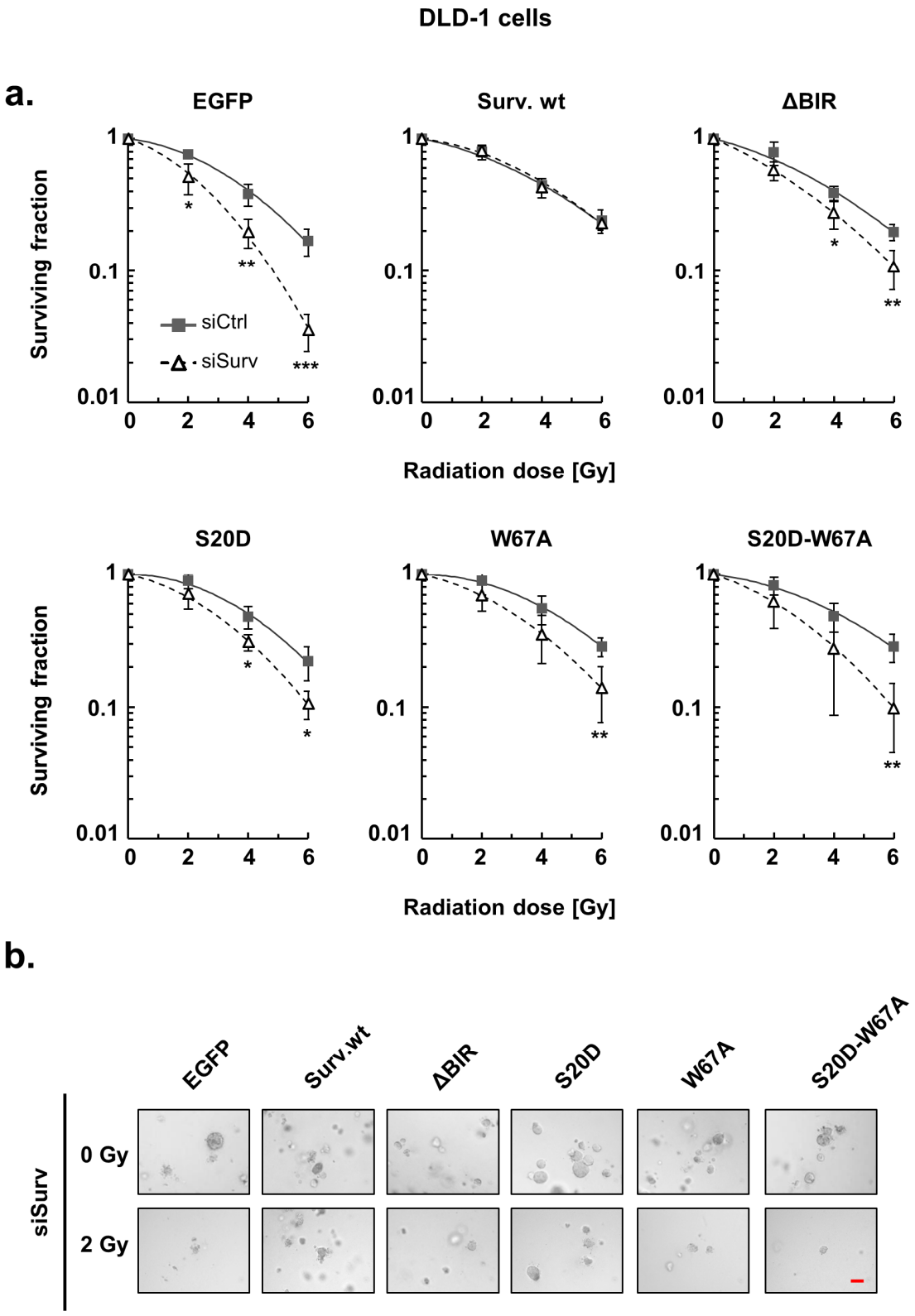

Figure 20. S20D, W67A, S20D-W67A and ΔBIR deletion mutant radiosensitize 3D-cultured DLD-1 colorectal cancer cells. (**a**) Clonogenic radiation survival of the EGFP, Surv. wt, BIR, S20D, W67A and S20D-W67A mutant-expressing DLD-1 3D cells after knockdown of endogenous Survivin (siSurv) or control siRNA (siCtrl) transfected cells were measured after irradiation with 0, 2, 4 or 6 Gy (single dose) using a 3D colony-forming assay. Results represent means ± SD ($n \geq 3$; * $p < 0.05$; ** $p < 0.01$; *** $p < 0.001$; t-test). (**b**) Representative pictures of 3D DLD-1 cell colonies (Axio Observer Z1; 10x objective). Scale bar: 100 μm.

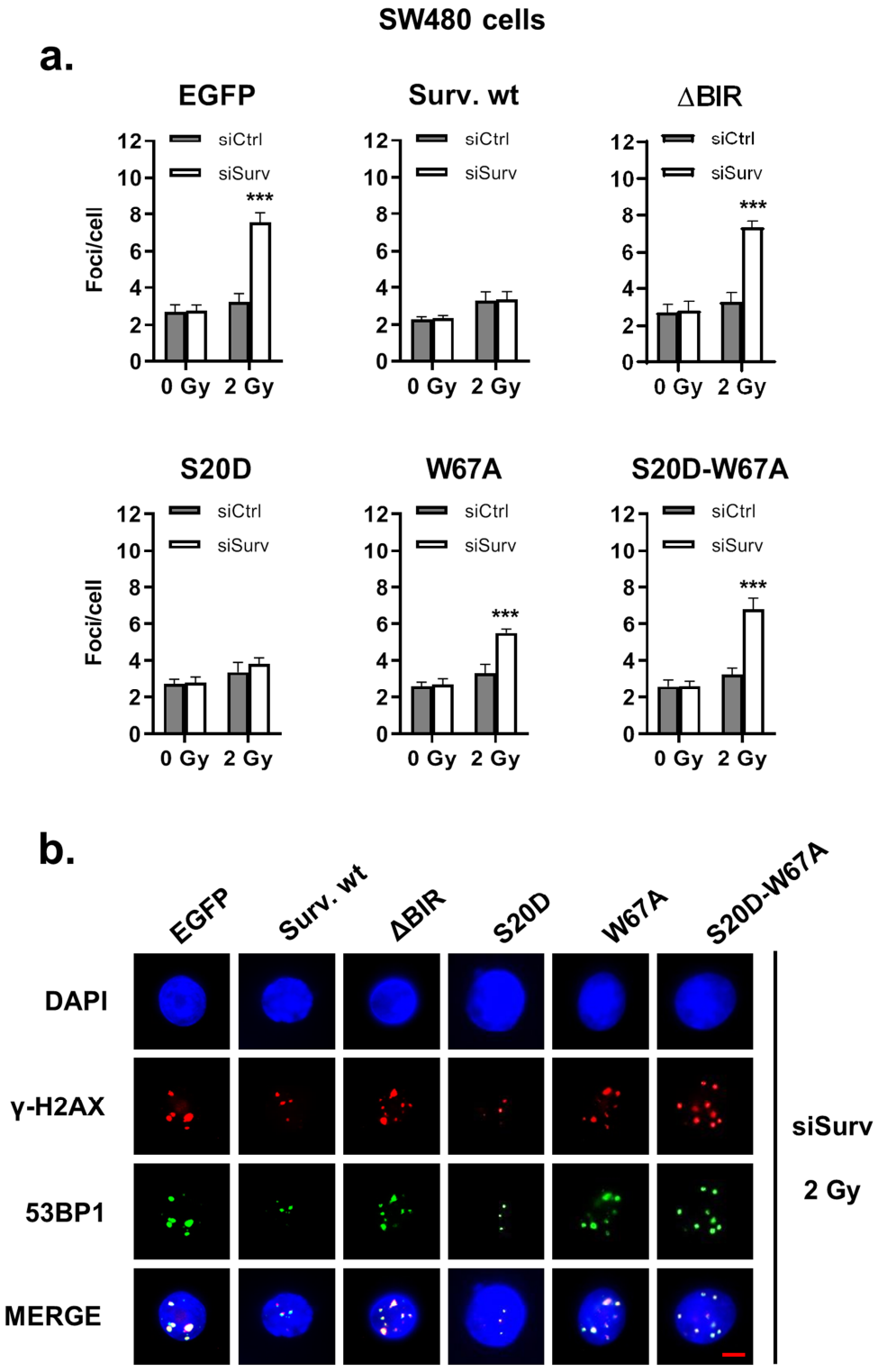

Figure 21. W67A, S20D-W67A mutation and ΔBIR deletion hamper the radiation-induced DNA repair in 3D-cultured SW480 colorectal cancer cells. (**a**) SW480 cells, stably expressing indicated Survivin mutants were subjected to siRNA transfection (siCtrl, non-specific control siRNA; siSurv, Survivin siRNA) and subsequently irradiated with 2 Gy. At 24 h after irradiation, cells were fixed and stained for γH2AX/53BP1 while nuclei were counterstained with DAPI. Nuclear γH2AX/53BP1 foci were microscopically counted (50 nuclei per experiment). Results represent mean foci per cell ± SD (n ≥ 3; *** $p < 0.001$; t-test). (**b**) Representative microscopic pictures of foci detection 24 h after 2 Gy irradiation of 3D SW480 cells under indicated conditions (Zeiss Axio Imager A1; 63x objective). Scale bar: 5 μm.

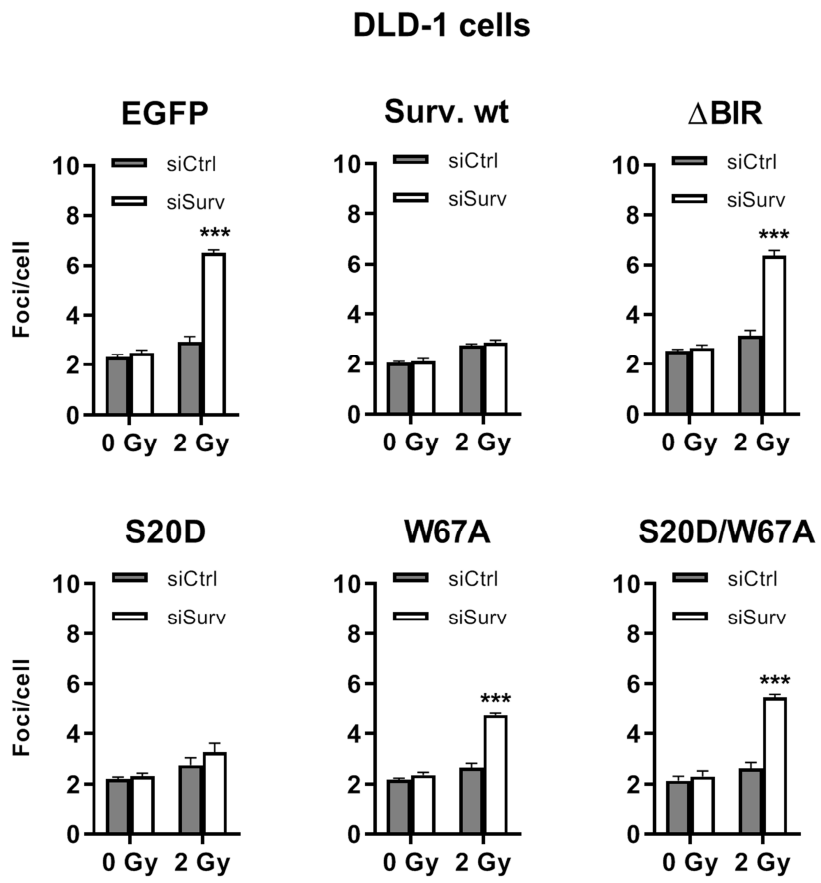

Figure 22. W67A single, S20D-W67A double mutation and ΔBIR deletion hamper the radiation-induced DNA repair in 3D-cultured DLD-1 colorectal cancer cells. DLD-1 colorectal cancer cells, stably expressing indicated Survivin mutants were subjected to siRNA transfection (siCtrl, non-specific control siRNA; siSurv, Survivin siRNA) and subsequently irradiated with 2 Gy. At 24 h after irradiation, cells were fixed and stained for γH2AX/53BP1 while nuclei were counterstained with DAPI. Nuclear γH2AX/53BP1 foci were microscopically counted (50 nuclei per experiment). Results represent mean foci per cell ± SD (n ≥ 3; *** $p < 0.001$; t-test).

4.6. Molecular docking and molecular dynamics simulations suggest a heterotetramer complex of Survivin-DNA-PKcs interaction

Given that the previous docking approach (~150 poses, **Figure 12**) indicate two prominent poses, placing S20 and W67 in close proximity to the PI3K region of DNA-PKcs, next an extended interaction analysis in a broader scale docking (~100k poses) was performed. By this, the minimum distance $d_{BIR} = min\{|\vec{x} - \vec{y}| : x \in \mathcal{R}_{PI3K}, y \in \mathcal{R}_{\mathcal{BIR}}\}$ between any docked Survivin BIR domain and the entire PI3K region atoms was calculated. Here $\mathcal{R}_{PI3K}$ is the collection of atom coordinates from the PI3K site and $\mathcal{R}_{\mathcal{BIR}}$ is the collection of atom coordinates from the docked Survivin BIR domain. The minimum distance between any of these atoms covers a sensible distance measure for examining if and what extent these domains touch.

The two-dimensional histograms indicate the distribution of the molecular distances and interface scores of large-scale molecular docking data between the Survivin BIR domain and PI3K domain of DNA-PKcs (**Figure 23a, 23b**). Histograms revealed the existence of two clusters concentrated on 20 to 40 Å (**Figure 23a**), and 1 to 2 Å (**Figure 23b**) distances. The

second cluster (**Figure 23b**) suggests the potential binding between the BIR and the PI3K domains. According to the preliminary molecular *in silico* approach and experimental findings in Figure 12, 16 and 17, respectively, large-scale global docking results were filtered for spatial proximity of S20 and W67 residues of Survivin to the PI3K domain of DNA-PKcs. Two differing states were found for S20 and W67, showing different configurations and orientations towards the PI3K domain (between 3747-4015 residues), while for geometrical constraints, it is not possible to fulfil both poses at the same time. Thus, a heterotetramer hypothesis was generated covering a structure requiring Survivin monomers within the dimer to interact with two head domains of DNA-PKcs by the help of S20 and W67 residues, which fulfils the spatial constraints (**Figure 23c**). The generated heterotetramer structure also incorporates an interface between the FKBP-rapamycin-binding (FRB) (between 3540-3746 residues, located between FAT and PI3K domains) and FAT (between 2906-3539 residues) domains of two head domains independent of Survivin binding (head-dimer). To experimentally confirm the live-cell occurrence of the predicted heterotetramer complex interaction, a FACS-FRET assay was employed. Briefly, SW480 cells were co-transfected with ECFP and EYFP fusion constructs of recombinant PI3K domain under different conditions, additional transfection of mock, control siRNA, Survivin siRNA or Survivin-Flag construct respectively. The PI3K domain indicates a clear dimerization in mock as well as control siRNA transfected conditions while the condition with Survivin siRNA did not show changes. Most importantly, Survivin overexpression (Survivin-Flag construct transfected) revealed a significant enhancement of ~40% on the dimerization of the PI3K domain of DNA-PKcs (**Figure 23d**). Furthermore, as mentioned before, it was observed by the *in silico* approach that dimerization of the PI3K domain without Survivin (head-dimer) was well-fitting to the FRB – FAT interface. These findings suggested that the heterotetramer can be produced by Survivin binding to a pre-existing DNA-PKcs dimer.

To confirm the energetic suitability of the heterotetramer structure, three individual molecular dynamics simulations were performed on heterotetramer, head-dimer and a reference model. All simulations are illustrated as animations in the weblinks given at **Section 3.2.8**. The head-dimer produced by deletion of Survivin from the heterotetramer structure consisted of two head domains interacting via the FRB and FAT regions. The reference model covers the result of an *in-silico* docking of two identical sites within DNA-PKcs, known as the FRB Domain. Since the FRB domain is a small sub-domain not located within the PI3K region, which was concluded that potential structural changes due to kinase dimerization cannot be observed in this model. The heterotetramer convergence in RMSD was observed for both head domains (Chain A and D) after ~50ns, although Chain A stabilized much faster (**Figure 24a**). The reference model showed a different behaviour compared to the other two models in both, RMSD and radius of gyration in the case of chain D (**Figure 24a, 24b**). The RMSD was stable for Survivin Chain B where S20 was in proximity to the PI3K domain (**Figure 24c**). In particular, Survivin Chain C, where W67 was in proximity to the PI3K domain, shows deviations between 30ns – 80ns for both RMSD and radius of gyration, suggesting potential structural changes (**Figure 24c, 24d**). The RMSD and radius of gyration results of the head-dimer were essentially identical to the heterotetramer for both head domains (Chain A and D).

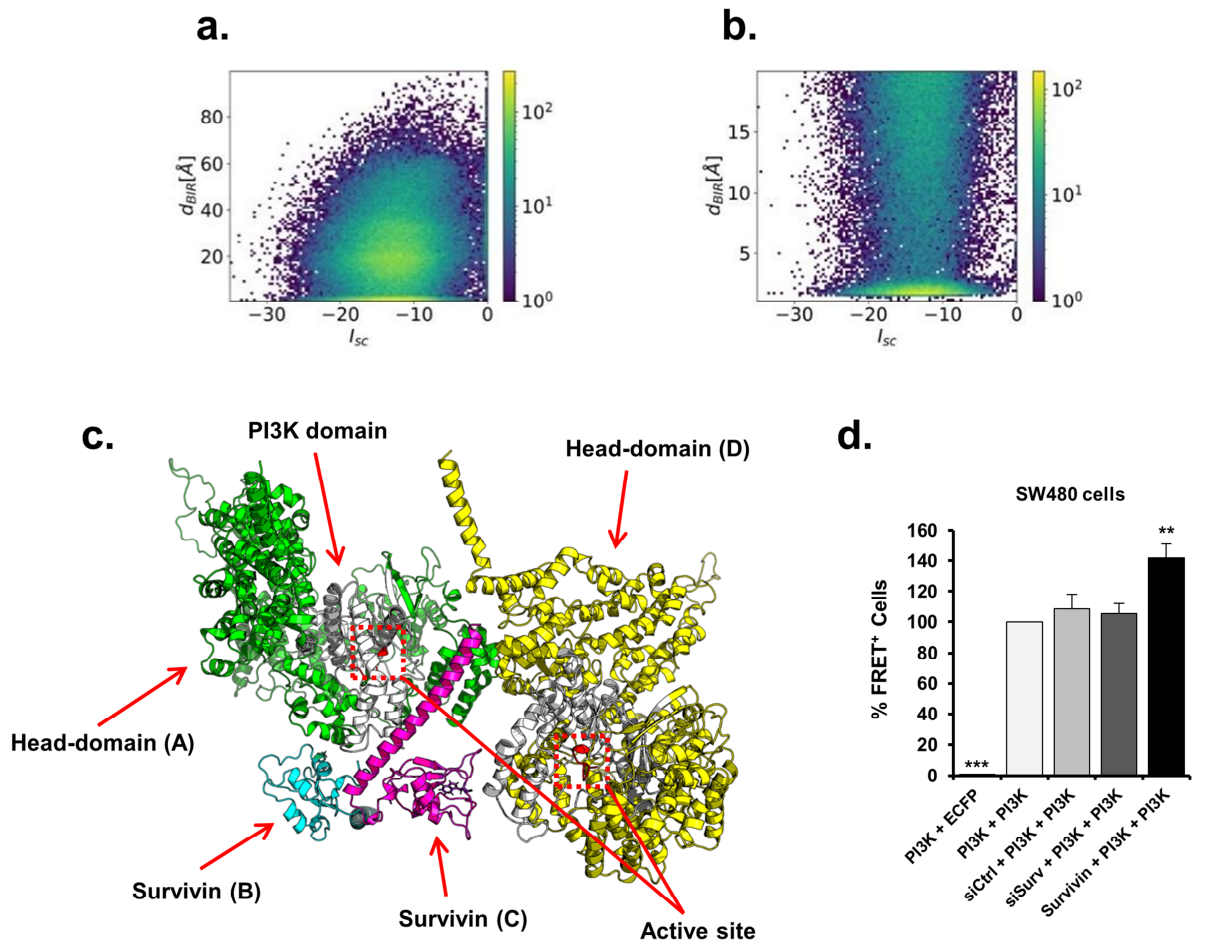

Figure 23. ***In silico*** **molecular docking results in a DNA-PKcs – Survivin – DNA-PKcs heterotetramer complex.** **(a)** Two-dimensional distribution for distance to active site d_{BIR} [Å] for any BIR atom in poses, versus interface score I_{sc}, quantifying the quality of docking poses. **(b)** Next to the region where BIR domain atoms are at least within 20 Å of the PI3K domain ($d_{BIR} \leq 20$), is shown to emphasize the BIR – PI3K interaction. **(c)** Filtering the large-scale docking results unravelled two docking poses. Aligning these poses on Survivin minimizes the distance between residues W67, S20 and the PI3K domain in DNA-PKcs. This results in the constitution of a heterotetramer complex whose constituents are Chain A head domain (green), Chain B Survivin (cyan), Chain C Survivin (purple), Chain D head domain (yellow), PI3K domains of both head domains (white), and active sites (red) depicted in relevant colors. **(d)** Experimental confirmation of the heterotetramer complex interaction assayed by FACS-FRET methodology. Briefly, SW480 cells were co-transfected with ECFP and EYFP fusion constructs of recombinant PI3K domain under different conditions by additional transfection of mock, control siRNA, Survivin siRNA, or Survivin-Flag construct respectively. Survivin overexpression was significantly enhanced, while knockdown of endogenous Survivin was not hampering the dimerization of PI3K domain. Results represent mean ± SD (n = 4; * $p < 0.05$; ** $p < 0.01$; *** $p < 0.001$; t-test)

The particle density for Chain A of the reference model was almost constant, while Chain D exhibited a downward trend after 50ns suggesting a partial opening of active site cavity. The head dimer showed a downward trend till ~150ns and shows a favourable opening of the active site for both chains. The heterotetramer exhibited far greater surface accessibility for chain D, while density for chain A was almost constant (**Figure 25a**). Particularly active site region of heterotetramer structure Chain D (green line) was clearly diverging (**Figure 25a**)

and resulted in a more accessible active site region (red in **Figure 25b** and 25**c**) at the simulation end (**Figure 25c**) compared to the beginning (**Figure 25b**).

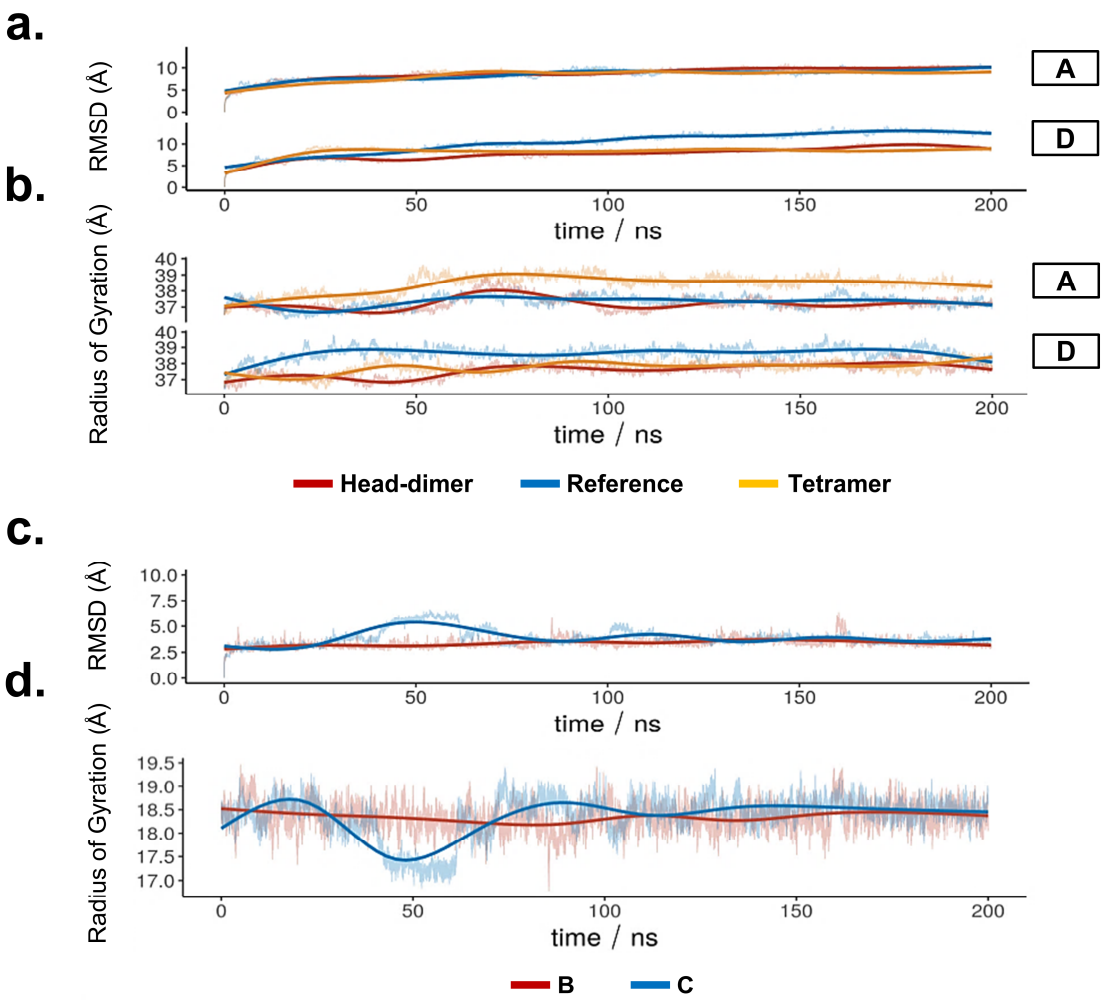

Figure 24. RMSD and radius of gyration of heterotetramer complex are predominantly stable over the molecular dynamics simulation. (**a**) RMSD atomic position and (**b**) radius of gyration analyses during the MD simulations of heterotetramer (red), head dimer (blue), and reference model (orange) structures over the course of 200 ns simulation time. (**c**) RMSD atomic position and (**d**) radius of gyration analyses during the MD simulations of Survivin chain B (red) and chain C (blue) structures over the course of 200 ns simulation time.

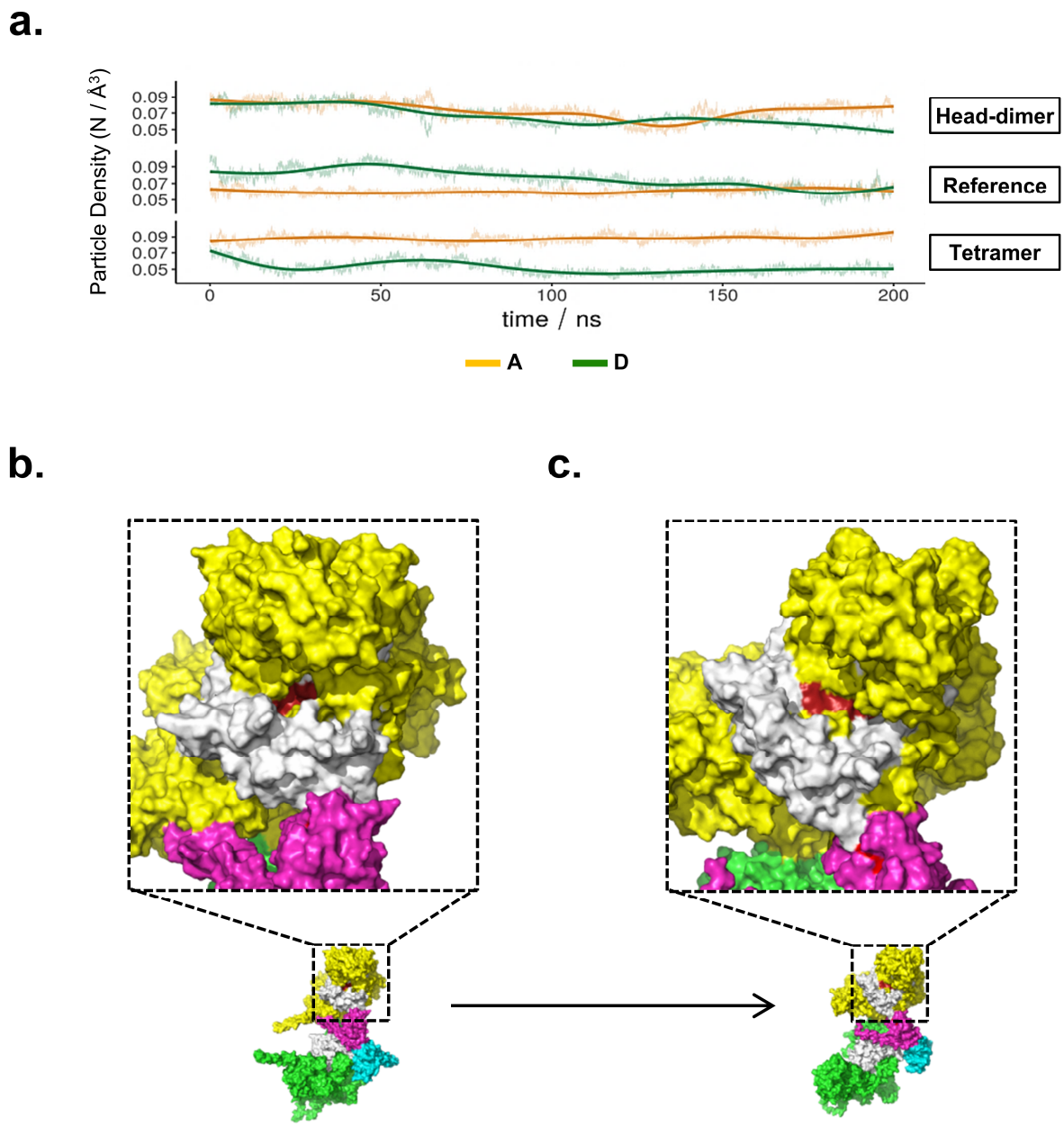

Figure 25. Particle density analysis revealed a heterotetramer complex with increased accessibility for the active site of the PI3K domain. (**a**) Particle density analysis of the atoms located above the active site region of PI3K domain for both chains A (orange) and D (green). (**b**) Visualization of the energy minimized and equilibrated heterotetramer at the start of MD simulation revealed relatively closed active site cavity, (**c**) while it became more accessible at the end of the simulation, (Colors: Chain A head domain (green), Chain B Survivin (cyan), Chain C Survivin (purple), Chain D head domain (yellow), PI3K domains of both head domains (white) and active sites (red)).

4.7. Survivin enhances the kinase activity of DNA-PKcs

To quantify the effect of Survivin binding on the kinase activity of DNA-PKcs, an *in vitro* methodology by modifying the SignaTECT DNA-Dependent Protein Kinase Assay System was designed. Stably EGFP or EGFP-tagged Survivin expressing SW480 cells were depleted for endogenous Survivin by siRNA-treatment. Next, immunoprecipitations were performed by using GFP antibody and densitometrically equal amounts of proteins were added into the

kinase reactions. Radioactive phosphor-quantification results indicate that the presence of Surv.wt significantly increased the kinase activity ~45% (**Figure 26**).

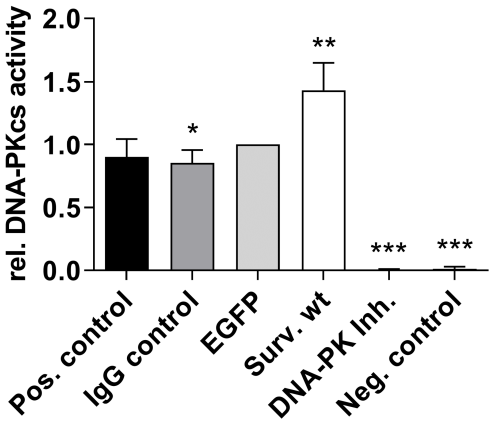

Figure 26. Survivin enhances the kinase activity of DNA-PKcs. Effect of Survivin on the kinase activity of DNA-PKcs was assayed by using the SignaTECT DNA-Dependent Protein Kinase Assay System and purified DNA-PK. SW480 cells stably expressing EGFP or Surv-EGFP were subjected to Survivin siRNA transfection and subsequently irradiated with 4 Gy. At 1 h after irradiation, cells were lysed and immunoprecipitation was performed with an EGFP antibody or IgG rabbit antibody. Densitometrically equal amounts of immunoprecipitated proteins were added to *in vitro* DNA-PKcs kinase reaction tubes and after kinase reaction probed to the membrane (provided by the kit) and exposition quantified with a Phosphoimager. Results represent means ± SD (n≥4; * $p < 0.05$; ** $p < 0.01$; *** $p < 0.001$; t-test vs. EGFP), (Abbreviations: *Pos. control*, DNA-PK + substrate peptide; *IgG control*, DNA-PK + substrate peptide + IgG pull-down; *EGFP*, DNA-PK + substrate peptide + EGFP pull-down; *Surv. wt*, DNA-PK + substrate peptide + Surv. wt pull-down; *DNA-PK Inh.*, DNA-PK + substrate peptide + DNA-PK inhibitor (1μM); *Neg. control*, DNA-PK).

4.8. Phosphoproteomics and proteomics approaches revealed post-translational phospho-regulatory and translational expression-regulatory functions of Survivin-DNA-PKcs interaction

Due to the enhanced kinase activity of DNA-PKcs in the presence of Survivin in the *in vitro* kinase reaction, next a putative regulatory function of Survivin on the phosphorylation status of the substrates of DNA-PKcs was addressed by performing LC-MS2 and LC-MS3 phosphoproteomics and proteomics analyses, respectively. The experimental setup consists of five conditions such as DNA-PK inhibitor treatment (*DNA-PK inh.*), mock (si*Ctrl*), endogenous Survivin knockdown (*siSurv*), EGFP overexpression (*EGFP*), and Survivin-EGFP overexpression (*Surv-EGFP*), accompanied by control siRNA or Survivin siRNA treatments. For the evaluation of experimental setup conditions, we have defined three comparison conditions, *DNA-PK inh. vs. siCtrl*, *siSurv vs. siCtrl*, and *Surv-EGFP vs. EGFP* (**Figure 27**). To classify the regulatory effect, we have defined two hypotheses by applying certain Log_2 fold change thresholds, naming as *direct* or *inverse* (*inverse* is for proteomics) effect. In the direct effect hypothesis, an increased phosphorylation/expression of phosphosites/proteins upon overexpression of Survivin and decreased phosphorylation/expression upon endogenous Survivin knockdown and DNA-PK inhibitor treatment was expected. In contrast, for the inverse effect hypothesis, a decreased expression of proteins upon overexpression of Survivin and increased expression upon endogenous Survivin knockdown and DNA-PK inhibitor

treatment was expected. For the direct effect mechanism, Log_2 fold change thresholds were set as [≤ -0.25], [≤ -0.25], and [≥ 0.25] for DNA-PK inh. vs. siCtrl, siSurv vs. siCtrl, and Surv-EGFP vs. EGFP evaluation conditions, respectively. For the inverse mechanism, Log_2 fold change thresholds were defined as [≥ 0.25], [≥ 0.25], and [≤ -0.25] for DNA-PK inh. vs. siCtrl, siSurv vs. siCtrl, and Surv-EGFP vs. EGFP evaluation conditions, respectively.

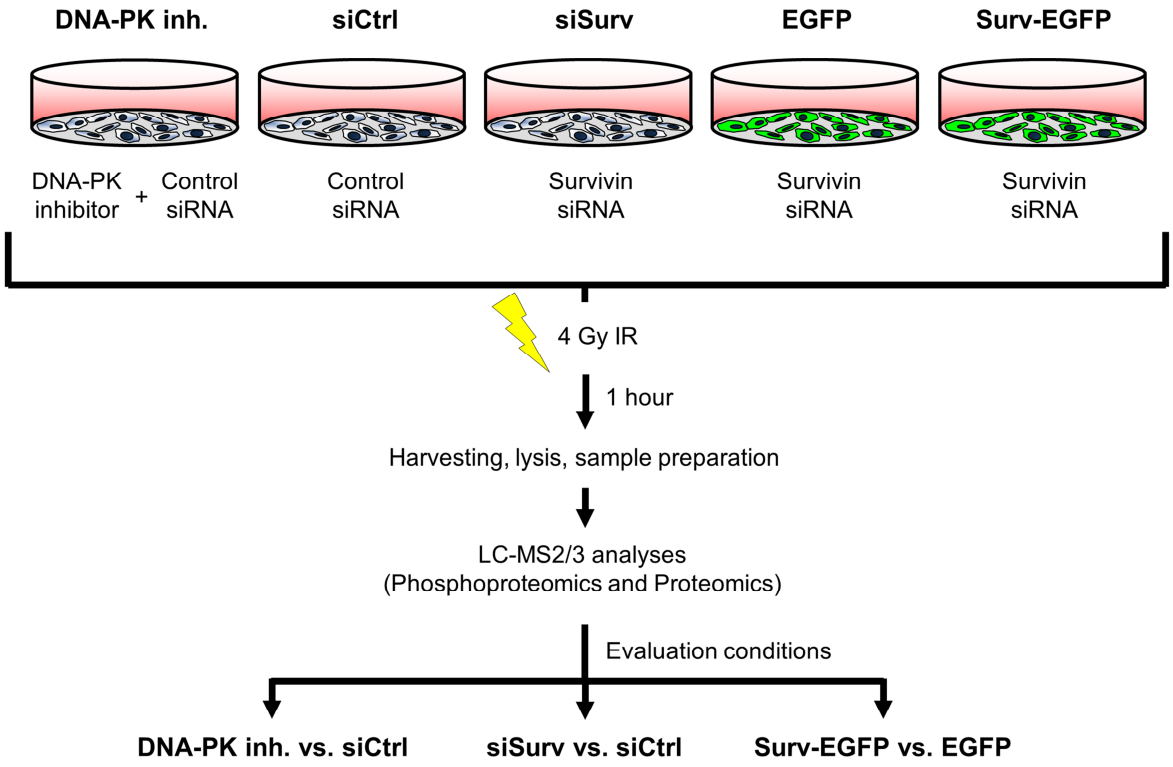

Figure 27. Schematic representation of the experimental setup and workflow of phosphoproteomics and proteomics analyses. Briefly, SW480 colorectal cancer cells, including EGFP and Surv-EGFP stably expressing cells, were transfected with control siRNA or Survivin siRNA. For DNA-PK inhibitor conditions, cells were further treated with DNA-PK inhibitor (1 h before irradiation). All cultures were irradiated with 4 Gy. At 1 h after irradiation, cells were harvested, lyzed, and samples were prepared for MS analyses. Subsequently, phosphoproteomics –LC-MS2– and proteomics –LC-MS3– analyses were performed and evaluations were carried out considering three comparisons: DNA-PK inh. vs. Ctrl, siSurv vs. Ctrl, Surv-EGFP vs. EGFP. Two independent experiments have been performed.

4.8.1. Phosphoproteomics analysis

Evaluation conditions yielded over 16 thousand phosphosites, which clustered by hierarchical clustering method with default Euclidean distance. The analysis revealed a similar clustering of the evaluation conditions of both separate experiments (**Figure 28**).

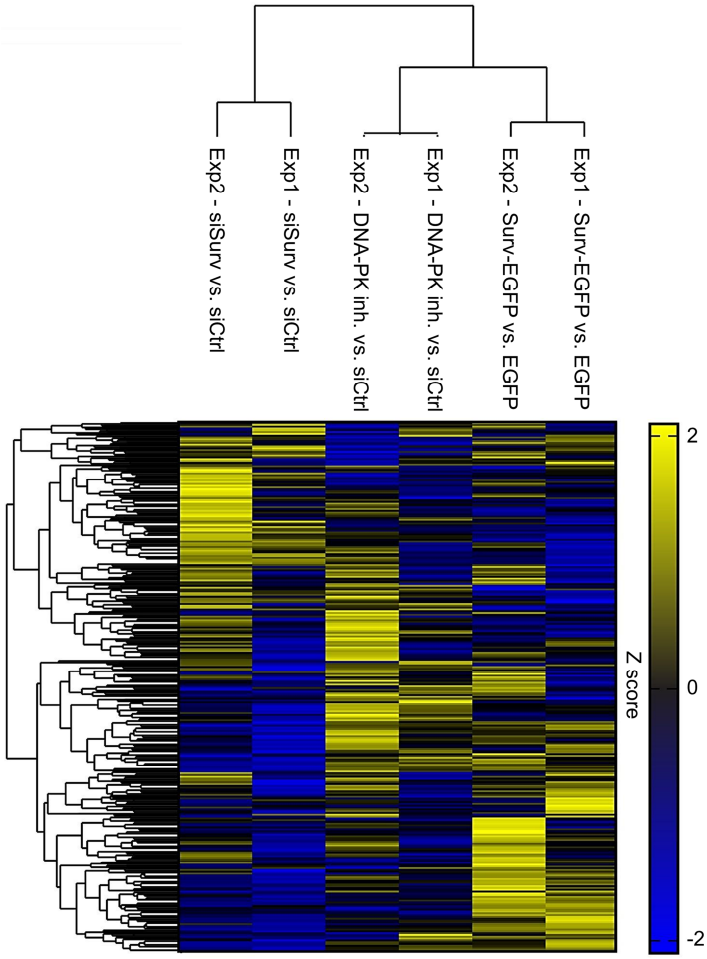

Figure 28. Hierarchical clustering of phosphoproteomics conditions. LC-MS2 quantification of TMT-labeled, phospho-enriched, and fractionated phospho-peptides revealed a similarly clustered differential phosphorylation profile of phosphosites. Computation of Z scores are derived from the centered data by dividing by the standard deviations.

All phosphosites were next displayed in a volcano plot by setting Log_2 fold change thresholds of effect mechanisms of siSurv vs. siCtrl and Surv-EGFP vs. EGFP evaluation conditions (**Figure 29a**). The qualified portion of regulated phosphosites (orange-colored in Figure 29a) were used as input for another volcano plot distribution to also consider the effect of DNA-PK inhibitor by setting Log_2 fold change thresholds of effect mechanism of DNA-PK inh. vs. siCtrl evaluation condition (**Figure 29b**).

The second-step qualified portion of regulated phosphosites (orange-colored in Figure 29b) were normalized with the related proteome data, then fold changes were represented in a heatmap graph (**Figure 30a**). Pathway analysis of regulated phosphosites revealed predominant involvement in DNA damage/repair, as well as in chromosome organization, cell cycle, (post)-transcriptional regulation, apoptosis, adhesion and ion transport (**Figure 30b**).

Particularly, FOXO3 is one of the notable candidates which has both direct (Shiga et al., 2020) and indirect (Barragan et al., 2006; Carew et al., 2011; Chen et al., 2007b; Haque et al., 2015; Niedan et al., 2014; Singh et al., 2010; Zheng et al., 2000) relationships with DNA damage/repair and DNA-PKcs. For validation purposes, the phosphorylation status of FOXO3 S253 residue was analysed by western immunoblot. Data given in **Figure 31** indicate that in

response to Survivin overexpression, the phosphorylation status of FOXO3 S253 was increased by 64% compared to EGFP control while in response to DNA-PK inhibitor treatment, the phosphorylation was decreased by 55% compared to siCtrl conditions in SW480 cells. These findings suggested that particularly an increase in the phosphorylation status of FOXO3 S253 residue was both Survivin and DNA-PK activity-dependent while a decrease was Survivin-independent.

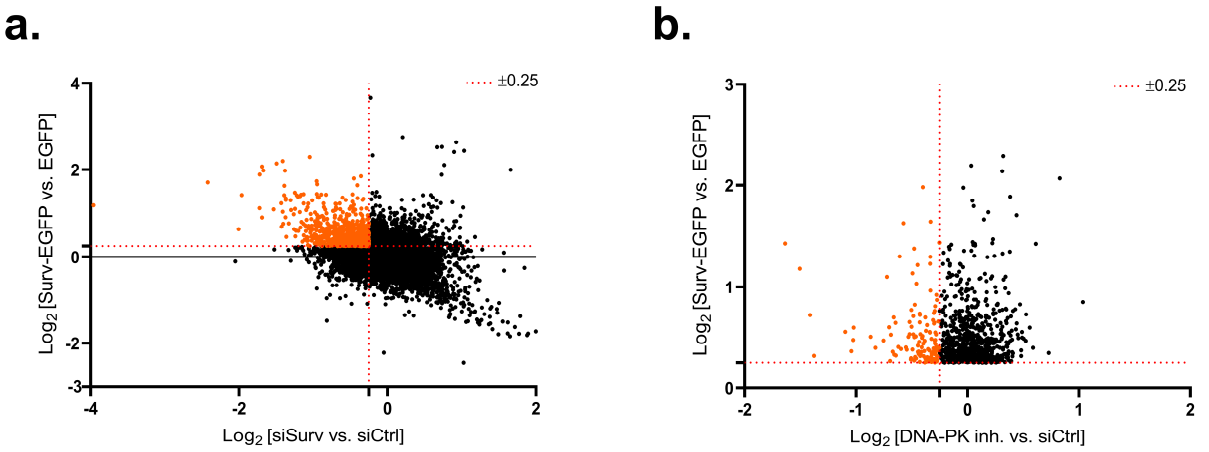

Figure 29. Qualification of phosphoproteomics candidates. (**a**) Analysis of directly (orange) regulated hits by setting Log_2 fold change cut-offs as follows: [≥ 0.25] for Surv-EGFP vs. EGFP, [≤ -0.25] for DNA-PK inh. vs. siCtrl and siSurv vs. siCtrl conditions by comparative distribution representations of the status of phosphosites as Volcano plot graphics. (**b**) Qualified phosphosites (orange-colored in Figure 29a) were used as input for further analysis to consider also the effect of DNA-PK inhibitor. Results represent mean Log_2 fold change value (n=2).

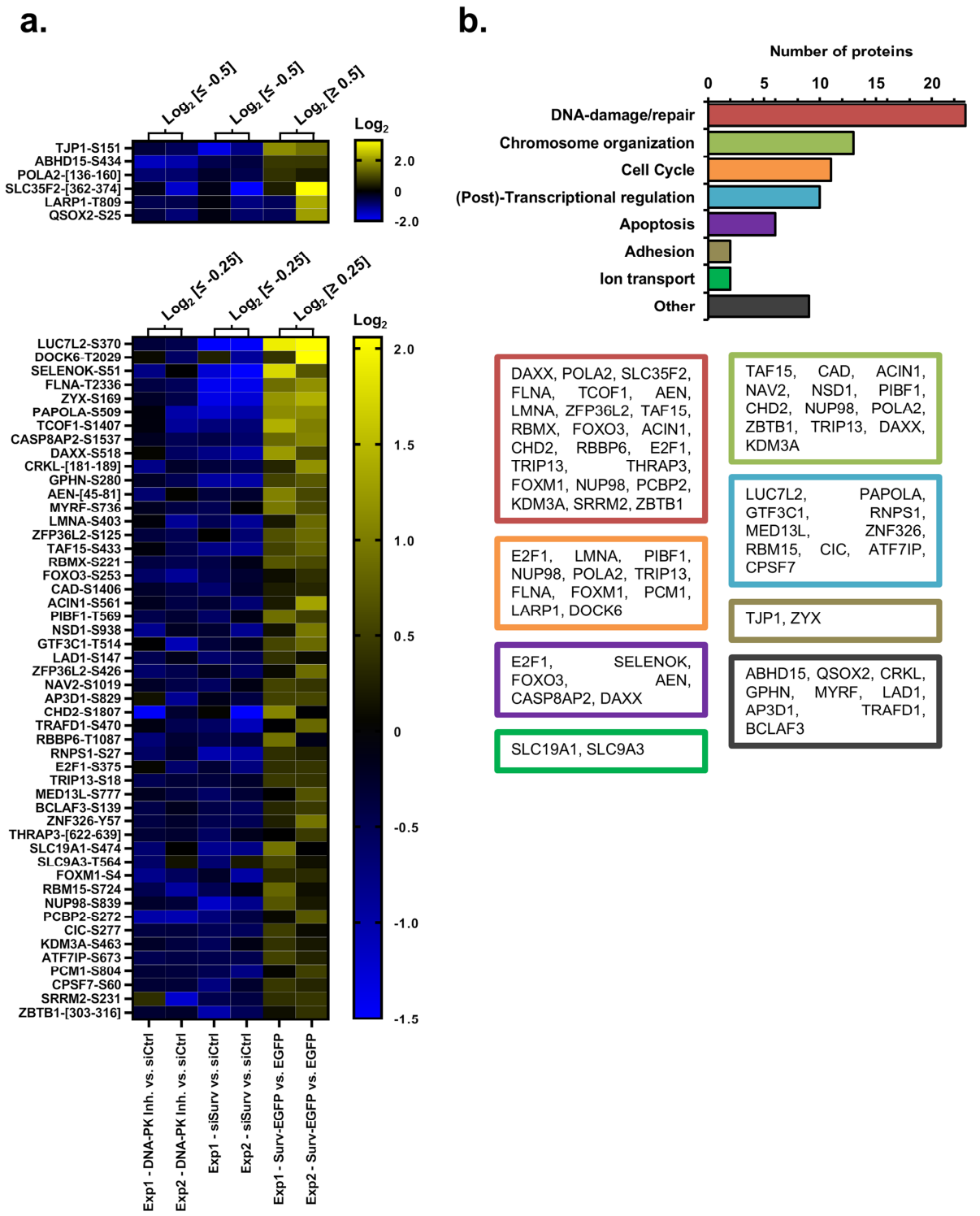

Figure 30. Regulated final candidate phosphosites. (**a**) The final set of regulated phosphosites (orange-colored in Figure 29b) were normalized with proteome data then presented by two heatmap graphs; first with high Log_2 fold change cut-offs [≤ -0.5], [≤ -0.5] and [≥ 0.5], second with low Log_2 fold change cut-offs [≤ -0.25], [≤ -0.25] and [≥ 0.25] for DNA-PK inh. vs. siCtrl, siSurv vs. siCtrl and Surv-EGFP vs. EGFP, respectively. (**b**) Pathway analysis by considering Pathway Commons (https://www.pathwaycommons.org) terms and related individual studies from literature.

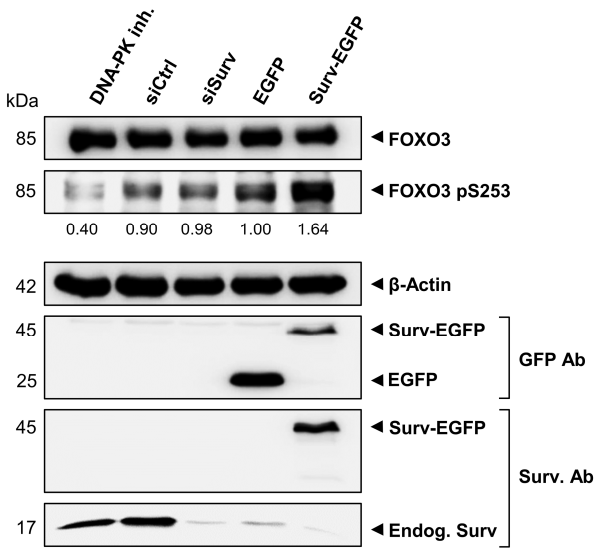

Figure 31. Western immunoblotting verification of FOXO3 S253 residue phosphorylation. Western immunoblotting revealed decreased phosphorylation of FOXO3 S253 residue in response to DNA-PK inhibitor and increased phosphorylation in response to Survivin overexpression in SW480 cells. (Abbreviations: DNA-PK inh, control siRNA + DNA-PK inhibitor treated (1μM). siCtrl, control siRNA treated. siSurv, Survivin siRNA treated. EGFP, Survivin siRNA + EGFP overexpression treated. Surv-EGFP, Survivin siRNA + Survivin-EGFP overexpression treated). Densitometric analysis performed by Analysis module of LI-COR Image Studio™ Software ver. 5.2.5.

Next, regulated phosphosites (**Figure 30a**) were further analyzed for a potential consensus phosphorylation motif and for this purpose, amino acid sequence profile alignment and weighted logo generator Seq2Logo 2.0 Server (http://www.cbs.dtu.dk/biotools/Seq2Logo/) was employed. Consensus motif analysis of phosphosites revealed high conservation of S/T-Hydr motifs (hydrophobic residues: G, A, V, L, I, P, F, M, W) with 60.5%, particularly high conservation on S/T-P motif with 33.3% including FOXO3 S253, *flna*/Filamin-A T2336. Interestingly, the well-known DNA-PKcs phosphorylation motif S/T-Q was conserved only in 1.2% (**Figure 32**). Besides, in addition to the well-known consensus phosphorylation motif (S/T-Q), the enrichment of S/T-P motif was also previously found in response to DNA damage (Bennetzen et al., 2010).

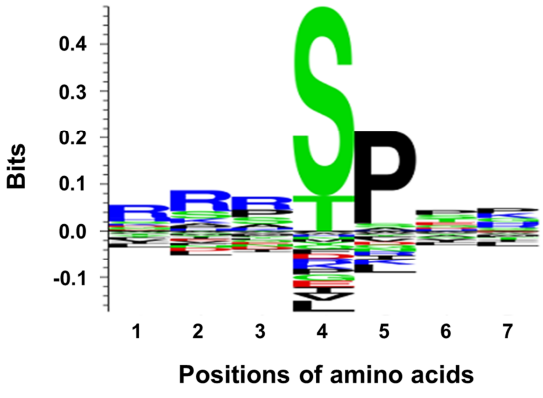

Figure 32. Consensus motif analysis of final candidate phosphosites revealed a highly conserved S/T-P motif. Bits states the information content units as the weighted prevalence frequency of indicated motif generated by Seq2Logo. The input motifs were used from the hits in Figure 30a. Generation of logo based on ‚Probability Weighted Kullback-Leibler´ logo type and Hobohm algorithm for sequence weighting type).

4.8.2. Proteomics analysis

Proteomics analyses performed in parallel to the phosphoproteomics assessment as reported before revealed differential expression of proteins in response to Survivin overexpression as well as Survivin knockdown and DNA-PK inhibitor treatment. Evaluation conditions yielded over 7 thousand peptides/proteins which clustered by the hierarchical clustering method with default Euclidean distance. The analysis revealed a similar clustering of the evaluation conditions of both experiments (**Figure 33**).

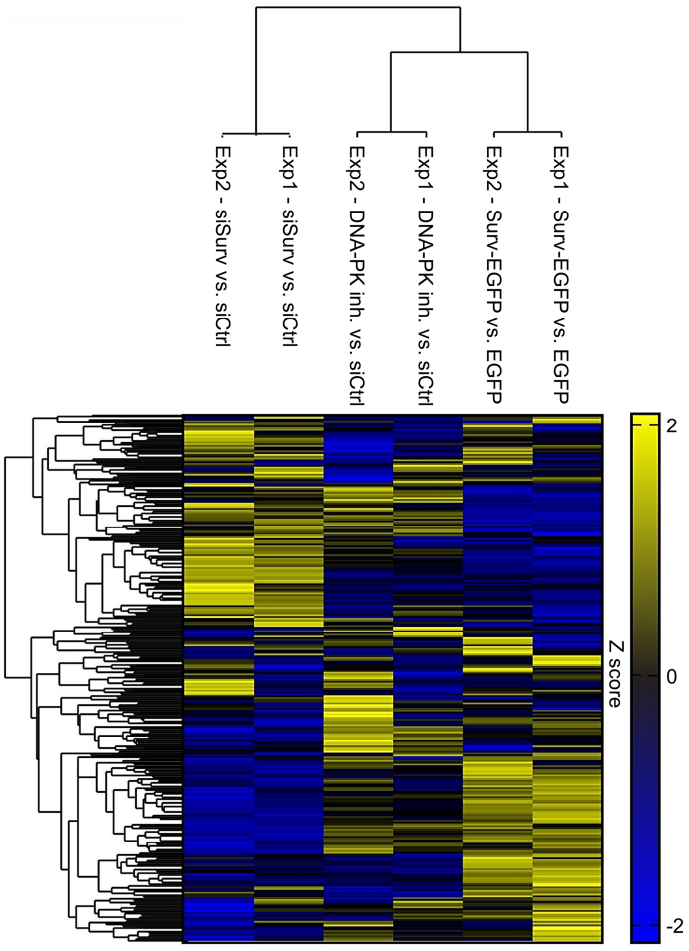

Figure 33. Hierarchical clustering of proteomics conditions. LC-MS3 quantification of TMT-labeled and fractionated peptides revealed a similarly clustered differential expression profile of proteins.

All proteins were distributed in a volcano plot, and sorted by setting Log_2 fold change thresholds of directly and inversely regulated proteins of siSurv vs. siCtrl and Surv-EGFP vs. EGFP conditions (**Figure 34a**). The qualified portion of directly (orange-colored in Figure 34a), and inversely (purple-colored in Figure 34a) regulated proteins were used as input for a volcano plot distribution to consider the effect of DNA-PK inhibitor by setting Log_2 fold change thresholds of DNA-PK inh. vs. siCtrl evaluation condition (**Figure 34b**).

Next, the fold changes of the second-step qualified portion of regulated proteins were represented in two separate heatmap graphs as directly (**Figure 35a**) and inversely (**Figure 35b**) regulated final candidate proteins. Notably, both directly and inversely regulated

candidate proteins are predominantly involved in DNA damage/repair (labeled with asterisk (*), **Figure 35**).

It was previously shown that DNA-PKcs has a remarkable modulatory function on gene expression of proteins via regulating transcription (Goodwin et al., 2015; Woodard et al., 1999). However, there was no clear statement about the role of the activity of DNA-PKcs on transcriptional regulation except a study which suggested a potential limited gene-specific transcriptional regulatory function may depend on the activity of DNA-PKcs (Bryntesson et al., 2001). According to our findings, the activity of DNA-PKcs seems to have an expressional regulatory role on a variety of proteins. The directly regulated proteins (**Figure 35a**) mainly involved in DNA damage/repair including proteins like cell division cycle associated 2 (*cdca2*/Repo-Man) (Peng et al., 2010), regulator of sister chromatid separation (*pttg1*/Securin) (Mjelle et al., 2015), sumo specific peptidase 5 (SENP5) (Jin et al., 2016), stimulated by retinoic acid gene 13 protein (STRA13) (Thin et al., 2007), and DNA topoisomerase II alpha (TOP2A) (de Campos-Nebel et al., 2010; Morimoto et al., 2019). Particularly, *cdca2*/Repo-Man plays a role in ATM activation (Peng et al., 2010), while SENP5 is involved in ATRIP inhibition (Jin et al., 2016) that suggest potential inhibitory roles of Survivin and DNA-PKcs on ATM and ATR-dependent pathways via regulating the expressions of *cdca2*/Repo-Man and SENP5.

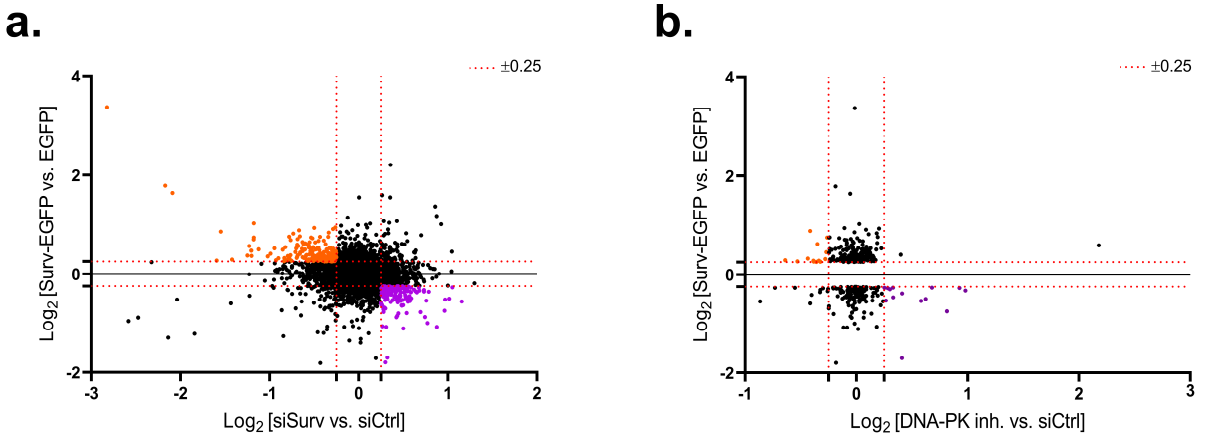

Figure 34. Qualification of proteomics candidates. (**a**) Analysis of directly (orange) and inversely (purple) regulated hits by setting Log_2 fold change cut-offs as followed: Directly regulated hits, [≥ 0.25] for Surv-EGFP vs. EGFP, [≤ -0.25] for DNA-PK inh. vs. siCtrl and siSurv vs. siCtrl; inversely regulated hits, [≤ -0.25] for Surv-EGFP vs. EGFP, [≥ 0.25] for DNA-PK inh. vs. siCtrl and siSurv vs. siCtrl conditions by comparative distribution representations of the status of expression as Volcano plot graphics. (**b**) Qualified proteins (orange and purple colored in Figure 34a) used as input for further qualification to consider also the effect of DNA-PK inhibitor. Results represent mean Log_2 fold change value (n = 2).

Interestingly, the inversely regulated proteins (**Figure 35b**) such as HIRA interacting protein 3 (HIRIP3), retinoblastoma binding protein 8 (*rbbp8*/CtIP), high mobility group at-hook (HMGA) and high mobility group nucleosome binding domain (HMGN) family members (HMGA1, HMGA2, HMGN1, HMGN2 and HMGN5) are reported to be involved in DNA damage/repair. Studies revealed their particular involvement in HR and ATM/ATR dependent pathways (Adamson et al., 2012; Hoa et al., 2015; Kim et al., 2009; Makharashvili et al., 2014; Natarajan et al., 2013; Palmieri et al., 2011; Quennet et al., 2011; Singh et al., 2015;

Wang et al., 2018b) that suggest a potential inhibitory regulation role of Survivin and DNA-PKcs on HR and ATM/ATR dependent pathways.

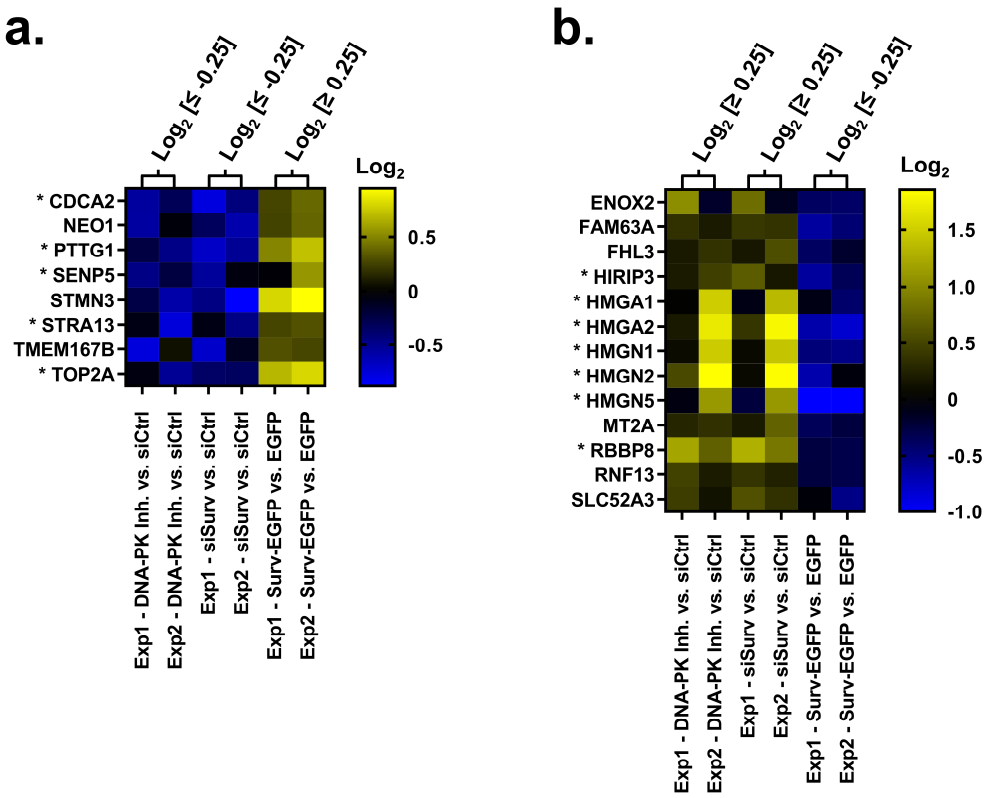

Figure 35. Directly and inversely regulated candidate proteins. (**a**) Final set of directly regulated proteins (orange-colored in Figure 34b) qualified by Log_2 fold change cut-offs [≤ -0.25], [≤ -0.25] and [≥ 0.25] for DNA-PK inh. vs. siCtrl, siSurv vs. siCtrl and Surv-EGFP vs. EGFP, respectively, are presented as heatmap graph. (**b**) The final set of inversely regulated proteins (purple colored in Figure 34b) qualified by Log_2 fold change cut-offs [≥ 0.25], [≥ 0.25], and [≤ -0.25] for DNA-PK inh. vs. siCtrl, siSurv vs. siCtrl, and Surv-EGFP vs. EGFP, respectively, are presented as heatmap graph. (asterisk (*) indicates the involvement in DNA damage/repair).

To specifically focus on the effect of Survivin overexpression and knockdown, we classified the qualified proteins by employing a pairwise intersection matrix representation considering different cut-off Log_2 values. For the directly (orange-colored in Figure 34a) and inversely (purple colored in Figure 34a) regulated proteins, Log_2 fold changes were determined as low [± 0.25], high [± 0.5] and highest [± 1.0] differentially regulated candidate proteins in response to Survivin overexpression and Survivin knockdown by representing the Log_2 fold change levels as heatmap graphs (**Figure 36**). The proteins directly (**Figure 36a**) or inversely (**Figure 36b**) regulated by only Survivin are involved in a variety of pathways: Directly regulated proteins are predominantly involved in the regulation of apoptosis, cell cycle, and DNA damage/repair while inversely regulated proteins participate in transcriptional repression, nucleolar reorganization, immune response, motility/invasiveness, and general cellular metabolism.

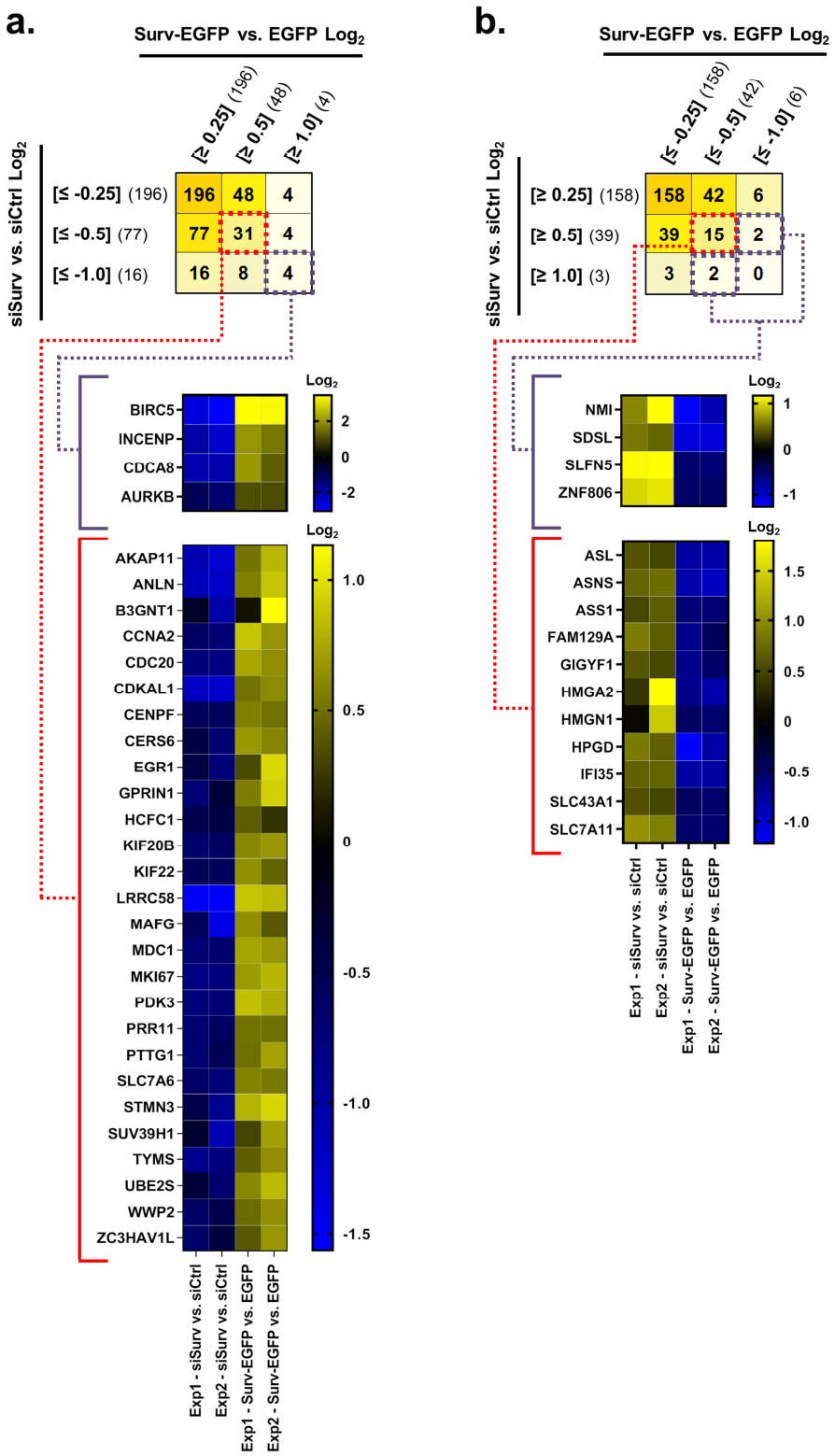

Figure 36. Directly and inversely Survivin-dependent regulated final candidate proteins. (a) Pairwise intersection matrix classifies directly regulated proteins (orange-colored in Figure 34a) by Log_2 fold changes as low [± 0.25], high [± 0.5] and highest [± 0.5] differentially expressed proteins in response to Survivin overexpression and Survivin knockdown by presenting the differential expression levels as heatmap graphs. (b) Pairwise intersection matrix classifies inversely regulated proteins (purple colored in Figure 34a) by Log_2 fold changes as low [± 0.25], high [± 0.5] and highest [± 0.5] differentially expressed proteins in response to Survivin overexpression and Survivin knockdown by presenting the differential expression levels as heatmap graphs.

4.9. Virtual screening approach to design an inhibitor aiming to prevent the interaction between Survivin and DNA-PKcs

Finally, analyses were performed to address the question whether Survivin-DNA-PKcs interaction is druggable. For that, a global virtual screening approach was performed by employing ~8 x 10^6 drug/drug-like ligands. Evaluation of candidates was based on four conditions: Attraction/interaction of ligand directly with S20 or W67 residue (via H-bond, Pi-Pi stacking, Pi-cation or Salt bridge), Virtual docking score (Extra Precision Glide docking score – XP Gscore), K_{DEEP} pK_d value –predicted dissociation constant– (ligand binding affinity), and ΔG binding free energy. The evaluation revealed a variety of candidate ligands for both S20 and W67 residues (**Table 11 and 12**). The top candidates for both S20 and W67 were used as representative figures (**Figure 37 and 38**). The surface of S20 and neighbouring residues is topologically less compatible for docking than the surface of W67 and neighbouring residues. This major restriction caused a limitation on the number of potential candidates and increased the XP Gscore for S20 targeting ligands. For this reason, the XP Gscore thresholds were set to ≤ -5.000 for S20, and ≤ -9.000 for W67. For S20 residue, M-000-631-284 labeled ligand was exhibiting the best XP GScore/pK_d/ΔG relative performance and hydrogen bonding directly with S20 residue (**Figure 37**). And for W67 residue, M-005-139-808 labeled ligand was displayed the best XP GScore/pK_d/ΔG relative performance and generated a direct Pi-cation attraction with W67 residue (**Figure 38**). Evaluation values suggest both candidates (Molport repository - M-000-631-284 and M-005-139-808 ligands) promise the potentials to target the related regions on Survivin efficiently.

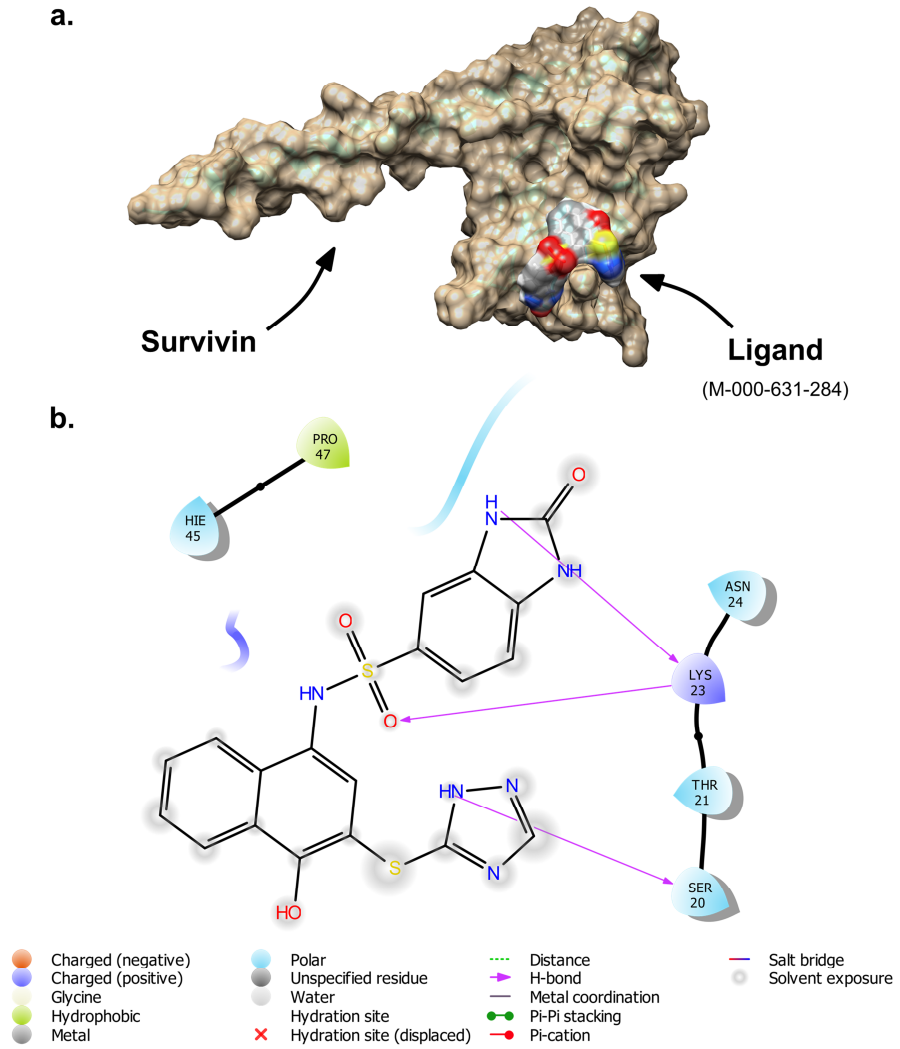

Figure 37. Docking of M-000-631-284 ligand into the S20 structural cavity. (**a**) Docking pose of Survivin and M-000-631-284 ligand as surface representation. The image was taken by Chimera version 1.14rc (Pettersen et al., 2004). (**b**) Direct hydrogen bonding between Survivin residues S20, K23 and M-000-631-284 ligand. The image was taken by Ligand Interaction Diagram - Maestro version 11.5 of Schrödinger Release 2018-1.

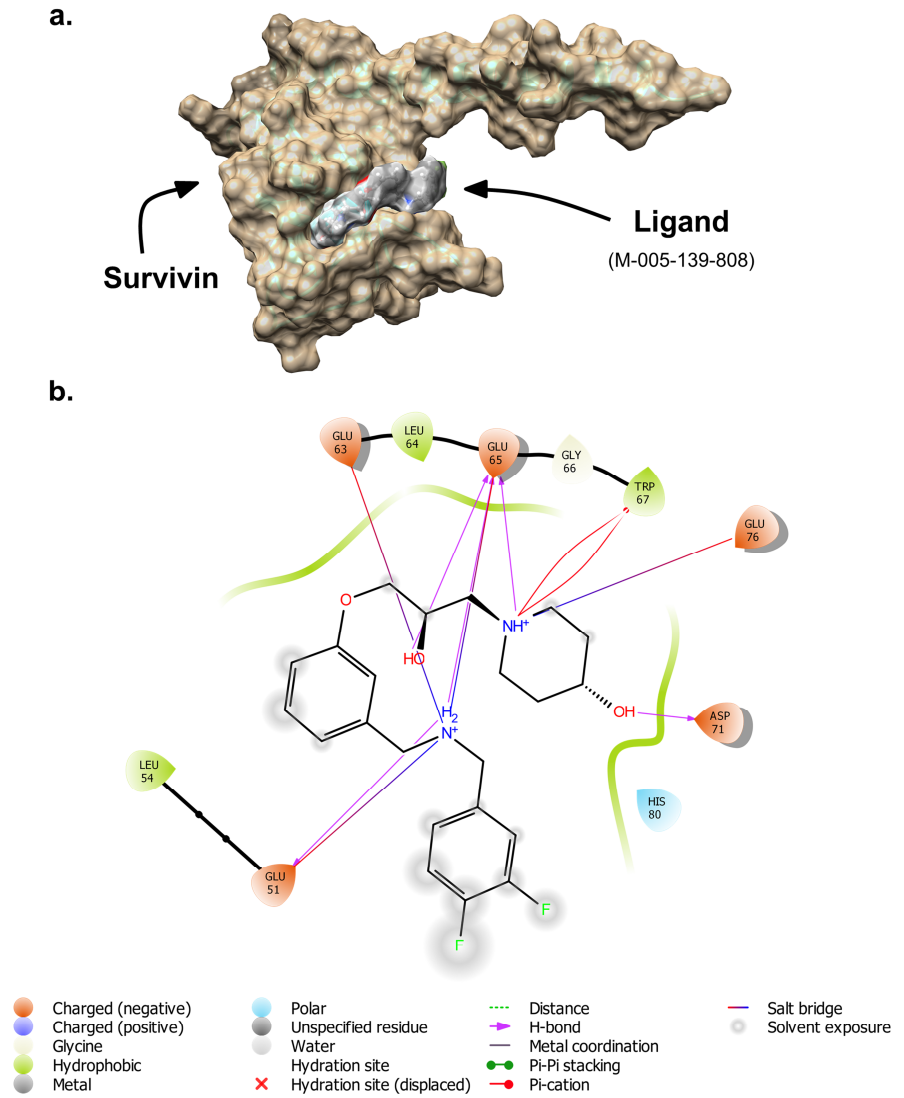

Figure 38. Docking of M-005-139-808 ligand into the W67 structural cavity. (**a**) Docking pose of Survivin and M-005-139-808 ligand as surface representation. The image was taken by Chimera version 1.14rc (Pettersen et al., 2004). (**b**) Multiple attraction and direct interactions (Hydrogen bonds, Pi-cation attractions, and Salt bridges) between Survivin residues E51, E63, E65, W67, D71, E76 and M-005-139-808 ligand. The image was taken by Ligand Interaction Diagram - Maestro version 11.5 of Schrödinger Release 2018-1.

5. Discussion

5.1. Radiation resistance role of Survivin BIR domain

The IAP family consists of eight members which all contain BIR domains mainly located in the N-terminal region (Oberoi-Khanuja et al., 2013; Srinivasula and Ashwell, 2008). Previously it was found that some of the members of IAP directly or indirectly play a role in the DDR and genetic instability (Ge et al., 2015; Hinz et al., 2010).

The activation of signal transduction pathways by ionizing radiation to induce DNA damage repair and regulate cell cycle progression/arrest and cell death is the main feature of the cellular radiation response (Dent et al., 2003). As there is substantial evidence for the involvement of Survivin in all of these pathways in line with a pronounced overexpression in tumor cells, Survivin is reported to be associated with a radiation-resistant phenotype. Moreover, Survivin has been recognized as a radiation-inducible factor (Badura et al., 2012; Rodel et al., 2003) clinically associated with an unfavorable prognosis, metastasis and resistance to conventional radiation or chemoradiation therapy in a multitude of tumors (Rodel et al., 2012; Sprenger et al., 2011). The complexity and molecular basis of Survivin's impact on radiation response, however, remains to be elucidated as it includes caspase-dependent as well as caspase-independent mechanisms (Chakravarti et al., 2004; Rodel et al., 2005; Rodel et al., 2011).

A radiosensitization of tumor cells analyzed by conventional 2D culture assays has been reported following attenuation of Survivin (Chakravarti et al., 2004; Iwasa et al., 2008; Rodel et al., 2005). There is, however, compelling evidence that tumor cell growth in extracellular matrix most pronounced under 3D cell culture conditions has an impact on radiation response due to altered gene expression, proliferation and survival (Hehlgans et al., 2008; Roskelley et al., 1994; Zschenker et al., 2012).

Survivin contains a single BIR domain which has been reported to be a protein interaction hub and mediates protein-protein interactions with multiple proteins including caspases, kinases, histones and chaperones. Besides, the extended amphipathic α-helical coiled-coil domain at the C-terminus predominantly mediates the interactions with microtubule-associated proteins (LaCasse et al., 1998; Verdecia et al., 2000). Our initial studies have analyzed the effect of Survivin domain deletion mutants on radiation response in 3D clonogenic assays that may reflect a physiological environment more closely than conventional 2D cultures (Eke et al., 2013; Storch et al., 2010). Under these conditions, cells stably expressing recombinant Survivin with a deletion of the BIR domain were significantly radiosensitized while the expression of Survivin mutants lacking the microtubules domain fully rescued radiation survival following siRNA-mediated knockdown of endogenous Survivin (Petraki, 2014). That suggested that the presence of the BIR domain (residues 18-88) is of pivotal importance for long term clonogenic radiation survival, whereas the microtubules domain does not seem to be involved.

5.2. Is the Survivin BIR domain a kinase/kinase-domain binding region?

The corroborative findings by initial global blind molecular docking analysis of Survivin and DNA-PKcs revealed predominant involvement of the BIR domain in the interaction with the PI3K domain of DNA-PKcs (**Figure 12**). In line with the potential interaction with the PI3K domain of DNA-PKcs, Survivin was previously found to directly interact with a variety of kinases/kinase domains such as Aurora kinase C, polo like kinase 1 (PLK1), cell division cycle 2 (CDC2), cyclin-dependent kinase 4 (CDK4) and Aurora kinase B (Chen et al., 2003; Colnaghi and Wheatley, 2010; O'Connor et al., 2000; Sasai et al., 2016; Suzuki et al., 2000). Particularly, the N-terminal region of Survivin, 1-90 residues –containing the BIR domain-, was found to more strongly co-immunoprecipitate with PLK1 compared to full-length Survivin, while N-terminal truncated Survivin, 98-142 residues –containing the Microtubules domain- was comparable with glutathione S-transferase (GST) negative control (Colnaghi and Wheatley, 2010). Additionally, Survivin was found to co-immunoprecipitate with the kinase domain of Aurora kinase B. Notably, the presence of Survivin in an *in vitro* Aurora kinase B kinase assay enhanced the kinase activity and increased the phosphorylation of Histone H3. Furthermore, siRNA-mediated knockdown of Survivin suppressed the phosphorylation of Histone H3 (Chen et al., 2003). In the light of these findings and our previous studies revealing a direct and kinase regulatory interaction of Survivin with DNA-PKcs (Capalbo et al., 2010; Reichert et al., 2011), we investigated the sequence specific interaction of Survivin with the different domain/regions of DNA-PKcs by employing FACS-FRET methodology. Our findings confirmed that the BIR domain of Survivin directly interacts with the PI3K domain of DNA-PKcs (**Figure 13 and 14**). Likewise, via immunoprecipitation analysis we observed that Survivin lacking the BIR domain does not co-immunoprecipitate with DNA-PKcs (and vice versa) in contrast to Surv. wt (**Figure 14**). Nevertheless, further investigations are needed to decipher the molecular and functional relationships of Survivin with the PI3K domain of DNA-PKcs and downstream kinases. However, considering all findings, it is conceivable that the BIR domain functions predominantly as kinase/kinase domain binding region of Survivin.

5.3. Involvement of the S20 and W67 residues of BIR domain in clonogenic radiation survival and DNA repair

Recent data demonstrate that nuclear accumulation of Survivin following irradiation and interaction with components of the DNA repair machinery like DNA-PKcs, KU70 and 53BP1 may comprise a further mechanism of Survivin-mediated radiation resistance mediated by regulation of DNA-PKcs kinase activity (Capalbo et al., 2010; Reichert et al., 2011; Wang et al., 2018c). In that context, knockdown of Survivin resulted in elevated numbers of DNA DSBs as measured by single cell gel electrophoresis (comet assay) (Chakravarti et al., 2004; Reichert et al., 2011) and increased phospho-histone-γH2AX foci detection in irradiated cells (Capalbo et al., 2010; Iwasa et al., 2008; Rodel et al., 2005; Wang et al., 2018c). Initial studies of our group demonstrated that SW480 cancer cells stably expressing the Survivin ΔBIR mutant were significantly radiosensitized upon knockdown of endogenous Survivin and also exhibited an increased number of residual γH2AX foci as compared to overexpression of Surv. wt and ΔMicTub constructs after irradiation with 2 Gy (Petraki, 2014).

A variety of different Survivin amino acids, which were determined as potential interaction sites by our initial global blind molecular docking analysis, and the known phosphorylation

sites were subjected to FACS-FRET analysis to investigate the interaction potential of Survivin and PI3K domain of DNA-PKcs on amino acids level. S20D, F27A, C31A, D53A and W67A from predicted sites and T34A and T34D from phosphorylation sites showed significant decrease in the interaction (**Figure 16a and 16b**). By further performing a variety of different double/triple mutant combinations, the S20D-W67A double mutant revealed the most significant decrease with about 70% diminution of binding (**Figure 16c**). Moreover, the importance of S20 and W67 on the interaction of Survivin with the PI3K domain of DNA-PKcs was verified additionally in DLD-1 and HCT-15 colorectal cancer cells (**Figure 16d and 16e**). In line with that, S20 and W67 amino acids of Survivin were among the top candidates according to ΔG binding free energy ranking in molecular docking analyses further suggesting a potential involvement in the interaction (**Figure 12a**). Moreover, *in silico* S20D and W67A mutagenesis resulted in a greater distance between interaction amino acid backbones/side chains and decreased the hydrogen bonding potential, which can be interpreted as a potential decrease in the interaction (**Figure 12b**). Further, co-immunoprecipitation validation of the most promising amino acid findings in FACS-FRET analysis clearly indicated that deletion of BIR domain completely disrupted the interaction while S20D, W67A, and S20D-W67A double mutant also showed a marked decrease in the interaction (**Figure 17a and 17b**). These data confirm the previous findings and support the contribution of specific amino acids located in the BIR domain of Survivin to the interaction with the PI3K domain of DNA-PKcs.

Furthermore, we focused on S20 and W67 amino acids of Survivin with respect to clonogenic radiation survival and DNA repair in 3D grown colorectal cancer cells. SW480 and DLD-1 colorectal cancer cells overexpressing the phospho-mimicking form of S20D were showing less radiosensitization while alanine substitution of W67A, S20D-W67A double mutant and BIR deletion displayed a significant radiosensitizing effect upon endogenous Survivin knockdown. By contrast, Surv.wt rescued the radiation survival of SW480 and DLD-1 colorectal cancer cells following attenuation of endogenous Survivin (**Figure 19 and 20**). These results strengthen the notion that mutations of these amino acids are important for the interaction with PI3K domain of DNA-PKcs and impact on clonogenic radiation survival of SW480 and DLD-1 colorectal cancer cells. In line with an increased radiation response, SW480 and DLD-1 colorectal cancer cells stably overexpressing Survivin W67A, S20D-W67A double mutant and BIR deletion mutant showed significantly increased numbers of residual γH2AX/53BP1 foci after knockdown of endogenous Survivin. By contrast S20D revealed a diminished increase on residual γH2AX/53BP1 foci and Surv. wt completely rescued the DNA damage repair (**Figure 21 and 22**). Thus, we consider that Survivin S20 and W67 amino acids are indispensable for DNA repair regulation, possibly via interaction with DNA-PKcs in SW480 and DLD-1 colorectal cancer cells.

5.4. The potential importance of S20 residue of Survivin in DDR

According to the above-mentioned findings, it is evident that Alanine substitution of S20 residue does not affect the interaction between Survivin and PI3K domain of DNA-PKcs while phospho-mimetic aspartic acid substitution significantly decreased binding (**Figure 16b**). That suggests S20 phosphorylation may have an inhibitory effect on the interaction of Survivin with DNA-PKcs. Studies revealed that Survivin S20 is phosphorylated by PLK1, Aurora kinase B, Aurora kinase C, and Protein kinase A (PKA) (Colnaghi and Wheatley, 2010; Dohi et al., 2007; Raab et al., 2015; Sasai et al., 2016). Phosphorylation of Survivin S20 by these kinases

appears important for both proper chromosome segregation and apoptosis inhibition. Overexpression of a non-phosphorylatable version, S20A, has been shown to be unable to correct spindle-attached chromosomes, which causes entering into anaphase with misoriented chromosomes and evading the spindle tension checkpoint. Moreover, the prevention of Survivin S20 phosphorylation by PKA in cytosol disrupts the binding interface between Survivin and XIAP which hampers anti-apoptotic functions of the Survivin-XIAP interrelationship (Colnaghi and Wheatley, 2010; Dohi et al., 2007; Raab et al., 2015; Sasai et al., 2016). Resembling the functional interaction of Survivin with DNA-PKcs, Survivin was previously found to interact with the kinase domain of Aurora kinase B and resulting in enhanced kinase activity (Chen et al., 2003). Furthermore, another study revealed that S20 phosphorylation of Survivin by PLK1 required for the centromeric activation of Aurora kinase B (Chu et al., 2011). These findings suggest that S20 residue of Survivin may function as a switch-regulator conferring different roles of Survivin in both nucleus and cytoplasm.

5.5. Heterotetramer complex formation by Survivin and DNA-PKcs

Our data suggested two distinct spatial binding conformations (Chain B of Survivin in close proximity via S20 to Chain A of the head-domain of DNA-PKcs, and Chain C of Survivin in close proximity via W67 to Chain A of the head-domain of DNA-PKcs) which resulted in a heterotetramer hypothesis where Survivin is bound to the surface of PI3K domains of a pre-existing DNA-PKcs dimer. The conformational opening of the surface of the active site region for the heterotetramer (particularly in Chain D) and partly in a head-dimer can be concluded as potentially increased accessibility by ATP and the substrates of DNA-PKcs, which might lead to enhanced kinase activity and could eventually result in increased phosphorylation. Indeed, *in vitro* kinase assays confirmed the *in silico* predicted increased catalytic activity potentials of the heterotetramer and head-dimer structures. DNA-PKcs already showed a basal level of phosphorylation in the absence of Survivin, while the addition of Survivin to the assay significantly enhanced the kinase activity approximately 45% (**Figure 26**). Consequently, the combination of findings from both *in silico* docking studies and experimental approaches showed a clear interaction between the BIR domain of Survivin and the PI3K domain of DNA-PKcs by generating a heterotetramer complex resulting in an increased kinase activity.

DNA-PKcs acts as a locomotive in DNA damage/repair by its catalytic enzyme function, which is activated by the DNA-PKcs-KU70/80-DNA holoenzyme complex formation. DNA accommodates into the tunnel formed by a KU70/80 heterodimer ring, which subsequently provides a binding platform for DNA-PKcs (Hill and Lee, 2010). Recent contradictory findings suggest that the DNA-PKcs is not important for the synapsis formation (Zhao et al., 2019), while many other recent findings by EM/cryoEM and SAXS studies concerning the symmetric/asymmetric homo/heterodimerization of DNA-PKcs showed the potential importance of DNA-PKcs in the synapsis process and brought novel perspectives to our current knowledge on NHEJ. Findings suggested either alone or as a holoenzyme with KU70/80, DNA-PKcs was able to generate differerent dimerization complexes by interacting with N-terminal HEAT repeats, mid part of cradle, and particularly FATKIN domains (Baretic et al., 2019; DeFazio et al., 2002; Hammel et al., 2010; Sibanda et al., 2017; Spagnolo et al., 2006). All these findings in correlation with our heterotetramer hypothesis further postulates the direct dimerization of the PI3K domain of DNA-PKcs and subsequent binding to two Survivin molecules which increases the binding potential, stability and kinase activity of DNA-PKcs.

Moreover, kinase activity (**Figure 26**) was enhanced in the presence of Survivin, while siRNA mediated knockdown of the IAP does not impact on complexation and basal level of phosphorylation. Accordingly, we do not consider Survivin binding to a preexisting DNA-PKcs PI3K dimer to cover an initial step in the NHEJ repair cascade, but may display a selective activation of the DNA-PKcs kinase activity at later stages of repair. In line with that, results from molecular simulations further indicate a change in kinase active site accessibility upon binding of Survivin that suggests enhanced accessibility of ATP and potential substrates to enter the active site. These results are comparable to reports, that histone H3 phosphorylated at threonine 3 is recognized by a binding pocket in the BIR domain of Survivin directing the CPC to chromosomes and resulting in an activation of its kinase subunit Aurora kinase B (Kelly et al., 2010). By contrast, cells depleted of Survivin display a lowered kinase activity and mislocalization of Aurora kinase B to its substrates including histone H3 (Chen et al., 2003; Kelly et al., 2010).

5.6. Change on phosphorylation motif of DNA-PK (S/T-Q → S/T-P)

Consensus motif analysis of phosphosites discovered in this study revealed highly conserved S/T-Hydr (Hydrophobic residues: G, A, V, L, I, P, F, M, W) particularly S/T-P motifs (**Figure 32**) and the enrichment of S/T-P motifs were also previously reported in response to DNA damage (Bennetzen et al., 2010). However, high throughput studies revealed over 900 Serine or Threonine, followed by Glutamine motif (S/T-Q) phosphorylation sites encompassing over 700 proteins in response to irradiation-triggered DNA damage response (Matsuoka et al., 2007). Like other PI3K family members, DNA-PK predominantly phosphorylates the S/T-Q motifs present in DNA-PKcs itself S2056/T2609, Artemis S516/S645, DNA ligase IV S672, H2AX S139, and KU70 S51 sequences. Nevertheless, DNA-PKcs is also capable of phosphorylating non-S/T-Q motifs (Lees-Miller and Anderson, 1989). Particularly, holoenzyme components KU70/80, DNA-PKcs itself and some other substrates covering a S/T-Hydr motif were shown to be efficiently phosphorylated by DNA-PK (Yu et al., 2003). All these findings and specific confirmation of FOXO3 S253 phosphorylation site (Motif: 250-R-A-V-**S**-M-D-N-256) by western immunoblotting strengthen the notion that Survivin binding redirects the substrate preference of DNA-PK to predominantly S/T-Hydr motifs, particularly S/T-P.

5.7. Phosphorylation of FOXO3 S253 and its dependence on DNA-PKcs

LC-MS analyses revealed a set of regulated phosphosites which were previously little-known to be related with DNA-PKcs. Pathway analysis was further revealed the predominant involvement of regulated phosphosites in DNA damage/repair, as well as in chromosome organization, cell cycle, (post)-transcriptional regulation, apoptosis, adhesion and ion transport (**Figure 30a and 30b**). One of the remarkable regulated phosphoproteins is FOXO3 which is a member of the forkhead family transcription factors that particularly functions on the transcriptional regulation of apoptosis and autophagy (Fitzwalter et al., 2018). The importance of FOXO3 S253 phosphorylation in relation with DNA damage/repair and DNA-PKcs is further supported by a variety of other studies: In three different studies, it was shown that FOXO3 S253 phosphorylation decreased upon LY294002 inhibitor treatment (Haque et

al., 2015; Singh et al., 2010; Zheng et al., 2000) which is a PI3K inhibitor with a known DNA-PK inhibitory effect (Rosenzweig et al., 1997). Besides, Wortmannin a PI3K inhibitor with a major DNA-PKcs inhibitory effect (Hashimoto et al., 2003), completely diminished FOXO3 S253 phosphorylation in rat granulosa and PC12 cells (Chen et al., 2007b; Zheng et al., 2000). Further, a study showed that HK-2 cells overexpressing FOXO3 revealed increased phosphorylation of S253 residue upon TGF-β1 treatment (Carew et al., 2011). The bottom line is that TGF- β1 has a key role in DNA damage response, which enhances the NHEJ pathway in irradiated cells via regulating the expression of DNA ligase IV (Kim et al., 2015). Likewise, the treatment of B-CLL cells with 10 nM Phorbal 12-myristate 13-acetate (PMA) revealed a significant increase in the phosphorylation of FOXO3 S253 residue (Barragan et al., 2006), and PMA-treated THP1 cells showed a remarkable increase in both DNA-PKcs expression and DNA-PKcs T2609 phosphorylation (So et al., 2013). In consideration of all these findings with our experimental support, it is suggested that DNA-PKcs regulates the phosphorylation of S253 residue of FOXO3 in a Survivin-DNA-PKcs interrelationship-dependent manner.

5.8. Additional phosphosites promise a better understanding of the relation of Survivin with DNA-PKcs

Not only FOXO3 S253, but also some other phosphosites investigated in the current study display a relation with DNA damage/repair. Such phosphosites are DNA polymerase α regulatory subunit (POLA2) S141 (Beli et al., 2012; Boeing et al., 2016) POLA2 S152, *flna*/Filamin-A T2336, zinc finger protein 36 C3H1 type-like 2 (ZFP36L2) S125, E2F transcription factor 1 (E2F1) S375, thyroid hormone receptor associated protein 3 (THRAP3) S622, nucleoporin 98 and 96 precursor (NUP98) S839 (Beli et al., 2012) and treacher collins-franceschetti syndrome 1 (TCOF1) S1407 (Boeing et al., 2016). Nucleocytoplasmic protein Filamin-A is a multi-complex interacting scaffold that anchors transmembrane receptors and actin filaments to glycoproteins. Besides, it interacts with breast cancer type 1/2 susceptibility proteins (BRCA1 and BRCA2), DNA-PKcs, integrins and second messengers to regulate DNA damage response, cell shape/size, ciliogenesis, cell-cell anchorage, and migration (Yue et al., 2013). Previous findings suggest that *flna*/Filamin-A is required to stabilize the interaction between components of the DNA-PK holoenzyme complex, particularly in between DNA-PKcs and KU80 via directly interacting with DNA-PKcs *in vivo*. Furthermore, *flna*-null cells were found to be deficient in DNA repair (Velkova et al., 2010). This suggests, that DNA-PK holoenzyme is a multi-effector dynamic protein complex by the recruitment of Survivin and probably some other proteins such as Filamin-A to expand its functional capacity.

POLA2 is required for the initiation of DNA replication by forming a primosome via an interaction with primase. Hereby, primosome synthesizes a short RNA:DNA primer which is used as a substrate for high fidelity polymerases δ and ε (Dang and Morales, 2020; Nunez-Ramirez et al., 2011). The recent study was revealed that POLA2 was directly involved in double strand break repair and regulation of genotoxic stress. *pola2*-deficient cells showed an increased number of 53BP1 foci and a significant decrease on the efficiency of both NHEJ and HR pathways. Moreover, *pola2*-deficient cells displayed a decreased cellular survival in response to IR (Dang and Morales, 2020). These findings and our phosphorylation findings potentially on POLA2 S141 and S152 residues suggest conceivably a DNA end polymerization

role for POLA2 in NHEJ pathway by the regulatory effect of Survivin-DNA-PKcs interrelationship.

5.9. Survivin-DNA-PKcs interrelationship has not only post-translational but also protein expression-level regulatory functions

Proteomics analysis revealed a vast amount of directly and inversely regulated proteins which function predominantly in DNA damage/repair such as *cdca2*/Repo-Man, SENP5, and HMGA family members (**Figure 35**). Particularly, inhibition of *cdca2*/Repo-Man enhances the ATM activation and autophosphorylation on S1981 (Peng et al., 2010). Additionally, SENP5 is found to interact with ATRIP and stimulated its desumoylation (Jin et al., 2016), which is essential for ATRIP to properly function and activate the ATR pathway (Wu et al., 2014). The increase in the expression of *cdca2*/Repo-Man and SENP5 in response to Survivin expression and decrease in response to Survivin knockdown and DNA-PK inhibitor treatment (**Figure 35a**) suggest that DNA-PKcs may have an inhibitory effect on ATM and ATR via regulating the expression of *cdca2*/Repo-Man and SENP5.

HMGA family proteins -HMGA1 and HMGA2- are chromatin-associated proteins that regulate the transcription via altering the chromatin architecture. HMGA2 particularly plays a role in the regulation of cell cycle, apoptosis, and chromosome condensation (Zhang et al., 2019). HMGA2 has an inhibitory effect on DNA-PKcs during the NHEJ process by altering the steady-state form of DNA-PK holoenzyme and delaying the release of DNA-PKcs from the DNA DSB ends (Li et al., 2009). That may indicate that DNA-PKcs and Survivin inversely regulate the expression of HMGA2 to preserve the functions and time-dependent regulation of NHEJ.

The studies with the synergistic effect of our proteomics findings strengthen the concept that the enhanced kinase activity of DNA-PKcs with the help of Survivin may change the repair preference to the DNA-PKcs-dependent pathway via dysregulation of HR and ATM/ATR-dependent pathways by regulating the expression of HIRIP3, *rbbp8*/CtIP, HMGA and HMGN family members (Adamson et al., 2012; Hoa et al., 2015; Kim et al., 2009; Makharashvili et al., 2014; Natarajan et al., 2013; Palmieri et al., 2011; Quennet et al., 2011; Singh et al., 2015; Wang et al., 2018b) (**Figure 35b**). However, a recent study suggests a dependence of efficient processing and resection of DNA ends on the phosphorylation of *rbbp8*/CtIP to DNA-PKcs (Deshpande et al., 2020).

Besides Survivin-DNA-PKcs interrelationship-dependent regulatory functions, Survivin has unique regulatory functions as well. As depicted in **Figure 36a**, INCENP, *cdca8*/Borealin and Aurora kinase B protein expressions were significantly increased in response to Survivin overexpression and decreased in response to Survivin knockdown. The cruces is that INCENP, *cdca8*/Borealin and Aurora kinase B together with Survivin are the members of the chromosomal passenger complex (CPC) which facilitates a vital step for mitotic cell division by accomplishing proper chromosome segregation (Carmena et al., 2012). It appears that, Survivin has a regulatory role on protein expression of the other CPC members that may define the fate of the cell.

5.10. Nucleus-directed drug targeting of Survivin – DNA-PKcs interaction

Since the relation of Survivin with cancer progression and therapy response was investigated shortly after its discovery, the protein was considered a valuable and attractive target for drug design approaches to target cancer cells. Our current study revealed novel candidate residues to particularly target the DNA-PKcs interaction interface of Survivin for radiosensitization of cancer cells. Thus far, there is no direct inhibitory approach in the literature targeting the amino acids revealed by current study to radiosensitize the cancer cells.

Recently, cytoplasmic/mitochondrial SMAC-Survivin interaction took attention of drug designers to stimulate apoptosis in cancer cells. The W67 residue is located in between the SMAC binding amino acids of Survivin (L64, D71 and L87) (Song et al., 2003) which partially provides some hydrophobic, π – π or π – cation attractions to the designed drugs (Park et al., 2019; Wang et al., 2018a; Xiao et al., 2015). But it is clearly observed that while L64A mutation conferred reduced binding, W67A nearly had no effect on the binding efficiency of inhibitors designed to target the same region (Park et al., 2019). In addition to this, Alanine and Arginine mutagenesis screening of Survivin have reported that R18A, W25A, C33R, C57A, and W67A mutations prevented the interaction with Histone H3 protein (Yamagishi et al., 2010). However, a more recent study generated the crystal structure of this interaction and findings revealed that only K62, E65, D71 and H80 residues but not W67 are responsible for the Survivin-Histone H3 interaction (Niedzialkowska et al., 2012). All these studies strengthen the hypothesis that W67 could be one of the unique amino acids for binding to DNA-PKcs in the nucleus.

Accumulation of drug molecules in the nucleus of cancer cells is of vital importance for specific targeting of Survivin-DNA-PKcs interaction and drug efficiency in our investigation. Recently, a polymeric drug delivery system was generated, which penetrates efficiently to cell nucleus. For selective delivery to the tumor cells, researchers designed self-assembled poly-(ethylene glycol)-*block*-poly(ε-caprolactone) nanocarriers fused with folic acid (FA-PECL). For the nucleus delivery, cell penetration peptide (CPP) fused with doxorubicin (DOX) resulted in a conjugate (CPP-DOX). The resulting drug-loaded delivery system is based on the the combination of both cell and nucleus delivery systems (FA-PECL/CPP-DOX). It is reported that it decreased a five times decreased tumor size in comparison to non-targeted therapies and is easy to implement to the other drugs instead of DOX (Hua et al., 2019). Besides to that, there are a variety of different nuclear delivery methods which can be implemented in our approach such as TAT-peptide conjugated mesoporous silica nanoparticles (MSNs-TAT) (Pan et al., 2012), targeted charge-reversal nanoparticles (TCRNs) comprised of poly(ε-caprolactone)-*block*-polyethyleneimine (PCL-PEI) (Xu et al., 2007), and biodegradable cross-linked *N*-(2-hydroxypropyl) methacrylamide (HPMA) copolymer micelles (Zhou et al., 2017b).

5.11. Future perspectives

Even under BIR domain deletion condition, we measured a small interaction potential (~15%) between Survivin and PI3K domain of DNA-PKcs by sensitive FACS-FRET approach (**Figure 13 and 16**). For that, alanine and phosphomimetic (for S/T/Y residues) screening of not only the rest of BIR domain, but also MicTub domain residues will provide a better understanding about the involvement of potential other residues, post-translational phospho-

regulatory functions, and exact spatial/structural interaction within the heterotetramer complex. Further, with the latest technological advancements in Cryo-EM and X-ray laser crystallography systems, the generation of the crystal structures of large multi-macromolecular complexes is feasible (Helliwell, 2017). Therefore, the generation of the condition-dependent dynamic crystal structure of Survivin – DNA-PKcs interaction will definitely provide a better understanding of the basis of molecular and functional roles. Investigation of the intracellular interaction dynamics can be further supplemented by the analyses with multiplexed super-resolution live-cell imaging and single-particle tracking microscopy studies.

The findings and/or hypotheses on the change of substrate recognition/phosphorylation motif (S/T-Hydr. and S/T-P) and potential inhibitory roles on HR and ATM/ATR-dependent pathways need be to further investigated to more closely unravel the translational and post-translational phospho-regulatory roles of the interaction of Survivin and DNA-PKcs. Particularly, FOXO3, *flna*/Filamin-A, POLA2, *cdca2*/Repo-Man, SENP5, HIRIP3, *rbbp8*/CtIP, and HMGA and HMGN family members seem to be of high importance.

To extend the knowledge on the dynamic interactome and interaction interfaces of Survivin – DNA-PKcs interrelationship, Proximity-dependent Biotin identification (BioID/BioID2/TurboID) technology may be implemented to capture both strong (stable interactors) and weak (transient interactors and substrates) interactors of the Survivin-DNA-PKcs interrelationship. Briefly, the plasmid construct including the bait protein (Survivin and DNA-PKcs) fused with either ascorbate peroxidase (APEX) or biotin ligase (BirA) enzymes should be recombinantly expressed in the cells. Afterwards, both APEX and BirA will be able to biotinylate the proteins in 10-15 nm proximity to the bait protein. This step is followed by a pull-down process by streptavidin beads to capture biotinylated protein which then can be subjected to LC-MS (Branon et al., 2018; Kim et al., 2016; Lam et al., 2015; Roux et al., 2012). After the pull-down step, samples can be further treated with protein-protein crosslinkers such as disuccinimidyl suberate (DSS) and bis(sulfosuccinimidyl)suberate (BS3) which covalently stabilize the protein-protein interactions and subsequent subjection to LC-MS analysis would provide essential data on protein interaction regions (Leitner et al., 2016; Rappsilber, 2011).

The *in vitro* cell-based testing of novel ligands that have *in silico* potential to target the S20 and W67 residues should give insight, whether a prevention of Survivin-DNA-PKcs interaction is a promising strategy for radiosensitization of cancer cells. In dependence on these preceding *in vitro* and *in vivo* experiments, our approach may open a new possibility within current radiosensitization strategies by targeting Survivin-DNA-PKcs interaction with hopefully fewer side effects.

Summary

In summary, our results confirm Survivin to act as a radiation resistance factor modulating cellular radiation responses by multiple mechanisms, including radiation survival and DNA DSB repair. For the first time, we indicate in a 3D cell culture system that S20 and W67 amino acids located in the BIR domain are essential for radiation survival and regulation of DNA damage repair, at least in part by disturbing protein interaction with the PI3K kinase domain of DNAPKcs. The involvement of Survivin in the enhancement of the kinase activity of DNA-

PKcs was further confirmed by a heterotetramer hypothesis employing both *in silico* and experimental approaches. Of particular importance, this novel hypothesis suggests the binding of Survivin to a pre-existing DNA-PKcs dimer which leads to a conformational change in the PI3K domain and results in the modulation of kinase activity and a differential change in DNA-PKcs' substrate specificity (**Figure 39**).

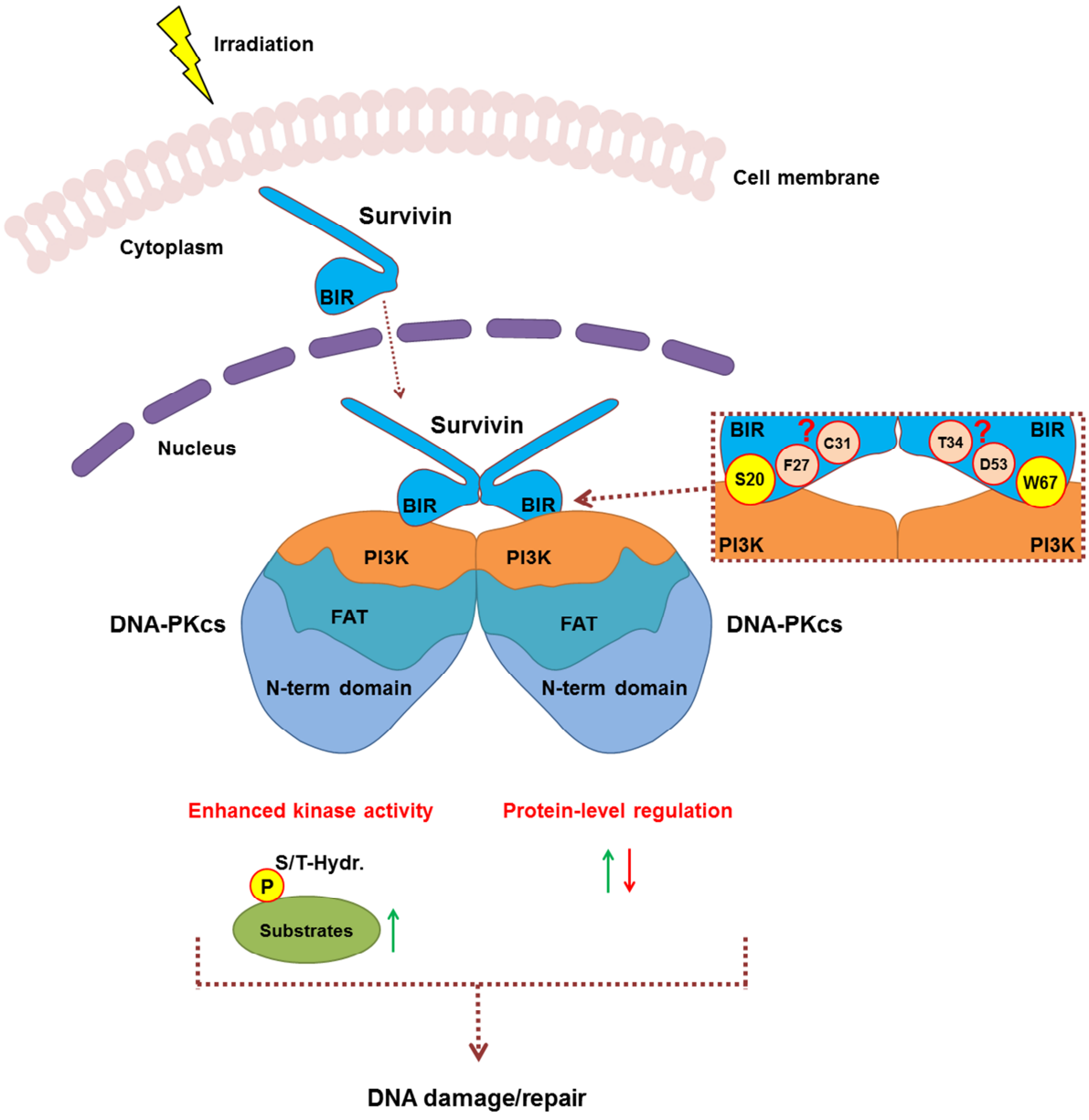

Figure 39. Functional overview of Survivin-DNA-PKcs interrelationship. Upon irradiation, Survivin accumulates in the nucleus and generates a heterotetramer via binding to a pre-existing DNA-PKcs dimer. This particular interaction is mediated mainly by S20, W67 and some other potential residues such as F27, C31, T34 and D53 of Survivin. Formation of the heterotetramer complex drives predominantly the phosphorylation of S/T-Hydr motifs (hydrophobic residues: G, A, V, L, I, P, F, M, W). Besides the regulatory functions on the phosphorylation pattern of substrates, the Survivin-DNA-PKcs interrelationship has essential functions on DNA damage/repair via modulating the expression levels of proteins.

6. References

Abraham, M.J., Murtola, T., Schulz, R., Páll, S., Smith, J.C., Hess, B., and Lindahl, E. (2015). GROMACS: High performance molecular simulations through multi-level parallelism from laptops to supercomputers. SoftwareX *1-2*, 19-25.

Adamson, B., Smogorzewska, A., Sigoillot, F.D., King, R.W., and Elledge, S.J. (2012). A genome-wide homologous recombination screen identifies the RNA-binding protein RBMX as a component of the DNA-damage response. Nat Cell Biol *14*, 318-328.

Ahnesorg, P., Smith, P., and Jackson, S.P. (2006). XLF interacts with the XRCC4-DNA ligase IV complex to promote DNA nonhomologous end-joining. Cell *124*, 301-313.

Alford, R.F., Leaver-Fay, A., Jeliazkov, J.R., O'Meara, M.J., DiMaio, F.P., Park, H., Shapovalov, M.V., Renfrew, P.D., Mulligan, V.K., Kappel, K.*, et al.* (2017). The Rosetta All-Atom Energy Function for Macromolecular Modeling and Design. J Chem Theory Comput *13*, 3031-3048.

Altieri, D.C. (2008). Survivin, cancer networks and pathway-directed drug discovery. Nat Rev Cancer *8*, 61-70.

Altieri, D.C. (2010). Survivin and IAP proteins in cell-death mechanisms. Biochem J *430*, 199-205.

Ambrosini, G., Adida, C., and Altieri, D.C. (1997). A novel anti-apoptosis gene, survivin, expressed in cancer and lymphoma. Nat Med *3*, 917-921.

Athanassiadou, P., Grapsa, D., Athanassiades, P., Gonidi, M., Athanassiadou, A.M., Tsipis, A., and Patsouris, E. (2008). The prognostic significance of COX-2 and survivin expression in ovarian cancer. Pathol Res Pract *204*, 241-249.

Badura, M., Braunstein, S., Zavadil, J., and Schneider, R.J. (2012). DNA damage and eIF4G1 in breast cancer cells reprogram translation for survival and DNA repair mRNAs. Proc Natl Acad Sci U S A *109*, 18767-18772.

Bajar, B.T., Wang, E.S., Zhang, S., Lin, M.Z., and Chu, J. (2016). A Guide to Fluorescent Protein FRET Pairs. Sensors (Basel) *16*.

Banning, C., Votteler, J., Hoffmann, D., Koppensteiner, H., Warmer, M., Reimer, R., Kirchhoff, F., Schubert, U., Hauber, J., and Schindler, M. (2010). A Flow Cytometry-Based FRET Assay to Identify and Analyse Protein-Protein Interactions in Living Cells. PLOS ONE *5*, e9344.

Baretic, D., Maia de Oliveira, T., Niess, M., Wan, P., Pollard, H., Johnson, C.M., Truman, C., McCall, E., Fisher, D., Williams, R.*, et al.* (2019). Structural insights into the critical DNA damage sensors DNA-PKcs, ATM and ATR. Prog Biophys Mol Biol *147*, 4-16.

Baretic, D., Pollard, H.K., Fisher, D.I., Johnson, C.M., Santhanam, B., Truman, C.M., Kouba, T., Fersht, A.R., Phillips, C., and Williams, R.L. (2017). Structures of closed and open conformations of dimeric human ATM. Sci Adv *3*, e1700933.

Barragan, M., de Frias, M., Iglesias-Serret, D., Campas, C., Castano, E., Santidrian, A.F., Coll-Mulet, L., Cosialls, A.M., Domingo, A., Pons, G.*, et al.* (2006). Regulation of Akt/PKB by phosphatidylinositol 3-kinase-dependent and -independent pathways in B-cell chronic lymphocytic leukemia cells: role of protein kinase C{beta}. J Leukoc Biol *80*, 1473-1479.

Beli, P., Lukashchuk, N., Wagner, S.A., Weinert, B.T., Olsen, J.V., Baskcomb, L., Mann, M., Jackson, S.P., and Choudhary, C. (2012). Proteomic investigations reveal a role for RNA processing factor THRAP3 in the DNA damage response. Mol Cell *46*, 212-225.

Bennetzen, M.V., Larsen, D.H., Bunkenborg, J., Bartek, J., Lukas, J., and Andersen, J.S. (2010). Site-specific phosphorylation dynamics of the nuclear proteome during the DNA damage response. Mol Cell Proteomics *9*, 1314-1323.

Blier, P.R., Griffith, A.J., Craft, J., and Hardin, J.A. (1993). Binding of Ku protein to DNA. Measurement of affinity for ends and demonstration of binding to nicks. J Biol Chem *268*, 7594-7601.

Boeing, S., Williamson, L., Encheva, V., Gori, I., Saunders, R.E., Instrell, R., Aygun, O., Rodriguez-Martinez, M., Weems, J.C., Kelly, G.P.*, et al.* (2016). Multiomic Analysis of the UV-Induced DNA Damage Response. Cell Rep *15*, 1597-1610.

Borrego-Soto, G., Ortiz-Lopez, R., and Rojas-Martinez, A. (2015). Ionizing radiation-induced DNA injury and damage detection in patients with breast cancer. Genet Mol Biol *38*, 420-432.

Brandsma, I., and Gent, D.C. (2012). Pathway choice in DNA double strand break repair: observations of a balancing act. Genome Integr *3*, 9.

Branon, T.C., Bosch, J.A., Sanchez, A.D., Udeshi, N.D., Svinkina, T., Carr, S.A., Feldman, J.L., Perrimon, N., and Ting, A.Y. (2018). Efficient proximity labeling in living cells and organisms with TurboID. Nat Biotechnol *36*, 880-887.

Bryntesson, F., Regan, J.C., Jeggo, P.A., Taccioli, G.E., and Hubank, M. (2001). Analysis of gene transcription in cells lacking DNA-PK activity. Radiat Res *156*, 167-176.

Capalbo, G., Dittmann, K., Weiss, C., Reichert, S., Hausmann, E., Rodel, C., and Rodel, F. (2010). Radiation-induced survivin nuclear accumulation is linked to DNA damage repair. Int J Radiat Oncol Biol Phys *77*, 226-234.

Carew, R.M., Browne, M.B., Hickey, F.B., and Brazil, D.P. (2011). Insulin receptor substrate 2 and FoxO3a signalling are involved in E-cadherin expression and transforming growth factor-beta1-induced repression in kidney epithelial cells. FEBS J *278*, 3370-3380.

Carmena, M., Wheelock, M., Funabiki, H., and Earnshaw, W.C. (2012). The chromosomal passenger complex (CPC): from easy rider to the godfather of mitosis. Nat Rev Mol Cell Biol *13*, 789-803.

Carter, T., Vancurová, I., Sun, I., Lou, W., and DeLeon, S. (1990). A DNA-activated protein kinase from HeLa cell nuclei. Molecular and Cellular Biology *10*, 6460.

Chakravarti, A., Zhai, G.G., Zhang, M., Malhotra, R., Latham, D.E., Delaney, M.A., Robe, P., Nestler, U., Song, Q., and Loeffler, J. (2004). Survivin enhances radiation resistance in primary human glioblastoma cells via caspase-independent mechanisms. Oncogene *23*, 7494-7506.

Chantalat, L., Skoufias, D.A., Kleman, J.P., Jung, B., Dideberg, O., and Margolis, R.L. (2000). Crystal structure of human survivin reveals a bow tie-shaped dimer with two unusual alpha-helical extensions. Mol Cell *6*, 183-189.

Chen, B.P., Chan, D.W., Kobayashi, J., Burma, S., Asaithamby, A., Morotomi-Yano, K., Botvinick, E., Qin, J., and Chen, D.J. (2005). Cell cycle dependence of DNA-dependent protein kinase phosphorylation in response to DNA double strand breaks. J Biol Chem *280*, 14709-14715.

Chen, B.P., Uematsu, N., Kobayashi, J., Lerenthal, Y., Krempler, A., Yajima, H., Lobrich, M., Shiloh, Y., and Chen, D.J. (2007a). Ataxia telangiectasia mutated (ATM) is essential for DNA-PKcs phosphorylations at the Thr-2609 cluster upon DNA double strand break. J Biol Chem *282*, 6582-6587.

Chen, J., Jin, S., Tahir, S.K., Zhang, H., Liu, X., Sarthy, A.V., McGonigal, T.P., Liu, Z., Rosenberg, S.H., and Ng, S.C. (2003). Survivin enhances Aurora-B kinase activity and localizes Aurora-B in human cells. J Biol Chem *278*, 486-490.

Chen, Y.J., Hsiao, P.W., Lee, M.T., Mason, J.I., Ke, F.C., and Hwang, J.J. (2007b). Interplay of PI3K and cAMP/PKA signaling, and rapamycin-hypersensitivity in TGFbeta1 enhancement of FSH-stimulated steroidogenesis in rat ovarian granulosa cells. J Endocrinol *192*, 405-419.

Chu, X.Y., Chen, L.B., Wang, J.H., Su, Q.S., Yang, J.R., Lin, Y., Xue, L.J., Liu, X.B., and Mo, X.B. (2012). Overexpression of survivin is correlated with increased invasion and metastasis of colorectal cancer. J Surg Oncol *105*, 520-528.

Chu, Y., Yao, P.Y., Wang, W., Wang, D., Wang, Z., Zhang, L., Huang, Y., Ke, Y., Ding, X., and Yao, X. (2011). Aurora B kinase activation requires survivin priming phosphorylation by PLK1. J Mol Cell Biol *3*, 260-267.

Chuang, G.Y., Kozakov, D., Brenke, R., Comeau, S.R., and Vajda, S. (2008). DARS (Decoys As the Reference State) potentials for protein-protein docking. Biophys J *95*, 4217-4227.

Chun, Y., and Kim, J. (2018). Autophagy: An Essential Degradation Program for Cellular Homeostasis and Life. Cells *7*.

Clegg, R.M. (1995). Fluorescence resonance energy transfer. Curr Opin Biotechnol *6*, 103-110.

Colnaghi, R., and Wheatley, S.P. (2010). Liaisons between survivin and Plk1 during cell division and cell death. J Biol Chem *285*, 22592-22604.

Crook, N.E., Clem, R.J., and Miller, L.K. (1993). An apoptosis-inhibiting baculovirus gene with a zinc finger-like motif. J Virol *67*, 2168-2174.

Dang, T.T., and Morales, J.C. (2020). Involvement of POLA2 in Double Strand Break Repair and Genotoxic Stress. Int J Mol Sci *21*.

Davis, A.J., Chen, B.P.C., and Chen, D.J. (2014). DNA-PK: a dynamic enzyme in a versatile DSB repair pathway. DNA repair *17*, 21-29.

de Campos-Nebel, M., Larripa, I., and Gonzalez-Cid, M. (2010). Topoisomerase II-mediated DNA damage is differently repaired during the cell cycle by non-homologous end joining and homologous recombination. PLoS One *5*.

DeFazio, L.G., Stansel, R.M., Griffith, J.D., and Chu, G. (2002). Synapsis of DNA ends by DNA-dependent protein kinase. EMBO J *21*, 3192-3200.

Dent, P., Yacoub, A., Contessa, J., Caron, R., Amorino, G., Valerie, K., Hagan, M.P., Grant, S., and Schmidt-Ullrich, R. (2003). Stress and radiation-induced activation of multiple intracellular signaling pathways. Radiat Res *159*, 283-300.

Deshpande, R.A., Myler, L.R., Soniat, M.M., Makharashvili, N., Lee, L., Lees-Miller, S.P., Finkelstein, I.J., and Paull, T.T. (2020). DNA-dependent protein kinase promotes DNA end processing by MRN and CtIP. Sci Adv *6*, eaay0922.

Dexter, D.L., Barbosa, J.A., and Calabresi, P. (1979). N,N-dimethylformamide-induced alteration of cell culture characteristics and loss of tumorigenicity in cultured human colon carcinoma cells. Cancer Res *39*, 1020-1025.

Dohi, T., Okada, K., Xia, F., Wilford, C.E., Samuel, T., Welsh, K., Marusawa, H., Zou, H., Armstrong, R., Matsuzawa, S.*, et al.* (2004). An IAP-IAP complex inhibits apoptosis. J Biol Chem *279*, 34087-34090.

Dohi, T., Xia, F., and Altieri, D.C. (2007). Compartmentalized phosphorylation of IAP by protein kinase A regulates cytoprotection. Mol Cell *27*, 17-28.

Du, C., Fang, M., Li, Y., Li, L., and Wang, X. (2000). Smac, a mitochondrial protein that promotes cytochrome c-dependent caspase activation by eliminating IAP inhibition. Cell *102*, 33-42.

Eke, I., Deuse, Y., Hehlgans, S., Gurtner, K., Krause, M., Baumann, M., Shevchenko, A., Sandfort, V., and Cordes, N. (2012). beta(1)Integrin/FAK/cortactin signaling is essential for human head and neck cancer resistance to radiotherapy. J Clin Invest *122*, 1529-1540.

Eke, I., Schneider, L., Forster, C., Zips, D., Kunz-Schughart, L.A., and Cordes, N. (2013). EGFR/JIP-4/JNK2 Signaling Attenuates Cetuximab-Mediated Radiosensitization of Squamous Cell Carcinoma Cells. Cancer Res *73*, 297-306.

Falzon, M., Fewell, J.W., and Kuff, E.L. (1993). EBP-80, a transcription factor closely resembling the human autoantigen Ku, recognizes single- to double-strand transitions in DNA. J Biol Chem *268*, 10546-10552.

Finzel, A., Grybowski, A., Strasen, J., Cristiano, E., and Loewer, A. (2016). Hyperactivation of ATM upon DNA-PKcs inhibition modulates p53 dynamics and cell fate in response to DNA damage. Mol Biol Cell *27*, 2360-2367.

Fiser, A., Do, R.K., and Sali, A. (2000). Modeling of loops in protein structures. Protein Sci *9*, 1753-1773.

Fitzwalter, B.E., Towers, C.G., Sullivan, K.D., Andrysik, Z., Hoh, M., Ludwig, M., O'Prey, J., Ryan, K.M., Espinosa, J.M., Morgan, M.J., *et al.* (2018). Autophagy Inhibition Mediates Apoptosis Sensitization in Cancer Therapy by Relieving FOXO3a Turnover. Dev Cell *44*, 555-565 e553.

Forster, T. (1946). Energiewanderung und Fluoreszenz. Naturwissenschaften *33*, 166-175.

Fortugno, P., Beltrami, E., Plescia, J., Fontana, J., Pradhan, D., Marchisio, P.C., Sessa, W.C., and Altieri, D.C. (2003). Regulation of survivin function by Hsp90. Proc Natl Acad Sci U S A *100*, 13791-13796.

Friesner, R.A., Banks, J.L., Murphy, R.B., Halgren, T.A., Klicic, J.J., Mainz, D.T., Repasky, M.P., Knoll, E.H., Shelley, M., Perry, J.K., *et al.* (2004). Glide: a new approach for rapid, accurate docking and scoring. 1. Method and assessment of docking accuracy. J Med Chem *47*, 1739-1749.

Friesner, R.A., Murphy, R.B., Repasky, M.P., Frye, L.L., Greenwood, J.R., Halgren, T.A., Sanschagrin, P.C., and Mainz, D.T. (2006). Extra precision glide: docking and scoring incorporating a model of hydrophobic enclosure for protein-ligand complexes. J Med Chem *49*, 6177-6196.

Galbo, P.M., Jr., Ciesielski, M.J., Figel, S., Maguire, O., Qiu, J., Wiltsie, L., Minderman, H., and Fenstermaker, R.A. (2017). Circulating CD9+/GFAP+/survivin+ exosomes in malignant glioma patients following survivin vaccination. Oncotarget *8*, 114722-114735.

Ge, C., Che, L., Ren, J., Pandita, R.K., Lu, J., Li, K., Pandita, T.K., and Du, C. (2015). BRUCE regulates DNA double-strand break response by promoting USP8 deubiquitination of BRIT1. Proc Natl Acad Sci U S A *112*, E1210-1219.

Goodarzi, A.A., Yu, Y., Riballo, E., Douglas, P., Walker, S.A., Ye, R., Harer, C., Marchetti, C., Morrice, N., Jeggo, P.A., *et al.* (2006). DNA-PK autophosphorylation facilitates Artemis endonuclease activity. EMBO J *25*, 3880-3889.

Goodwin, J.F., Kothari, V., Drake, J.M., Zhao, S., Dylgjeri, E., Dean, J.L., Schiewer, M.J., McNair, C., Jones, J.K., Aytes, A., *et al.* (2015). DNA-PKcs-Mediated Transcriptional Regulation Drives Prostate Cancer Progression and Metastasis. Cancer Cell *28*, 97-113.

Gray, J.J., Moughon, S., Wang, C., Schueler-Furman, O., Kuhlman, B., Rohl, C.A., and Baker, D. (2003). Protein-protein docking with simultaneous optimization of rigid-body displacement and side-chain conformations. J Mol Biol *331*, 281-299.

Halgren, T.A., Murphy, R.B., Friesner, R.A., Beard, H.S., Frye, L.L., Pollard, W.T., and Banks, J.L. (2004). Glide: a new approach for rapid, accurate docking and scoring. 2. Enrichment factors in database screening. J Med Chem *47*, 1750-1759.

Hammel, M., Yu, Y., Mahaney, B.L., Cai, B., Ye, R., Phipps, B.M., Rambo, R.P., Hura, G.L., Pelikan, M., So, S., *et al.* (2010). Ku and DNA-dependent protein kinase dynamic

conformations and assembly regulate DNA binding and the initial non-homologous end joining complex. J Biol Chem *285*, 1414-1423.

Hammel, M., Yu, Y., Radhakrishnan, S.K., Chokshi, C., Tsai, M.S., Matsumoto, Y., Kuzdovich, M., Remesh, S.G., Fang, S., Tomkinson, A.E.*, et al.* (2016). An Intrinsically Disordered APLF Links Ku, DNA-PKcs, and XRCC4-DNA Ligase IV in an Extended Flexible Non-homologous End Joining Complex. J Biol Chem *291*, 26987-27006.

Hao, Y., Sekine, K., Kawabata, A., Nakamura, H., Ishioka, T., Ohata, H., Katayama, R., Hashimoto, C., Zhang, X., Noda, T.*, et al.* (2004). Apollon ubiquitinates SMAC and caspase-9, and has an essential cytoprotection function. Nat Cell Biol *6*, 849-860.

Haque, I., Banerjee, S., De, A., Maity, G., Sarkar, S., Majumdar, M., Jha, S.S., McGragor, D., and Banerjee, S.K. (2015). CCN5/WISP-2 promotes growth arrest of triple-negative breast cancer cells through accumulation and trafficking of p27(Kip1) via Skp2 and FOXO3a regulation. Oncogene *34*, 3152-3163.

Harder, E., Damm, W., Maple, J., Wu, C., Reboul, M., Xiang, J.Y., Wang, L., Lupyan, D., Dahlgren, M.K., Knight, J.L.*, et al.* (2016). OPLS3: A Force Field Providing Broad Coverage of Drug-like Small Molecules and Proteins. Journal of Chemical Theory and Computation *12*, 281-296.

Hartley, K.O., Gell, D., Smith, G.C., Zhang, H., Divecha, N., Connelly, M.A., Admon, A., Lees-Miller, S.P., Anderson, C.W., and Jackson, S.P. (1995). DNA-dependent protein kinase catalytic subunit: a relative of phosphatidylinositol 3-kinase and the ataxia telangiectasia gene product. Cell *82*, 849-856.

Hashimoto, M., Rao, S., Tokuno, O., Yamamoto, K., Takata, M., Takeda, S., and Utsumi, H. (2003). DNA-PK: the major target for wortmannin-mediated radiosensitization by the inhibition of DSB repair via NHEJ pathway. J Radiat Res *44*, 151-159.

Hehlgans, S., Booms, P., Gullulu, O., Sader, R., Rodel, C., Balermpas, P., Rodel, F., and Ghanaati, S. (2018). Radiation Sensitization of Basal Cell and Head and Neck Squamous Cell Carcinoma by the Hedgehog Pathway Inhibitor Vismodegib. Int J Mol Sci *19*.

Hehlgans, S., Eke, I., and Cordes, N. (2012). Targeting FAK radiosensitizes 3-dimensional grown human HNSCC cells through reduced Akt1 and MEK1/2 signaling. Int J Radiat Oncol Biol Phys *83*, e669-676.

Hehlgans, S., Eke, I., Deuse, Y., and Cordes, N. (2008). Integrin-linked kinase: dispensable for radiation survival of three-dimensionally cultured fibroblasts. Radiother Oncol *86*, 329-335.

Hehlgans, S., Oppermann, J., Reichert, S., Fulda, S., Rodel, C., and Rodel, F. (2015). The SMAC mimetic BV6 sensitizes colorectal cancer cells to ionizing radiation by interfering with DNA repair processes and enhancing apoptosis. Radiat Oncol *10*, 198.

Hehlgans, S., Petraki, C., Reichert, S., Cordes, N., Rodel, C., and Rodel, F. (2013). Double targeting of Survivin and XIAP radiosensitizes 3D grown human colorectal tumor cells and decreases migration. Radiother Oncol *108*, 32-39.

Helliwell, J.R. (2017). New developments in crystallography: exploring its technology, methods and scope in the molecular biosciences. Biosci Rep *37*.

Hill, R., and Lee, P.W. (2010). The DNA-dependent protein kinase (DNA-PK): More than just a case of making ends meet? Cell Cycle *9*, 3460-3469.

Hinz, M., Stilmann, M., Arslan, S.C., Khanna, K.K., Dittmar, G., and Scheidereit, C. (2010). A cytoplasmic ATM-TRAF6-cIAP1 module links nuclear DNA damage signaling to ubiquitin-mediated NF-kappaB activation. Mol Cell *40*, 63-74.

Hoa, N.N., Kobayashi, J., Omura, M., Hirakawa, M., Yang, S.H., Komatsu, K., Paull, T.T., Takeda, S., and Sasanuma, H. (2015). BRCA1 and CtIP Are Both Required to Recruit Dna2 at Double-Strand Breaks in Homologous Recombination. PLoS One *10*, e0124495.

Hoffmann, M. (2017). Nachweis der Interaktion des Apoptoseinhibitors Survivin mit der PI3K-Domäne der DNA-abhängigen Proteinkinase (DNA-PKcs). In Biology (Darmstadt, Technische Universität Darmstadt), pp. 108.

Hua, Q., Qiang, Z., Chu, M., Shi, D., and Ren, J. (2019). Polymeric Drug Delivery System with Actively Targeted Cell Penetration and Nuclear Targeting for Cancer Therapy. ACS Applied Bio Materials *2*, 1724-1731.

Iwasa, T., Okamoto, I., Suzuki, M., Nakahara, T., Yamanaka, K., Hatashita, E., Yamada, Y., Fukuoka, M., Ono, K., and Nakagawa, K. (2008). Radiosensitizing effect of YM155, a novel small-molecule survivin suppressant, in non-small cell lung cancer cell lines. Clin Cancer Res *14*, 6496-6504.

Jacobson, M.P., Friesner, R.A., Xiang, Z., and Honig, B. (2002). On the role of the crystal environment in determining protein side-chain conformations. J Mol Biol *320*, 597-608.

Jacobson, M.P., Pincus, D.L., Rapp, C.S., Day, T.J., Honig, B., Shaw, D.E., and Friesner, R.A. (2004). A hierarchical approach to all-atom protein loop prediction. Proteins *55*, 351-367.

Jares-Erijman, E.A., and Jovin, T.M. (2003). FRET imaging. Nat Biotechnol *21*, 1387-1395.

Jeggo, P., and Lobrich, M. (2006). Radiation-induced DNA damage responses. Radiat Prot Dosimetry *122*, 124-127.

Jeyaprakash, A.A., Klein, U.R., Lindner, D., Ebert, J., Nigg, E.A., and Conti, E. (2007). Structure of a Survivin-Borealin-INCENP core complex reveals how chromosomal passengers travel together. Cell *131*, 271-285.

Jiang, W., Crowe, J.L., Liu, X., Nakajima, S., Wang, Y., Li, C., Lee, B.J., Dubois, R.L., Liu, C., Yu, X.*, et al.* (2015). Differential phosphorylation of DNA-PKcs regulates the interplay between end-processing and end-ligation during nonhomologous end-joining. Mol Cell *58*, 172-185.

Jin, Z.L., Pei, H., Xu, Y.H., Yu, J., and Deng, T. (2016). The SUMO-specific protease SENP5 controls DNA damage response and promotes tumorigenesis in hepatocellular carcinoma. Eur Rev Med Pharmacol Sci *20*, 3566-3573.

Jorgensen, W.L., Chandrasekhar, J., Madura, J.D., Impey, R.W., and Klein, M.L. (1983). Comparison of simple potential functions for simulating liquid water. The Journal of Chemical Physics *79*, 926-935.

Jung, S.A., Park, Y.M., Hong, S.W., Moon, J.H., Shin, J.S., Lee, H.R., Ha, S.H., Lee, D.H., Kim, J.H., Kim, S.M.*, et al.* (2015). Cellular inhibitor of apoptosis protein 1 (cIAP1) stability contributes to YM155 resistance in human gastric cancer cells. J Biol Chem *290*, 9974-9985.

Kantidze, O.L., Velichko, A.K., Luzhin, A.V., Petrova, N.V., and Razin, S.V. (2018). Synthetically Lethal Interactions of ATM, ATR, and DNA-PKcs. Trends Cancer *4*, 755-768.

Kanwar, J.R., Kamalapuram, S.K., and Kanwar, R.K. (2011). Targeting survivin in cancer: the cell-signalling perspective. Drug Discov Today *16*, 485-494.

Kanwar, J.R., Kamalapuram, S.K., and Kanwar, R.K. (2013). Survivin signaling in clinical oncology: a multifaceted dragon. Med Res Rev *33*, 765-789.

Kelly, A.E., Ghenoiu, C., Xue, J.Z., Zierhut, C., Kimura, H., and Funabiki, H. (2010). Survivin reads phosphorylated histone H3 threonine 3 to activate the mitotic kinase Aurora B. Science *330*, 235-239.

Kim, D.I., Jensen, S.C., Noble, K.A., Kc, B., Roux, K.H., Motamedchaboki, K., and Roux, K.J. (2016). An improved smaller biotin ligase for BioID proximity labeling. Mol Biol Cell *27*, 1188-1196.

Kim, M.R., Lee, J., An, Y.S., Jin, Y.B., Park, I.C., Chung, E., Shin, I., Barcellos-Hoff, M.H., and Yi, J.Y. (2015). TGFbeta1 protects cells from gamma-IR by enhancing the activity of the NHEJ repair pathway. Mol Cancer Res *13*, 319-329.

Kim, Y.C., Gerlitz, G., Furusawa, T., Catez, F., Nussenzweig, A., Oh, K.S., Kraemer, K.H., Shiloh, Y., and Bustin, M. (2009). Activation of ATM depends on chromatin interactions occurring before induction of DNA damage. Nat Cell Biol *11*, 92-96.

Koonin, E.V., and Aravind, L. (2000). The NACHT family - a new group of predicted NTPases implicated in apoptosis and MHC transcription activation. Trends Biochem Sci *25*, 223-224.

Kozakov, D., Brenke, R., Comeau, S.R., and Vajda, S. (2006). PIPER: An FFT-based protein docking program with pairwise potentials. Proteins: Structure, Function, and Bioinformatics *65*, 392-406.

Kunzmann, P., and Hamacher, K. (2018). Biotite: a unifying open source computational biology framework in Python. BMC Bioinformatics *19*, 346.

LaCasse, E.C., Baird, S., Korneluk, R.G., and MacKenzie, A.E. (1998). The inhibitors of apoptosis (IAPs) and their emerging role in cancer. Oncogene *17*, 3247-3259.

Lam, S.S., Martell, J.D., Kamer, K.J., Deerinck, T.J., Ellisman, M.H., Mootha, V.K., and Ting, A.Y. (2015). Directed evolution of APEX2 for electron microscopy and proximity labeling. Nat Methods *12*, 51-54.

Leaver-Fay, A., Tyka, M., Lewis, S.M., Lange, O.F., Thompson, J., Jacak, R., Kaufman, K., Renfrew, P.D., Smith, C.A., Sheffler, W.*, et al.* (2011). ROSETTA3: an object-oriented software suite for the simulation and design of macromolecules. Methods Enzymol *487*, 545-574.

Lees-Miller, S.P., and Anderson, C.W. (1989). The human double-stranded DNA-activated protein kinase phosphorylates the 90-kDa heat-shock protein, hsp90 alpha at two NH2-terminal threonine residues. J Biol Chem *264*, 17275-17280.

Leibovitz, A., Stinson, J.C., McCombs, W.B., 3rd, McCoy, C.E., Mazur, K.C., and Mabry, N.D. (1976). Classification of human colorectal adenocarcinoma cell lines. Cancer Res *36*, 4562-4569.

Leitner, A., Faini, M., Stengel, F., and Aebersold, R. (2016). Crosslinking and Mass Spectrometry: An Integrated Technology to Understand the Structure and Function of Molecular Machines. Trends Biochem Sci *41*, 20-32.

Li, A.Y., Boo, L.M., Wang, S.Y., Lin, H.H., Wang, C.C., Yen, Y., Chen, B.P., Chen, D.J., and Ann, D.K. (2009). Suppression of nonhomologous end joining repair by overexpression of HMGA2. Cancer Res *69*, 5699-5706.

Lieber, M.R. (2010). The mechanism of double-strand DNA break repair by the nonhomologous DNA end-joining pathway. Annu Rev Biochem *79*, 181-211.

Lin, T.Y., Chan, H.H., Chen, S.H., Sarvagalla, S., Chen, P.S., Coumar, M.S., Cheng, S.M., Chang, Y.C., Lin, C.H., Leung, E.*, et al.* (2019). BIRC5/Survivin is a novel ATG12-ATG5 conjugate interactor and an autophagy-induced DNA damage suppressor in human cancer and mouse embryonic fibroblast cells. Autophagy, 1-18.

Lipinski, C.A., Lombardo, F., Dominy, B.W., and Feeney, P.J. (2001). Experimental and computational approaches to estimate solubility and permeability in drug discovery and development settings. Adv Drug Deliv Rev *46*, 3-26.

Lopez, J., John, S.W., Tenev, T., Rautureau, G.J., Hinds, M.G., Francalanci, F., Wilson, R., Broemer, M., Santoro, M.M., Day, C.L., *et al.* (2011). CARD-mediated autoinhibition of cIAP1's E3 ligase activity suppresses cell proliferation and migration. Mol Cell *42*, 569-583.

Lotz, K., Pyrowolakis, G., and Jentsch, S. (2004). BRUCE, a giant E2/E3 ubiquitin ligase and inhibitor of apoptosis protein of the trans-Golgi network, is required for normal placenta development and mouse survival. Mol Cell Biol *24*, 9339-9350.

Ma, Y., Lu, H., Tippin, B., Goodman, M.F., Shimazaki, N., Koiwai, O., Hsieh, C.L., Schwarz, K., and Lieber, M.R. (2004). A biochemically defined system for mammalian nonhomologous DNA end joining. Mol Cell *16*, 701-713.

Ma, Y., Pannicke, U., Schwarz, K., and Lieber, M.R. (2002). Hairpin opening and overhang processing by an Artemis/DNA-dependent protein kinase complex in nonhomologous end joining and V(D)J recombination. Cell *108*, 781-794.

Maier, J.A., Martinez, C., Kasavajhala, K., Wickstrom, L., Hauser, K.E., and Simmerling, C. (2015). ff14SB: Improving the Accuracy of Protein Side Chain and Backbone Parameters from ff99SB. J Chem Theory Comput *11*, 3696-3713.

Makharashvili, N., Tubbs, A.T., Yang, S.H., Wang, H., Barton, O., Zhou, Y., Deshpande, R.A., Lee, J.H., Lobrich, M., Sleckman, B.P., *et al.* (2014). Catalytic and noncatalytic roles of the CtIP endonuclease in double-strand break end resection. Mol Cell *54*, 1022-1033.

Mandel, M., and Higa, A. (1970). Calcium-dependent bacteriophage DNA infection. J Mol Biol *53*, 159-162.

Mari, P.O., Florea, B.I., Persengiev, S.P., Verkaik, N.S., Bruggenwirth, H.T., Modesti, M., Giglia-Mari, G., Bezstarosti, K., Demmers, J.A., Luider, T.M., *et al.* (2006). Dynamic assembly of end-joining complexes requires interaction between Ku70/80 and XRCC4. Proc Natl Acad Sci U S A *103*, 18597-18602.

Marti-Renom, M.A., Stuart, A.C., Fiser, A., Sanchez, R., Melo, F., and Sali, A. (2000). Comparative protein structure modeling of genes and genomes. Annu Rev Biophys Biomol Struct *29*, 291-325.

Mashiach, E., Schneidman-Duhovny, D., Andrusier, N., Nussinov, R., and Wolfson, H.J. (2008). FireDock: a web server for fast interaction refinement in molecular docking. Nucleic Acids Res *36*, W229-232.

Matsuoka, S., Ballif, B.A., Smogorzewska, A., McDonald, E.R., 3rd, Hurov, K.E., Luo, J., Bakalarski, C.E., Zhao, Z., Solimini, N., Lerenthal, Y., *et al.* (2007). ATM and ATR substrate analysis reveals extensive protein networks responsive to DNA damage. Science *316*, 1160-1166.

McAlister, G.C., Nusinow, D.P., Jedrychowski, M.P., Wuhr, M., Huttlin, E.L., Erickson, B.K., Rad, R., Haas, W., and Gygi, S.P. (2014). MultiNotch MS3 enables accurate, sensitive, and multiplexed detection of differential expression across cancer cell line proteomes. Anal Chem *86*, 7150-7158.

Mehrotra, S., Languino, L.R., Raskett, C.M., Mercurio, A.M., Dohi, T., and Altieri, D.C. (2010). IAP regulation of metastasis. Cancer Cell *17*, 53-64.

Mimori, T., and Hardin, J.A. (1986). Mechanism of interaction between Ku protein and DNA. J Biol Chem *261*, 10375-10379.

Miura, K., Fujibuchi, W., Ishida, K., Naitoh, T., Ogawa, H., Ando, T., Yazaki, N., Watanabe, K., Haneda, S., Shibata, C., *et al.* (2011). Inhibitor of apoptosis protein family as diagnostic markers and therapeutic targets of colorectal cancer. Surg Today *41*, 175-182.

Mjelle, R., Hegre, S.A., Aas, P.A., Slupphaug, G., Drablos, F., Saetrom, P., and Krokan, H.E. (2015). Cell cycle regulation of human DNA repair and chromatin remodeling genes. DNA Repair (Amst) *30*, 53-67.

Morimoto, S., Tsuda, M., Bunch, H., Sasanuma, H., Austin, C., and Takeda, S. (2019). Type II DNA Topoisomerases Cause Spontaneous Double-Strand Breaks in Genomic DNA. Genes (Basel) *10*.

Natarajan, S., Hombach-Klonisch, S., Droge, P., and Klonisch, T. (2013). HMGA2 inhibits apoptosis through interaction with ATR-CHK1 signaling complex in human cancer cells. Neoplasia *15*, 263-280.

Nemoz, C., Ropars, V., Frit, P., Gontier, A., Drevet, P., Yu, J., Guerois, R., Pitois, A., Comte, A., Delteil, C.*, et al.* (2018). XLF and APLF bind Ku80 at two remote sites to ensure DNA repair by non-homologous end joining. Nat Struct Mol Biol *25*, 971-980.

Ng, A., and Xavier, R.J. (2011). Leucine-rich repeat (LRR) proteins: integrators of pattern recognition and signaling in immunity. Autophagy *7*, 1082-1084.

Niedan, S., Kauer, M., Aryee, D.N., Kofler, R., Schwentner, R., Meier, A., Potschger, U., Kontny, U., and Kovar, H. (2014). Suppression of FOXO1 is responsible for a growth regulatory repressive transcriptional sub-signature of EWS-FLI1 in Ewing sarcoma. Oncogene *33*, 3927-3938.

Niedzialkowska, E., Wang, F., Porebski, P.J., Minor, W., Higgins, J.M., and Stukenberg, P.T. (2012). Molecular basis for phosphospecific recognition of histone H3 tails by Survivin paralogues at inner centromeres. Mol Biol Cell *23*, 1457-1466.

Nunez-Ramirez, R., Klinge, S., Sauguet, L., Melero, R., Recuero-Checa, M.A., Kilkenny, M., Perera, R.L., Garcia-Alvarez, B., Hall, R.J., Nogales, E.*, et al.* (2011). Flexible tethering of primase and DNA Pol alpha in the eukaryotic primosome. Nucleic Acids Res *39*, 8187-8199.

O'Connor, D.S., Grossman, D., Plescia, J., Li, F., Zhang, H., Villa, A., Tognin, S., Marchisio, P.C., and Altieri, D.C. (2000). Regulation of apoptosis at cell division by p34cdc2 phosphorylation of survivin. Proc Natl Acad Sci U S A *97*, 13103-13107.

O'Connor, D.S., Wall, N.R., Porter, A.C., and Altieri, D.C. (2002). A p34(cdc2) survival checkpoint in cancer. Cancer Cell *2*, 43-54.

Oberoi-Khanuja, T.K., Murali, A., and Rajalingam, K. (2013). IAPs on the move: role of inhibitors of apoptosis proteins in cell migration. Cell Death Dis *4*, e784.

Palacios-Rodriguez, Y., Garcia-Lainez, G., Sancho, M., Gortat, A., Orzaez, M., and Perez-Paya, E. (2011). Polypeptide modulators of caspase recruitment domain (CARD)-CARD-mediated protein-protein interactions. J Biol Chem *286*, 44457-44466.

Palmieri, D., Valentino, T., D'Angelo, D., De Martino, I., Postiglione, I., Pacelli, R., Croce, C.M., Fedele, M., and Fusco, A. (2011). HMGA proteins promote ATM expression and enhance cancer cell resistance to genotoxic agents. Oncogene *30*, 3024-3035.

Pan, L., He, Q., Liu, J., Chen, Y., Ma, M., Zhang, L., and Shi, J. (2012). Nuclear-Targeted Drug Delivery of TAT Peptide-Conjugated Monodisperse Mesoporous Silica Nanoparticles. Journal of the American Chemical Society *134*, 5722-5725.

Pandey, A., Vishnoi, K., Mahata, S., Tripathi, S.C., Misra, S.P., Misra, V., Mehrotra, R., Dwivedi, M., and Bharti, A.C. (2015). Berberine and Curcumin Target Survivin and STAT3 in Gastric Cancer Cells and Synergize Actions of Standard Chemotherapeutic 5-Fluorouracil. Nutr Cancer *67*, 1293-1304.

Park, M.H., Kim, S.Y., Kim, Y.J., and Chung, Y.H. (2014). ALS2CR7 (CDK15) attenuates TRAIL induced apoptosis by inducing phosphorylation of survivin Thr34. Biochem Biophys Res Commun *450*, 129-134.

Park, S.H., Shin, I., and Kim, N.D. (2019). An Inhibitor of the Interaction of Survivin with Smac in Mitochondria Promotes Apoptosis. Chem Asian J.

Passmore, L.A., and Barford, D. (2004). Getting into position: the catalytic mechanisms of protein ubiquitylation. Biochem J *379*, 513-525.

Peng, A., Lewellyn, A.L., Schiemann, W.P., and Maller, J.L. (2010). Repo-man controls a protein phosphatase 1-dependent threshold for DNA damage checkpoint activation. Curr Biol *20*, 387-396.

Petraki, C.E. (2014). The role of the inhibitor of apoptosis protein Survivin in cellular radiation response. In Biology (Darmstadt, Technical University of Darmstadt), pp. 127.

Pettersen, E.F., Goddard, T.D., Huang, C.C., Couch, G.S., Greenblatt, D.M., Meng, E.C., and Ferrin, T.E. (2004). UCSF Chimera—A visualization system for exploratory research and analysis. Journal of Computational Chemistry *25*, 1605-1612.

Plenchette, S., Cathelin, S., Rebe, C., Launay, S., Ladoire, S., Sordet, O., Ponnelle, T., Debili, N., Phan, T.H., Padua, R.A.*, et al.* (2004). Translocation of the inhibitor of apoptosis protein c-IAP1 from the nucleus to the Golgi in hematopoietic cells undergoing differentiation: a nuclear export signal-mediated event. Blood *104*, 2035-2043.

Pohl, C., and Jentsch, S. (2008). Final stages of cytokinesis and midbody ring formation are controlled by BRUCE. Cell *132*, 832-845.

Potel, C.M., Lin, M.H., Heck, A.J.R., and Lemeer, S. (2018). Defeating Major Contaminants in Fe(3+)- Immobilized Metal Ion Affinity Chromatography (IMAC) Phosphopeptide Enrichment. Mol Cell Proteomics *17*, 1028-1034.

Quennet, V., Beucher, A., Barton, O., Takeda, S., and Lobrich, M. (2011). CtIP and MRN promote non-homologous end-joining of etoposide-induced DNA double-strand breaks in G1. Nucleic Acids Res *39*, 2144-2152.

Raab, M., Kramer, A., Hehlgans, S., Sanhaji, M., Kurunci-Csacsko, E., Dotsch, C., Bug, G., Ottmann, O., Becker, S., Pachl, F.*, et al.* (2015). Mitotic arrest and slippage induced by pharmacological inhibition of Polo-like kinase 1. Mol Oncol *9*, 140-154.

Radhakrishnan, S.K., and Lees-Miller, S.P. (2017). DNA requirements for interaction of the C-terminal region of Ku80 with the DNA-dependent protein kinase catalytic subunit (DNA-PKcs). DNA Repair (Amst) *57*, 17-28.

Rappsilber, J. (2011). The beginning of a beautiful friendship: cross-linking/mass spectrometry and modelling of proteins and multi-protein complexes. J Struct Biol *173*, 530-540.

Reichert, S., Rodel, C., Mirsch, J., Harter, P.N., Tomicic, M.T., Mittelbronn, M., Kaina, B., and Rodel, F. (2011). Survivin inhibition and DNA double-strand break repair: a molecular mechanism to overcome radioresistance in glioblastoma. Radiother Oncol *101*, 51-58.

Rodel, C., Haas, J., Groth, A., Grabenbauer, G.G., Sauer, R., and Rodel, F. (2003). Spontaneous and radiation-induced apoptosis in colorectal carcinoma cells with different intrinsic radiosensitivities: survivin as a radioresistance factor. Int J Radiat Oncol Biol Phys *55*, 1341-1347.

Rodel, F., Hoffmann, J., Distel, L., Herrmann, M., Noisternig, T., Papadopoulos, T., Sauer, R., and Rodel, C. (2005). Survivin as a radioresistance factor, and prognostic and therapeutic target for radiotherapy in rectal cancer. Cancer Res *65*, 4881-4887.

Rodel, F., Reichert, S., Sprenger, T., Gaipl, U.S., Mirsch, J., Liersch, T., Fulda, S., and Rodel, C. (2011). The role of survivin for radiation oncology: moving beyond apoptosis inhibition. Curr Med Chem *18*, 191-199.

Rodel, F., Sprenger, T., Kaina, B., Liersch, T., Rodel, C., Fulda, S., and Hehlgans, S. (2012). Survivin as a prognostic/predictive marker and molecular target in cancer therapy. Curr Med Chem *19*, 3679-3688.

Röntgen, W.C. (1895). Ueber eine neue Art von Strahlen. In Sitzungsberichte der Wuerzburger Physik-medic Gesellschaft Würzburg (Würzburg), pp. 137-147.

Rosenzweig, K.E., Youmell, M.B., Palayoor, S.T., and Price, B.D. (1997). Radiosensitization of human tumor cells by the phosphatidylinositol3-kinase inhibitors wortmannin and LY294002 correlates with inhibition of DNA-dependent protein kinase and prolonged G2-M delay. Clin Cancer Res *3*, 1149-1156.

Roskelley, C.D., Desprez, P.Y., and Bissell, M.J. (1994). Extracellular matrix-dependent tissue-specific gene expression in mammary epithelial cells requires both physical and biochemical signal transduction. Proc Natl Acad Sci U S A *91*, 12378-12382.

Roux, K.J., Kim, D.I., Raida, M., and Burke, B. (2012). A promiscuous biotin ligase fusion protein identifies proximal and interacting proteins in mammalian cells. J Cell Biol *196*, 801-810.

Roy, S., de Melo, A.J., Xu, Y., Tadi, S.K., Negrel, A., Hendrickson, E., Modesti, M., and Meek, K. (2015). XRCC4/XLF Interaction Is Variably Required for DNA Repair and Is Not Required for Ligase IV Stimulation. Mol Cell Biol *35*, 3017-3028.

Sali, A., and Blundell, T.L. (1993). Comparative protein modelling by satisfaction of spatial restraints. J Mol Biol *234*, 779-815.

Samuel, T., Okada, K., Hyer, M., Welsh, K., Zapata, J.M., and Reed, J.C. (2005). cIAP1 Localizes to the nuclear compartment and modulates the cell cycle. Cancer Res *65*, 210-218.

Sasai, K., Katayama, H., Hawke, D.H., and Sen, S. (2016). Aurora-C Interactions with Survivin and INCENP Reveal Shared and Distinct Features Compared with Aurora-B Chromosome Passenger Protein Complex. PLoS One *11*, e0157305.

Sastry, G.M., Adzhigirey, M., Day, T., Annabhimoju, R., and Sherman, W. (2013). Protein and ligand preparation: parameters, protocols, and influence on virtual screening enrichments. J Comput Aided Mol Des *27*, 221-234.

Schneidman-Duhovny, D., Wolfson, H.J., Nussinov, R., and Inbar, Y. (2005). PatchDock and SymmDock: servers for rigid and symmetric docking. Nucleic Acids Research *33*, W363-W367.

Shapovalov, M.V., and Dunbrack, R.L., Jr. (2011). A smoothed backbone-dependent rotamer library for proteins derived from adaptive kernel density estimates and regressions. Structure *19*, 844-858.

Shiga, S., Murata, Y., Hashimoto, T., Urushihara, Y., Fujishima, Y., Kudo, K., Sonohara, Y., Kurusu, M., Takeda, K., Jingu, K.*, et al.* (2020). DNA-PKcs is activated under nutrient starvation and activates Akt, MST1, FoxO3a, and NDR1. Biochem Biophys Res Commun *521*, 668-673.

Sibanda, B.L., Chirgadze, D.Y., Ascher, D.B., and Blundell, T.L. (2017). DNA-PKcs structure suggests an allosteric mechanism modulating DNA double-strand break repair. Science *355*, 520-524.

Singh, A., Ye, M., Bucur, O., Zhu, S., Tanya Santos, M., Rabinovitz, I., Wei, W., Gao, D., Hahn, W.C., and Khosravi-Far, R. (2010). Protein phosphatase 2A reactivates FOXO3a through a dynamic interplay with 14-3-3 and AKT. Mol Biol Cell *21*, 1140-1152.

Singh, I., Ozturk, N., Cordero, J., Mehta, A., Hasan, D., Cosentino, C., Sebastian, C., Kruger, M., Looso, M., Carraro, G.*, et al.* (2015). High mobility group protein-mediated transcription requires DNA damage marker gamma-H2AX. Cell Res *25*, 837-850.

Singh, M., Hunt, C.R., Pandita, R.K., Kumar, R., Yang, C.R., Horikoshi, N., Bachoo, R., Serag, S., Story, M.D., Shay, J.W., *et al.* (2013). Lamin A/C depletion enhances DNA damage-induced stalled replication fork arrest. Mol Cell Biol *33*, 1210-1222.

So, E.Y., Kozicki, M., and Ouchi, T. (2013). Roles of DNA Damage Response Proteins in Mitogen-Induced Thp-1 Differentiation into Macrophage. J Cancer Biol Res *1*.

Song, Z., Yao, X., and Wu, M. (2003). Direct interaction between survivin and Smac/DIABLO is essential for the anti-apoptotic activity of survivin during taxol-induced apoptosis. J Biol Chem *278*, 23130-23140.

Spagnolo, L., Rivera-Calzada, A., Pearl, L.H., and Llorca, O. (2006). Three-dimensional structure of the human DNA-PKcs/Ku70/Ku80 complex assembled on DNA and its implications for DNA DSB repair. Mol Cell *22*, 511-519.

Sprenger, T., Rodel, F., Beissbarth, T., Conradi, L.C., Rothe, H., Homayounfar, K., Wolff, H.A., Ghadimi, B.M., Yildirim, M., Becker, H., *et al.* (2011). Failure of downregulation of survivin following neoadjuvant radiochemotherapy in rectal cancer is associated with distant metastases and shortened survival. Clin Cancer Res *17*, 1623-1631.

Srinivasula, S.M., and Ashwell, J.D. (2008). IAPs: what's in a name? Mol Cell *30*, 123-135.

Stone, S.L., Hauksdottir, H., Troy, A., Herschleb, J., Kraft, E., and Callis, J. (2005). Functional analysis of the RING-type ubiquitin ligase family of Arabidopsis. Plant Physiol *137*, 13-30.

Storch, K., Eke, I., Borgmann, K., Krause, M., Richter, C., Becker, K., Schrock, E., and Cordes, N. (2010). Three-dimensional cell growth confers radioresistance by chromatin density modification. Cancer Res *70*, 3925-3934.

Su, V., and Lau, A.F. (2009). Ubiquitin-like and ubiquitin-associated domain proteins: significance in proteasomal degradation. Cell Mol Life Sci *66*, 2819-2833.

Sun, Y., Rombola, C., Jyothikumar, V., and Periasamy, A. (2013). Forster resonance energy transfer microscopy and spectroscopy for localizing protein-protein interactions in living cells. Cytometry A *83*, 780-793.

Suzuki, A., Ito, T., Kawano, H., Hayashida, M., Hayasaki, Y., Tsutomi, Y., Akahane, K., Nakano, T., Miura, M., and Shiraki, K. (2000). Survivin initiates procaspase 3/p21 complex formation as a result of interaction with Cdk4 to resist Fas-mediated cell death. Oncogene *19*, 1346-1353.

Tang, E.D., Wang, C.Y., Xiong, Y., and Guan, K.L. (2003). A role for NF-kappaB essential modifier/IkappaB kinase-gamma (NEMO/IKKgamma) ubiquitination in the activation of the IkappaB kinase complex by tumor necrosis factor-alpha. J Biol Chem *278*, 37297-37305.

Thin, T.H., Li, L., Chung, T.K., Sun, H., and Taneja, R. (2007). Stra13 is induced by genotoxic stress and regulates ionizing-radiation-induced apoptosis. EMBO Rep *8*, 401-407.

Vanommeslaeghe, K., Hatcher, E., Acharya, C., Kundu, S., Zhong, S., Shim, J., Darian, E., Guvench, O., Lopes, P., Vorobyov, I., *et al.* (2010). CHARMM general force field: A force field for drug-like molecules compatible with the CHARMM all-atom additive biological force fields. J Comput Chem *31*, 671-690.

Velkova, A., Carvalho, M.A., Johnson, J.O., Tavtigian, S.V., and Monteiro, A.N. (2010). Identification of Filamin A as a BRCA1-interacting protein required for efficient DNA repair. Cell Cycle *9*, 1421-1433.

Verdecia, M.A., Huang, H., Dutil, E., Kaiser, D.A., Hunter, T., and Noel, J.P. (2000). Structure of the human anti-apoptotic protein survivin reveals a dimeric arrangement. Nat Struct Biol *7*, 602-608.

Vizcaino, J.A., Csordas, A., del-Toro, N., Dianes, J.A., Griss, J., Lavidas, I., Mayer, G., Perez-Riverol, Y., Reisinger, F., Ternent, T.*, et al.* (2016). 2016 update of the PRIDE database and its related tools. Nucleic Acids Res *44*, D447-456.

Vizcaino, J.A., Deutsch, E.W., Wang, R., Csordas, A., Reisinger, F., Rios, D., Dianes, J.A., Sun, Z., Farrah, T., Bandeira, N.*, et al.* (2014). ProteomeXchange provides globally coordinated proteomics data submission and dissemination. Nat Biotechnol *32*, 223-226.

Walker, A.I., Hunt, T., Jackson, R.J., and Anderson, C.W. (1985). Double-stranded DNA induces the phosphorylation of several proteins including the 90 000 mol. wt. heat-shock protein in animal cell extracts. The EMBO journal *4*, 139-145.

Wang, F., Dai, J., Daum, J.R., Niedzialkowska, E., Banerjee, B., Stukenberg, P.T., Gorbsky, G.J., and Higgins, J.M. (2010). Histone H3 Thr-3 phosphorylation by Haspin positions Aurora B at centromeres in mitosis. Science *330*, 231-235.

Wang, H.W., and Wang, J.W. (2017). How cryo-electron microscopy and X-ray crystallography complement each other. Protein Sci *26*, 32-39.

Wang, Q., Arnst, K.E., Xue, Y., Lei, Z.N., Ma, D., Chen, Z.S., Miller, D.D., and Li, W. (2018a). Synthesis and biological evaluation of indole-based UC-112 analogs as potent and selective survivin inhibitors. Eur J Med Chem *149*, 211-224.

Wang, W.Y., Cao, Y.X., Zhou, X., Wei, B., Zhan, L., and Fu, L.T. (2018b). HMGA2 gene silencing reduces epithelial-mesenchymal transition and lymph node metastasis in cervical cancer through inhibiting the ATR/Chk1 signaling pathway. Am J Transl Res *10*, 3036-3052.

Wang, X., Beitler, J.J., Huang, W., Chen, G., Qian, G., Magliocca, K., Patel, M.R., Chen, A.Y., Zhang, J., Nannapaneni, S.*, et al.* (2018c). Honokiol Radiosensitizes Squamous Cell Carcinoma of the Head and Neck by Downregulation of Survivin. Clin Cancer Res *24*, 858-869.

Wang, X., Chu, H., Lv, M., Zhang, Z., Qiu, S., Liu, H., Shen, X., Wang, W., and Cai, G. (2016). Structure of the intact ATM/Tel1 kinase. Nat Commun *7*, 11655.

Wang, X., Ran, T., Zhang, X., Xin, J., Zhang, Z., Wu, T., Wang, W., and Cai, G. (2017). 3.9 A structure of the yeast Mec1-Ddc2 complex, a homolog of human ATR-ATRIP. Science *358*, 1206-1209.

Wang, Y.G., Nnakwe, C., Lane, W.S., Modesti, M., and Frank, K.M. (2004). Phosphorylation and regulation of DNA ligase IV stability by DNA-dependent protein kinase. J Biol Chem *279*, 37282-37290.

Waterman, D.P., Haber, J.E., and Smolka, M.B. (2020). Checkpoint Responses to DNA Double-Strand Breaks. Annu Rev Biochem.

Webb, B., and Sali, A. (2016). Comparative Protein Structure Modeling Using MODELLER. Curr Protoc Bioinformatics *54*, 5 6 1-5 6 37.

Wheatley, S.P., and Altieri, D.C. (2019). Survivin at a glance. J Cell Sci *132*.

Wheatley, S.P., Barrett, R.M., Andrews, P.D., Medema, R.H., Morley, S.J., Swedlow, J.R., and Lens, S.M. (2007). Phosphorylation by aurora-B negatively regulates survivin function during mitosis. Cell Cycle *6*, 1220-1230.

Woodard, R.L., Anderson, M.G., and Dynan, W.S. (1999). Nuclear extracts lacking DNA-dependent protein kinase are deficient in multiple round transcription. J Biol Chem *274*, 478-485.

Wu, C.S., Ouyang, J., Mori, E., Nguyen, H.D., Marechal, A., Hallet, A., Chen, D.J., and Zou, L. (2014). SUMOylation of ATRIP potentiates DNA damage signaling by boosting multiple protein interactions in the ATR pathway. Genes Dev *28*, 1472-1484.

Xiao, M., Wang, J., Lin, Z., Lu, Y., Li, Z., White, S.W., Miller, D.D., and Li, W. (2015). Design, Synthesis and Structure-Activity Relationship Studies of Novel Survivin Inhibitors with Potent Anti-Proliferative Properties. PLOS ONE *10*, e0129807.

Xu, P., Van Kirk, E.A., Zhan, Y., Murdoch, W.J., Radosz, M., and Shen, Y. (2007). Targeted charge-reversal nanoparticles for nuclear drug delivery. Angew Chem Int Ed Engl *46*, 4999-5002.

Yajima, H., Lee, K.J., and Chen, B.P. (2006). ATR-dependent phosphorylation of DNA-dependent protein kinase catalytic subunit in response to UV-induced replication stress. Mol Cell Biol *26*, 7520-7528.

Yamagishi, Y., Honda, T., Tanno, Y., and Watanabe, Y. (2010). Two histone marks establish the inner centromere and chromosome bi-orientation. Science *330*, 239-243.

Yaneva, M., Kowalewski, T., and Lieber, M.R. (1997). Interaction of DNA-dependent protein kinase with DNA and with Ku: biochemical and atomic-force microscopy studies. EMBO J *16*, 5098-5112.

Yu, Y., Wang, W., Ding, Q., Ye, R., Chen, D., Merkle, D., Schriemer, D., Meek, K., and Lees-Miller, S.P. (2003). DNA-PK phosphorylation sites in XRCC4 are not required for survival after radiation or for V(D)J recombination. DNA Repair (Amst) *2*, 1239-1252.

Yue, J., Huhn, S., and Shen, Z. (2013). Complex roles of filamin-A mediated cytoskeleton network in cancer progression. Cell Biosci *3*, 7.

Zhang, S., Mo, Q., and Wang, X. (2019). Oncological role of HMGA2 (Review). Int J Oncol *55*, 775-788.

Zhao, B., Watanabe, G., and Lieber, M.R. (2020). Polymerase mu in non-homologous DNA end joining: importance of the order of arrival at a double-strand break in a purified system. Nucleic Acids Res *48*, 3605-3618.

Zhao, B., Watanabe, G., Morten, M.J., Reid, D.A., Rothenberg, E., and Lieber, M.R. (2019). The essential elements for the noncovalent association of two DNA ends during NHEJ synapsis. Nat Commun *10*, 3588.

Zheng, W.H., Kar, S., and Quirion, R. (2000). Insulin-like growth factor-1-induced phosphorylation of the forkhead family transcription factor FKHRL1 is mediated by Akt kinase in PC12 cells. J Biol Chem *275*, 39152-39158.

Zhou, Y., Lee, J.H., Jiang, W., Crowe, J.L., Zha, S., and Paull, T.T. (2017a). Regulation of the DNA Damage Response by DNA-PKcs Inhibitory Phosphorylation of ATM. Mol Cell *65*, 91-104.

Zhou, Z., Liu, Y., Wu, L., Li, L., and Huang, Y. (2017b). Enhanced nuclear delivery of anti-cancer drugs using micelles containing releasable membrane fusion peptide and nuclear-targeting retinoic acid. Journal of Materials Chemistry B *5*, 7175-7185.

Zschenker, O., Streichert, T., Hehlgans, S., and Cordes, N. (2012). Genome-wide gene expression analysis in cancer cells reveals 3D growth to affect ECM and processes associated with cell adhesion but not DNA repair. PLoS One *7*, e34279.

7. Appendix

7.1. Virtual Screening Hits

Table 11. Virtual screening final candidate ligands for S20 residue of Survivin. (A, Asinex repository. C, ChemBridge repository. M, MolPort repository.)

Id	Structure	Mol. weight (g/mol)	pK_d	ΔG (kcal/mol)	XP Gscore
A-194858	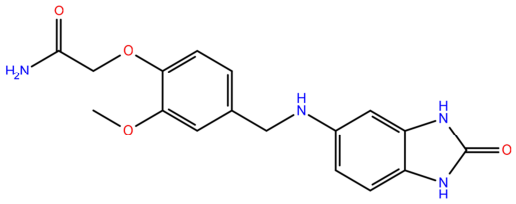	342.13	2.1	-2.83	-5.561
C-479488	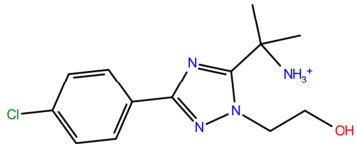	281.12	2.58	-3.48	-5.498
M-000-631-284	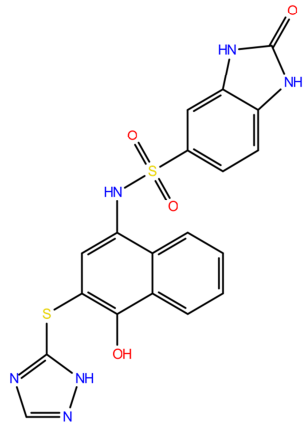	454.05	4.29	-5.79	-5.321

Table 12. Virtual screening final candidate ligands for W67 residue of Survivin. (C, ChemBridge repository. M, MolPort repository. S, Specs repository.)

Id	Structure	Mol. weight (g/mol)	pK_d	ΔG (kcal/mol)	XP Gscore
C-433489	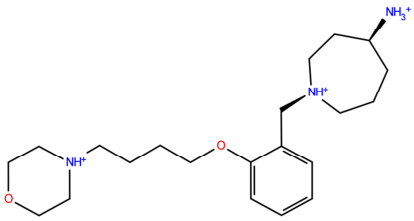	364,29	4,89	-6,61	-9,963
C-556129	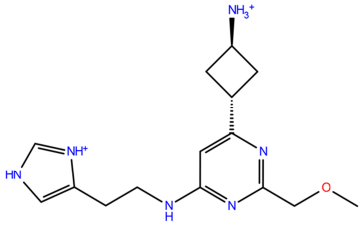	304,2	4,51	-6,08	-9,881
C-190989	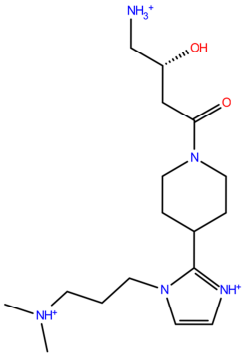	340,27	5,05	-6,82	-9,783
C-506743	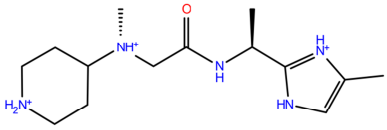	282,23	3,65	-4,93	-9,586
M-005-139-808	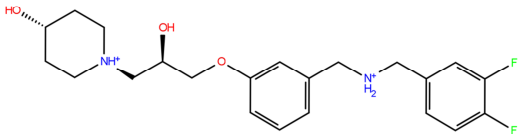	408,22	5,79	-7,82	-9,586
C-595802	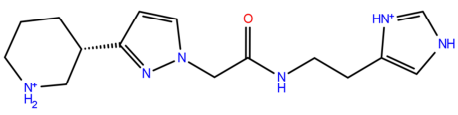	304,2	5,08	-6,86	-9,525
C-2952	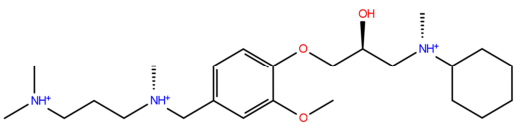	424,35	5,32	-7,18	-9,513
C-181550	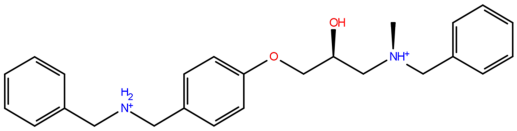	392,25	4,78	-6,45	-9,507

Id	Structure	Mol. weight (g/mol)	pK_d	ΔG (kcal/mol)	XP Gscore
C-224979	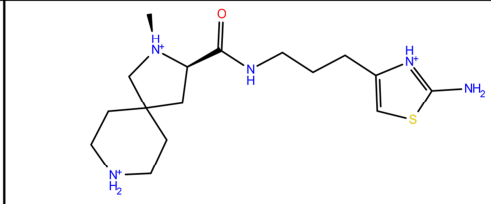	340,22	5,22	-7,04	-9,443
C-48286	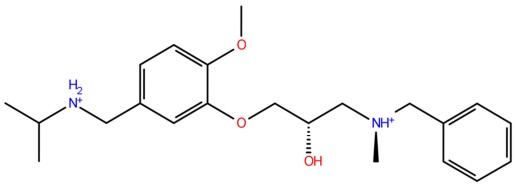	374,26	4,88	-6,58	-9,400
C-249176	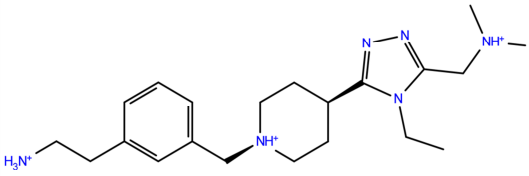	373,31	5,55	-7,49	-9,265
M-000-002-141	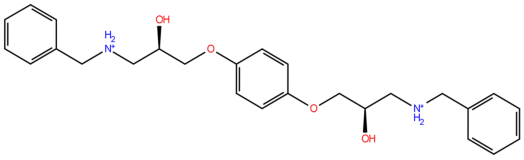	438,25	4,49	-6,07	-9,231
C-423769	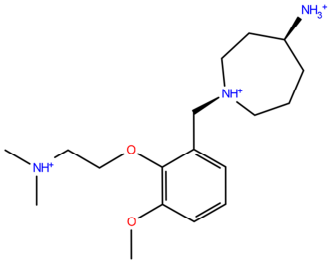	324,26	4,34	-5,85	-9,193
M-005-148-815	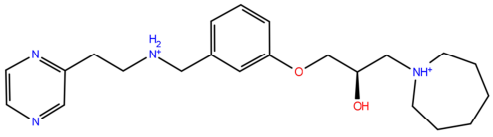	386,27	5,41	-7,3	-9,146
S-414361	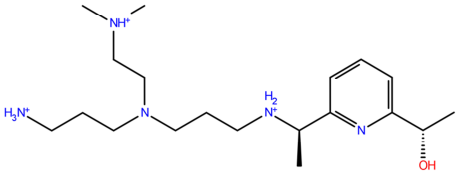	354,32	4,36	-5,89	-9,119

Id	Structure	Mol. weight (g/mol)	pK_d	ΔG (kcal/mol)	XP Gscore
C-61592	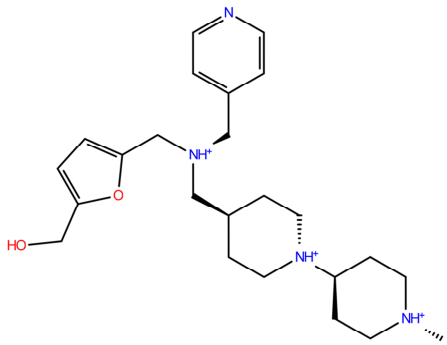	415,31	4,2	-5,67	-9,117
C-12848	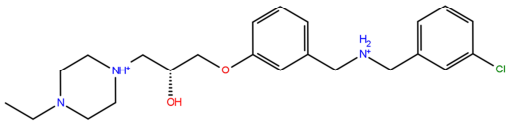	419,23	5,79	-7,81	-9,078
C-578799	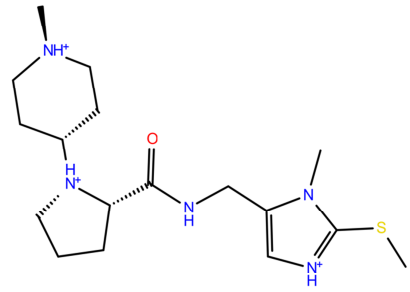	354,23	4,94	-6,67	-9,068
C-393833	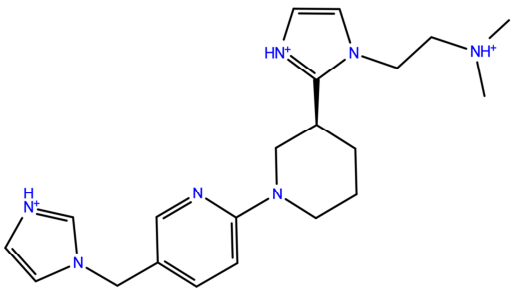	382,27	5,59	-7,55	-9,021
C-5707	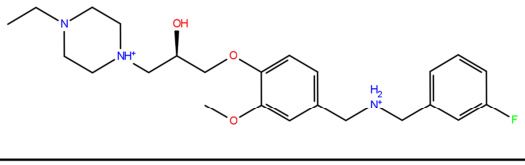	433,27	5,71	-7,71	-9,006

7.2. DNA sequences

Survivin wt

GGTGCCCCGACGTTGCCCCCTGCCTGGCAGCCCTTTCTCAAGGACCACCGCATCTCTACATTCA
AGAACTGGCCCTTCTTGGAGGGCTGCGCCTGCACCCCGGAGCGGATGGCCGAGGCTGGCTTCA
TCCACTGCCCCACTGAGAACGAGCCAGACTTGGCCCAGTGTTTCTTCTGCTTCAAGGAGCTGGA
AGGCTGGGAGCCAGATGACGACCCCATAGAGGAACATAAAAAGCATTCGTCCGGTTGCGCTTT
CCTTTCTGTCAAGAAGCAGTTTGAAGAATTAACCCTTGGTGAATTTTTGAAACTGGACAGAGAA
AGAGCCAAGAACAAAATTGCAAAGGAAACCAACAATAAGAAGAAAGAATTTGAGGAAACTGCG
GAGAAAGTGCGCCGTGCCATCGAGCAGCTGGCTGCCATGGAT

PI3K-DNA-PKcs

ATGGAACACCCTTTCCTGGTGAAGGGTGGCGAGGACCTGCGGCAGGACCAGCGCGTGGAGCAG
CTCTTCCAGGTCATGAATGGGATCCTGGCCCAAGACTCCGCCTGCAGCCAGAGGGCCCTGCAG
CTGAGGACCTATAGCGTTGTGCCCATGACCTCCAGGTTAGGATTAATTGAGTGGCTTGAAAATA
CTGTTACCTTGAAGGACCTTCTTTTGAACACCATGTCCCAAGAGGAGAAGGCGGCTTACCTGAG
TGATCCCAGGGCACCGCCGTGTGAATATAAAGATTGGCTGACAAAAATGTCAGGAAAACATGAT
GTTGGAGCTTACATGCTAATGTATAAGGGCGCTAATCGTACTGAAACAGTCACGTCTTTTAGAA
AACGAGAAAGTAAAGTGCCTGCTGATCTCTTAAAGCGGGCCTTCGTGAGGATGAGTACAAGCC
CTGAGGCTTTCCTGGCGCTCCGCTCCCACTTCGCCAGCTCTCACGCTCTGATATGCATCAGCCA
CTGGATCCTCGGGATTGGAGACAGACATCTGAACAACTTTATGGTGGCCATGGAGACTGGCGG
CGTGATCGGGATCGACTTTGGGCATGCGTTTGGATCCGCTACACAGTTTCTGCCAGTCCCTGAG
TTGATGCCTTTTCGGCTAACTCGCCAGTTTATCAATCTGATGTTACCAATGAAAGAAACGGGCC
TTATGTACAGCATCATGGTACACGCACTCCGGGCCTTCCGCTCAGACCCTGGCCTGCTCACCAA
CACCATGGATGTGTTTGTCAAGGAGCCCTCCTTTGATTGGAAAAAT

HEAT1-DNA-PKcs

ATGGCGGGCTCCGGAGCCGGTGTGCGTTGCTCCCTGCTGCGGCTGCAGGAGACCTTGTCCGCT
GCGGACCGCTGCGGTGCTGCCCTGGCCGGTCATCAACTGATCCGCGGCCTGGGGCAGGAATGC
GTCCTGAGCAGCAGCCCCGCGGTGCTGGCATTACAGACATCTTTAGTTTTTTCCAGAGATTTCG
GTTTGCTTGTATTTGTCCGGAAGTCACTCAACAGTATTGAATTTCGTGAATGTAGAGAAGAAAT
CCTAAAGTTTTTATGTATTTTCTTAGAAAAAATGGGCCAGAAGATCGCACCTTACTCTGTTGAAA
TTAAGAACACTTGTACCAGTGTTTATACAAAAGATAGAGCTGCTAAATGTAAAATTCCAGCCCT
GGACCTTCTTATTAAGTTACTTCAGACTTTTAGAAGTTCTAGACTCATGGATGAATTTAAAATTG
GAGAATTATTTAGTAAATTCTATGGAGAACTTGCATTGAAAAAAAAAATACCAGATACAGTTTTA
GAAAAAGTATATGAGCTCCTAGGATTATTGGGTGAAGTTCATCCTAGTGAGATGATAAATAATG
CAGAAAACCTGTTCCGCGCTTTTCTGGGTGAACTTAAGACCCAGATGACATCAGCAGTAAGAGA
GCCCAAACTACCTGTTCTGGCAGGATGTCTGAAGGGGTTGTCCTCACTTCTGTGCAACTTCACT
AAGTCCATGGAAGAAGATCCCCAGACTTCAAGGGAGATTTTTAATTTTGTACTAAAGGCAATTC
GTCCTCAGATTGATCTGAAGAGATATGCTGTGCCCTCAGCTGGCTTGCGCCTATTTGCCCTGCA
TGCATCTCAGTTTAGCACCTGCCTTCTGGACAACTACGTGTCTCTATTTGAAGTCTTGTTAAAGT
GGTGTGCCCACACAAATGTAGAATTGAAAAAAGCTGCACTTTCAGCCCTGGAATCCTTTCTGAA

ACAGGTTTCTAATATGGTGGCGAAAAATGCAGAAATGCATAAAAATAAACTGCAGTACTTTATG
GAGCAGTTTTATGGAATCATCAGAAATGTGGATTCGAACAACAAGGAGTTATCTATTGCTATCC
GTGGATATGGACTTTTTGCAGGACCGTGCAAGGTTATAAAC

FATC-DNA-PKcs

ATGCTGAAAAAAGGAGGGTCATGGATTCAAGAAATAAATGTTGCTGAAAAAAATTGGTACCCCC
GACAGAAAATATGTTACGCTAAGAGAAAGTTAGCAGGTGCCAATCCAGCAGTCATTACTTGTGA
TGAGCTACTCCTGGGTCATGAGAAGGCCCCTGCCTTCAGAGACTATGTGGCTGTGGCACGAGG
AAGCAAAGATCACAACATTCGTGCCCAAGAACCAGAGAGTGGGCTTTCAGAAGAGACTCAAGT
GAAGTGCCTGATGGACCAGGCAACAGACCCCAACATCCTTGGCAGAACCTGGGAAGGATGGGA
GCCCTG

PI3K-ATM

ATGGTGGACCACACAGGAGAATATGGAAATCTGGTGACTATACAGTCATTTAAAGCAGAATTTC
GCTTAGCAGGAGGTGTAAATTTACCAAAAATAATAGATTGTGTAGGTTCCGATGGCAAGGAGAG
GAGACAGCTTGTTAAGGGCCGTGATGACCTGAGACAAGATGCTGTCATGCAACAGGTCTTCCA
GATGTGTAATACATTACTGCAGAGAAACACGGAAACTAGGAAGAGGAAATTAACTATCTGTACT
TATAAGGTGGTTCCCCTCTCTCAGCGAAGTGGTGTTCTTGAATGGTGCACAGGAACTGTCCCCA
TTGGTGAATTTCTTGTTAACAATGAAGATGGTGCTCATAAAAGATACAGGCCAAATGATTTCAG
TGCCTTTCAGTGCCAAAAGAAAATGATGGAGGTGCAAAAAAAGTCTTTTGAAGAGAAATATGAA
GTCTTCATGGATGTTTGCCAAAATTTTCAACCAGTTTTCCGTTACTTCTGCATGGAAAAATTCTT
GGATCCAGCTATTTGGTTTGAGAAGCGATTGGCTTATACGCGCAGTGTAGCTACTTCTTCTATT
GTTGGTTACATACTTGGACTTGGTGATAGACATGTACAGAATATCTTGATAAATGAGCAGTCAG
CAGAACTTGTACATATAGATCTAGGTGTTGCTTTTGAACAGGGCAAAATCCTTCCTACTCCTGA
GACAGTTCCTTTTAGACTCACCAGAGATATTGTGGATGGCATGGGCATTACGGGTGTTGAAGGT
GTCTTCAGAAGATGCTGTGAGAAAACCATGGAAGTGATGAGAAACTCTCAGGAAACTCTGTTAA
CCATTGTAGAGGTCCTTCTATATGATCCACTCTTTGACTGGACCATGAATCCTTTGAAAGCTTTG
TATTTACAGCAGAGG

7.3. Curriculum Vitae

Name: Ömer Güllülü

Day of birth: 27.11.1990

Place of birth: Gebze, Turkey

Nationality: Turkish

Education:

07/2017 – 12/2020	Technical University of Darmstadt, Germany PhD student and scholar within the GRK 1657 Subject: Spatial and functional interrelationship of a heterotetramer Survivin-DNA-PKcs complex in the repair of DNA double-strand breaks. Project accomplished at the Molecular Radiation Biology research group, Department of Radiotherapy and Oncology, Goethe-University Frankfurt, Germany, Principal investigator: Prof. Dr. Franz Rödel
02/2015 – 07/2017	Gebze Technical University, Turkey Master of Science, Molecular Biology and Genetics Subject: Regulation of subcellular localization and functions of coiled-coil domain-containing 124 (CCDC124) protein by post translational mechanisms
09/2011 – 06/2014	Gebze Institute of Technology, Turkey Bachelor of Science, Molecular Biology and Genetics Subject: From midbody protein-protein interactions to possible interactions of coiled-coil domain-containing 124 (CCDC124) protein
09/2004 – 06/2008	Sezai Türkes Feyzi Akkaya Vocational and Technical Anatolian High School, Turkey Division: Mechatronics Subject: Remote-controlled mobile watering system for the people with disabilities and older people
09/1996 – 06/2004	Cumhuriyet Elementary School, Turkey

Publications:

- Hehlgans, S.; Booms, P.; Güllülü, Ö.; Sader, R.; Rödel, C.; Balermpas, P.; Rödel, F.; Ghanaati, S. Radiation Sensitization of Basal Cell and Head and Neck Squamous Cell Carcinoma by the Hedgehog Pathway Inhibitor Vismodegib. Int. J. Mol. Sci. 2018, 19, 2485.

Conference proceedings:

- Investigations on the interaction regions of Survivin and DNA-PKcs by combining *in silico* and FACS-FRET methods (Poster)

  Güllülü Ö., Hehlgans S., Weipert F., Hoffmann M., Rödel C., Rödel F.

  24. Jahrestagung der Deutschen Gesellschaft für Radioonkologie e.V. (DEGRO), 21-24/06/2018, Leipzig

- Identification of the interaction regions of Survivin and DNA-PKcs by combining structure-based molecular docking and site directed mutagenesis (Talk)

  Güllülü Ö., Hoffmann M., Rödel C., Hehlgans S., Rödel F.

  Gesellschaft für Biologische Strahlenforschung e.V. (GBS) 21. Annual Meeting, 17-19/09/2018, Frankfurt

- Combining the structural bioinformatics and FACS-FRET methods to investigate the interaction interfaces of Survivin and DNA-PKcs on a molecular resolution level (Poster)

  Güllülü Ö., Hoffmann M., Rödel C., Hehlgans S., Rödel F.

  Universitäres Centrum für Tumorerkrankungen (UCT) Frankfurt Cancer Conference, 25-27/09/2018, Frankfurt

- Survivin regulates the DNA Damage Repair by modulating the kinase activity of DNA-PKcs (Poster)

  Güllülü Ö., Hoffmann M., Rödel C., Hehlgans S., Rödel F.

  25. Jahrestagung der Deutschen Gesellschaft für Radioonkologie e.V. (DEGRO), 13-16/06/2019, Münster

- Survivin modulates the DNA damage-dependent radiosensitivity of colorectal cancer cells (Poster)

  Güllülü Ö., Hoffmann M., Rödel C., Hehlgans S., Rödel F.

  9th Universitäres Centrum für Tumorerkrankungen (UCT) Science Day, 04/09/2019, Frankfurt

- Survivin impacts on the radiation response of colorectal cancer cells by increasing the kinase activity of DNA-PKcs (Talk)

  Güllülü Ö., Hoffmann M., Rödel C., Hehlgans S., Rödel F.

  Deutsche Gesellschaft für Biologische Strahlenforschung e.V. (deGBS), 22. Annual Meeting, 23-25/09/2019, Mannheim

7.4. Own Work

Experiments, data analysis and writing of this thesis were all done by myself with exception of the following items:

Figure 10 taken from the PhD thesis of Chrysi Petraki (Petraki, 2014) to mention the importance of the Survivin BIR domain in previous findings in the context of 3D clonogenic radiation survival and DNA damage repair.

Large-scale molecular docking and molecular dynamics simulations in Figure 6, 7, 23a,b,c, 24 and 25 were performed by Benjamin Mayer, Maximilian Dombrowsky, Patrick Kunzmann and Prof. Dr. Kay Hamacher in a GRK1657 collaboration study (Computational Biology and Simulation Group – Department of Biology, Technical University of Darmstadt).

Phosphoproteomics and proteomics analyses/raw data, and Figure 28 and 33 were provided by Ines Gößner and Dr. Christian Münch in a collaboration study (Institute of Biochemistry II, Faculty of Medicine, Goethe University Frankfurt).

7.5. Acknowledgments

I would like to thank Prof. Dr. Franz Rödel for providing me an opportunity to work on this interesting Survivin project in his laboratory. It is crucial to state that this project has catched the fire with his great supervision, guidance, support, encouragements and scientific discussions.

I don't know how to thank Dr. Stephanie Hehlgans because it was impossible to bring the story to this point without her scientific vision, knowledge, and efforts over the years. And she was all the time friendly, kind, and complaisant as a colleague. I deeply appreciate you, and I am happy and grateful to work with you.

I would like to thank Prof. Dr. Claus Rödel and Prof. Dr. Emmanouil Fokas for their interest in this project and liberality on the usage of department facilities.

I would like to thank all former and present members of the research group of Prof. Dr. Franz Rödel, all were friendly, humble and great colleagues. Particularly, Melanie Hoffmann, Dr. Chrysi Petraki, Dr. Fabian Weipert, Dr. Gianni Capalbo and Dr. Sebastian Reichert, by the help of their initial works, our current work stepped forward. Especially, I would like to express my best appreciations that without the great help of Julius Oppermann, we couldn't make it. Also, I thank Jeannie Peifer for her help and valued colleagueship.

I thank all employees of the Department of Radiotherapy and Oncology (University Hospital Frankfurt), specially to medical physicists, and medical technical assistants for taking care of the daily dosimetry of LINACs.

I am grateful to Prof. Dr. Franz Rödel and Prof. Dr. Markus Löbrich for being my supervisors and Prof. Dr. Alexander Löwer and Prof. Dr. Kay Hamacher for being my examiners, as well as for their constructive comments and criticisms over the course of my study.

I also thank Prof. Dr. Markus Löbrich to realize the GRK1657 graduate school project, and to the funder German Research Foundation (DFG) as well, that provided me a wide range of opportunities such as regular retreats, biological colloqiums, support for symposiums/congresses/workshops and much more to get scientifically well-equipped and prepared.

I am thankful to the contributions of Benjamin Mayer, Maximilian Dombrowsky, Patrick Kunzmann, and Prof. Dr. Kay Hamacher in a great collaboration under the GRK1657 project. And, a huge thanks to Ines Gößner and Dr. Christian Münch for the great work and contributions.

I would like to thank the research groups of Prof. Dr. Klaus Strebhardt and Prof. Dr. Juping Yuan for their help and weekly journal clubs full of novel aspects of science. Notedly, I want to thank Dr. Nina-Naomi Kreis for her help on kinase assays.

Finally, I express heartful thanks to my family. Their support and love are my source of energy and motivation; so glad I have all you…

7.6. List of abbreviations

Abbreviation	Full name
ΔG	Binding free energy
γH2AX	S139 phosphorylated H2A histone family member X
3D	Three dimensional
53BP1	P53-binding protein 1
5-FU	5-fluorouracil
ABHD15	Abhydrolase domain containing 15
ACIN1	Apoptotic chromatin condensation inducer 1
ADME	Absorption, distribution, metabolism, and excretion
AEN	Apoptosis enhancing nuclease
AKAP11	A-kinase anchoring protein 11
Akt/PKB	Akr thymoma serine/threonine-specific protein kinase; protein kinase B
ANLN	Anillin actin binding protein
AP3D1	Adaptor related protein complex 3 subunit delta 1
Apaf1	Apoptotic protease-activating factor 1
APS	Ammonium persulfate
ASL	Argininosuccinate lyase
ASNS	Asparagine synthetase (glutamine-hydrolyzing)
ASS1	Argininosuccinate synthase 1
ATF7IP	Activating transcription factor 7 interacting protein
ATG5/12/16	Autophagy related protein 5/12/16
ATM	Ataxia telangiectasia mutated protein kinase
ATP [γ-32P]	Adenosine triphosphate, labeled on the gamma phosphate group with ^{32}P
ATR	Ataxia telangiectasia and RAD3 related protein
ATRIP	ATR interacting protein
AURKB	Aurora kinase B
B3GNT1	Beta-1,4-glucuronyltransferase 1
BCA	Bicinchoninic acid
BCLAF3	BCLAF1 and THRAP3 family member 3
BECLIN-1	Coiled-coil myosin-like BCL2-interacting protein
BIR/ΔBIR	Baculoviral IAP repeat / deletion of BIR domain
BIRC1/2/3/4/5/6/7/8	Baculoviral IAP repeat containing 1/2/3/4/5/6/7/8
BRCA1/2	Breast cancer type 1/2 susceptibility protein
BRIT1	BRCT-repeat inhibitor of TERT expression 1
BRUCE	BIR repeat containing ubiquitin-conjugating enzyme
BS3	Bis(sulfosuccinimidyl)suberate
BSA	Bovine serum albumin
C, Cys	Cysteine
C31A	Alanine mutation on cysteine 31 residue of Survivin
CAD	Carbamoyl-phosphate synthetase 2, aspartate transcarbamylase, and

	dihydroorotase
CARD	Caspase recruitment domain
CASP8AP2	Caspase 8 associated protein 2
CCNA2	Cyclin A2
CDC20	Cell division cycle 20
CDCA2/8	Cell division cycle associated 2/8
CDK1/CDC2	Cyclin-dependent kinase 1; Cell division control protein 2
CDK4	Cyclin-dependent kinase 4
CDKAL1	CDK5 regulatory subunit associated protein 1 like 1
CENPF	Centromere protein F
CERS6	Ceramide synthase 6
CHD2/4	Chromodomain helicase DNA binding protein 2/4
c-IAP1/2	Cellular-IAP1/2
CIC	Capicua transcriptional repressor
CPC	Chromosomal passenger complex
CPP	Cell penetration peptide
CPSF7	Cleavage and polyadenylation specific factor 7
CRKL	CRK like proto-oncogene, adaptor protein
D, Asp	Aspartic acid
D53A	Alanine mutation on aspartic acid 53 residue of Survivin
Da/kDa	Dalton/kilodalton
DAPI	4′.6-diamidin-2-phenylindol
DAXX	Death domain associated protein
DCA	Dichloroacetic acid
DDR	DNA damage response
DMEM	Dulbecco’s modified eagle medium
DMSO	Dimethyl sulfoxide
DNA	Deoxyribonucleic acid
DNA-PKcs	DNA-dependent protein kinase, catalytic subunit
dNTP	Deoxynucleotides
DOCK6	Dedicator of cytokinesis 6
DOX	Doxorubicin
DSB	Double strand break
DSS	Disuccinimidyl suberate
DTT	Dithiothreitol
E, Glu	Glutamic acid
E29A	Alanine mutation on glutamic acid 29 residue of Survivin
E76A	Alanine mutation on glutamic acid 76 residue of Survivin
E2F1	E2F transcription factor 1
ECFP/EGFP/EYFP	Enhanced cyan/green/yellow fluorescent protein
ECL	Enhanced chemiluminescent
EGFR	Epidermal growth factor receptor
EGR1	Early growth response 1
EDTA	Ethylenediaminetetraacetic acid
E. coli	*Escherichia coli*

EM/cryo-EM	Electron microscopy; cryogenic EM
ENOX2	Ecto-nox disulfide-thiol exchanger 2
ERRFI1	ERBB receptor feedback inhibitor 1
eV	Electron volt
EWS	EWS RNA binding protein 1
F, Phe	Phenylalanine
F27A	Alanine mutation on phenylalanine 27 residue of Survivin
FA	Folic acid
FACS-FRET	Flow cytometry-based förster resonance energy transfer
FAK	Focal adhesion kinase
FAM63A/MINDY1	Family with sequence similarity 63 member a; Mindy lysine 48 deubiquitinase 1
FAM129A/NIBAN1	Family with sequence similarity 129 member a; Niban apoptosis regulator 1
FAT	FRAP, ATM, TRRAP domain
FATC	C-terminal of FAT
FATKIN	FAT and kinase domain
FBS	Fetal bovine serum
FHL3	Four and a half LIM domains 3
FLI1	FLI-1 proto-oncogene, ets transcription factor
FLNA	Filamin A
FOXM1	Forkhead box M1
FOXO3/FOXO3A	Forkhead box O3/A
FPs	Florescence proteins
FRET	Förster resonance energy transfer
GIGYF1	GRB10 interacting GYF protein 1
GPHN	Gephyrin
GPRIN1	G protein regulated inducer of neurite outgrowth 1
Gscore	Glide docking score
GST	Glutathione S-transferase
GTF3C1	General transcription factor IIIC subunit 1
Gy	Gray
HBXIP	Hepatitis B X-interacting protein
HCFC1	Host cell factor C1
HEAT	Huntingtin, elongation factor 3, regulatory subunit a of PP2A, TOR1
hILP2	Human inhibitor of apoptosis-like protein 2
HIRIP3	Hira interacting protein 3
HMGA1/2	High mobility group at-hook ½
HMGN1/2/5	High mobility group nucleosome binding domain 1/2/5
HNSCC	Head and neck squamous cell carcinoma
HPGD	15-hydroxyprostaglandin dehydrogenase
HPMA	*N*-(2-hydroxypropyl) methacrylamide
HPV	Human papillomavirus
HR	Homologous recombination
HRP	Horse radish peroxidase

Hsp90	Heat shock protein 90
HTVS	High-throughput virtual screening
Hydr	Hydrophobic
IAP	Inhibitor of apoptosis
IFI35	Interferon induced protein 35
IgG	Immunglobulin G
INCENP	Inner centromere protein
IP / co-IP	Immunoprecipitation / co-immunoprecipitation
IR	Ionizing radiation
K, Lys	Lysine
K79A	Alanine mutation on lysine 79 residue of Survivin
Kan	Kanamycin
kb	Kilo base pairs
K_d	Dissociation constant (binding affinity)
KD	Kinase-dead
KDM3A	Lysine Demethylase 3a
kg	Kilogram
KIF20B	Kinesin family member 20b
KIF22	Kinesin family member 22
KU70/80	Lupus KU autoantigen protein p70/80
L, Leu	Leucine
L28A	Alanine mutation on leucine 28 residue of Survivin
LAD1	Ladinin 1
LARP1	LA ribonucleoprotein 1, translational regulator
LC-MS	Liquid chromatography-mass spectrometry
LEMD3	LEM domain containing 3
Lig4	DNA ligase IV
LMNA	Lamin A
LRR	Leucine-rich repeats
LRRC58	Leucine rich repeat containing 58
LUC7L2	LUC7 like 2, pre-mRNA splicing factor
MAFG	MAF BZIP transcription factor G
MD	Molecular dynamics
MDC1	Mediator of DNA damage checkpoint protein 1
MED13L	Mediator Complex Subunit 13l
MKI67	Marker of proliferation KI-67
MOPS	3-(n-morpholino)propanesulfonic acid
MSN	Mesoporous silica nanoparticle
MT2A	Metallothionein 2A
MYRF	Myelin regulatory factor
NACHT	NAIP-C2TA-HETE-TEP1 nucleotide binding and oligomerization domain
NAIP	Neuronal apoptosis inhibitory protein
NAV2	Neuron navigator 2
NEO1	Neogenin 1

NF-κB	Nuclear factor-kappa B
NHEJ	Non-homologous end joining
NMI	N-MYC and STAT interactor
NP-40	Nonidet P-40
NSD1	Nuclear receptor binding set domain protein 1
NUP98	Nucleoporin 98 and 96 precursor
P, Pro	Proline
PAPOLA	Poly(A) polymerase alpha
PBS	Dulbecco's phosphate buffered saline
PCBP2	Poly(RC) binding protein 2
PCL	Poly(ε-caprolactone)
PCM1	Pericentriolar material 1
PCR	Polymerase chain reaction
PDK3	Pyruvate dehydrogenase kinase 3
PECL	Poly-(ethylene glycol)-*block*-poly(ε-caprolactone)
PEI	Polyethyleneimine
PI3K	Phosphatidylinositol-3-kinase
PIBF1	Progesterone immunomodulatory binding factor 1
PIKK	Phosphatidylinositol 3-kinase-related kinases
PKA	Protein kinase A
PLK1	Polo-like kinase 1
PMA	Phorbal 12-myristate 13-acetate
PNKP	Polynucleotide kinase-phosphatase
POLA2	DNA polymerase alpha 2, regulatory subunit
PRKCE	Protein kinase C epsilon
PRR11	Proline rich 11
PTTG1	PTTG1 regulator of sister chromatid separation, Securin
QSOX2	Quiescin sulfhydryl oxidase 2
R, Arg	Arginine
RAD51	Rad51 recombinase
RBBP6	Rb binding protein 6, ubiquitin ligase
RBBP8	Rb binding protein 8, endonuclease
RBM15	RNA binding motif protein 15
RBMX	RNA binding motif protein x-linked
RING	Really interesting new gene
RIPA	Radio-immunoprecipitation assay
RMSD	Root-mean-square deviation
RNA	Ribonucleic acid
RNF13	Ring finger protein 13
RNPS1	RNA binding protein with serine rich domain 1
RPMI	Roswell park memorial institute
RT	Room temperature
S, Ser	Serine
S20	Serine 20 residue of Survivin

S20A	Alanine mutation on serine 20 residue of Survivin
S20D	Aspartic acid mutation on serine 20 residue of Survivin
SAXS	Small angle X-ray scattering
SDS	Sodium dodecylsulfate
SDSL	Serine dehydratase like
SDS-PAGE	Sodium dodecyl sulphate polyacrylamide gel electrophoresis
SELENOK	Selenoprotein K
SENP5	Sumo specific peptidase 5
SLC19A1	Solute carrier family 19 member 1
SLC35F2	Solute carrier family 35 member F2
SLC43A1	Solute carrier family 43 member 1
SLC52A3	Solute carrier family 52 member 3
SLC7A11	Solute carrier family 7 member 11
SLC7A6	Solute carrier family 7 member 6
SLC9A3	Solute carrier family 9 member A3
SMAC	Second mitochondria derived activator of caspase
SP	Standard precision
SRC	C-sarcoma
SRRM2	Serine/arginine repetitive matrix 2
SSB	Single strand break
STMN3	Stathmin 3
STRA13	Stimulated by retinoic acid gene 13 protein
STX8	Syntaxin 8
Surv.wt	Survivin wild type
SUV39H1	Suppressor of variegation 3-9 homolog 1
T, Thr	Threonine
T34A	Alanine mutation on threonine 34 residue of Survivin
T34D	Aspartic acid mutation on threonine 34 residue of Survivin
T117A	Alanine mutation on threonine 117 residue of Survivin
T117D	Aspartic acid mutation on threonine 117 residue of Survivin
TAE	Tris acetate EDTA
TAF15	Tata-box binding protein associated factor 15
TAT	HIV cell penetrating tat peptide
TBS	Tris-buffered saline
TBS-T	TBS-Tween 20
TCA	Trichloroacetic acid
TCOF1	Treacher collins-franceschetti syndrome 1
TCRN	Targeted charge-reversal nanoparticles
TEMED	Tetramethylethylenediamin
TGF-β1	Transforming growth factor beta 1
THRAP3	Thyroid hormone receptor associated protein 3
TJP1	Tight junction protein 1
TMEM167B	Transmembrane protein 167B
TOP2A	DNA topoisomerase II alpha

TRAFD1	Traf-type zinc finger domain containing 1
TRD3	Tetratricopeptide repeat domain 3
TRIP13	Thyroid hormone receptor interactor 13
TRIS	Tris hydroxymethyl aminomethane
TYMS	Thymidylate synthetase
UBA	Ubiquitin-associated domain
UBC	Ubiquitin conjugating domain
UBE2S	Ubiquitin conjugating enzyme E2 S
USP8	Ubiquitin specific peptidase 8
UV	Ultraviolet
VS.	Versus
W, Trp	Tryptophane
W67A	Alanine mutation on tryptophane 67 residue of Survivin
wt	Wild type
WWP2	WW domain containing E3 ubiquitin protein ligase 2
XAF1	XIAP-associating factor 1
XIAP	X-linked inhibitor of apoptosis protein
XLF	XRCC4-like factor
XP	Extra precision
XRCC4	X-ray cross-complementing protein 4
ZBTB1	Zinc finger and BTB domain containing 1
ZC3HAV1L	Zinc finger CCCH-type containing, antiviral 1 like
ZFP36L2	Zinc finger protein 36, C3H1 type-like 2
ZNF326	Zinc finger protein 326
ZNF806	Zinc finger protein 806
ZYX	Zyxin